UNIVERSIDADE DE SÃO PAULO

INSTITUTO DE FÍSICA
CAIXA POSTAL 20516
01498 - SÃO PAULO - SP
BRASIL

PUBLICAÇÕES

IFUSP/P-871

THEORY OF NEAR-CRITICAL-ANGLE SCATTERING FROM A CURVED INTERFACE

N. Fiedler-Ferrari
Instituto de Física, Universidade de São Paulo

H.M. Nussenzveig* and **W.J. Wiscombe**
NASA Goddard Space Flight Center, Greenbelt,
MD 20771, U.S.A.

*Permanent address: Departamento de Física, Pontifícia Universidade Católica, 22452 Rio de Janeiro, RJ, Brasil

Setembro/1990

THEORY OF NEAR-CRITICAL-ANGLE SCATTERING FROM A CURVED INTERFACE†

N. Fiedler-Ferrari

Instituto de Física, Universidade de São Paulo
C.P. 20516, 01498 São Paulo, SP, Brasil

H.M. Nussenzveig* and W.J. Wiscombe

NASA Goddard Space Flight Center, Greenbelt, MD 20771, U.S.A.

† To appear in *Physical Review A*.

* Permanent address: Departamento de Física, Pontifícia Universidade Católica, 22452 Rio de Janeiro, RJ, Brasil.

ABSTRACT

A new type of diffraction effect, different from the standard semiclassical ones (rainbow, glory, forward peak, orbiting), takes place near the critical angle for total reflection at a curved interface between two homogeneous media. A theoretical treatment of this new effect is given for Mie scattering, e. g., light scattering by an air bubble in water; it can readily be extended to more general curved interface problems in a variety of different fields (quantum mechanics, acoustics, seismic waves).

The relatively slowly-varying Mie diffraction pattern associated with near-critical scattering is obscured by rapid fine-structure oscillations due to interference with unrelated "farside" contributions. These contributions are evaluated and subtracted from the Mie amplitudes to yield the relevant "nearside" effects.

A zero-order transitional CAM (complex angular momentum) approximation to the nearside amplitude is developed. The most important contributions arise from partial and total reflection, represented by two new diffraction integrals, designated Fresnel-Fock and Pearcey-Fock respectively. The total reflection contribution is strongly affected by tunneling, giving rise to a generalized version of the Goos-Hänchen shift.

In terms of short-wave asymptotics, in a generalized Huygens-Fresnel-type integral representation, the new diffraction features arise from non-analyticity of the integrand amplitude function within the range of a saddle point.

Also discussed are the WKB approximation, a known physical optics approximation and a new modified version of this approximation: they are compared with the "exact" nearside Mie amplitude obtained by numerical partial-wave summation, at scatterer size parameters (circumference/wavelength) ranging from 1,000 to 10,000. It is found that the physical optics approximations lead to large errors in the near-critical region, whereas the zero-order CAM approximation is in good agreement with the exact solution, accounting for the new diffraction effects in near-critical scattering.

1. INTRODUCTION

The standard critical situations in semiclassical scattering, where primitive semiclassical approximations fail and diffraction effects become important, are associated with near-forward diffractive scattering, rainbow scattering, forward and backward glory scattering, and orbiting, usually related with resonance scattering.[1]

In the present work, we deal with a new type of diffraction effect, which takes place in the vicinity of total reflection from a curved interface (a plane interface, for which the theory has already been partially developed, is included as a limiting case). The effect was identified long ago by Pulfrich,[2] who believed it to be connected with the rainbow, through a sort of reciprocity relation. Pulfrich observed scattering of white light from a cloud of air bubbles in water, rather than a cloud of water droplets in air. He saw pale colors near the critical scattering angle $\theta_t = 2\cos^{-1} N$ at which incident light is totally reflected, where N is the relative refractive index (for air bubbles in water, $N = 0.75$ and $\theta_t \approx 82.8°$). According to Pulfrich, θ_t would play a role analogous to the rainbow angle.

However, although it is tempting to draw analogies between the two phenomena, in reality they are quite different. In geometrical optics (or classical mechanics), a rainbow scattering angle is a caustic direction, corresponding to an infinite discontinuity in the scattered intensity, while the critical scattering angle is connected with a weaker singularity, which one may call a *weak caustic*: a continuous scattered intensity with an infinite discontinuity in *slope*. This singularity arises from the behavior of the Fresnel reflectivities at the critical angle: their slope shifts from vertical to horizontal, producing a cusp.[3] The diffraction pattern to which this gives rise has a superficial similarity with that for the rainbow: "supernumerary" oscillations on the total reflection ("bright") side, and rapid decay on the partial reflection ("dark") side. Like the rainbow, the pattern is modulated by much more rapid fine-structure oscillations, arising from interference with paths that are entirely unrelated with the effect under consideration.

As a theoretical model, we choose light scattering by a homogeneous sphere with relative refractive index $N < 1$, such as an air bubble in water, because the availability of the exact Mie solution[4] allows us to perform precise numerical tests of the accuracy of the proposed approximations. The Mie solution is in excellent agreement with experiment, as was verified in high-resolution observations by Langley and Marston.[5]

However, like the rainbow (but unlike the glory), the effect is structurally stable, being preserved even under large deformations, e. g., from spherical to cylindrical geometry. Actually, observations with cylindrical "bubbles" were made both by Pulfrich and by Marston and coworkers (including photographs of colors).[6] As will be pointed out in the concluding section, the theory developed in the present paper can be carried over with only trivial changes for the cylindrical case.

The results also apply to nonrelativistic quantum scattering by a two or three-dimensional square potential barrier (conceivably of interest in connection with quantum electron devices), as well as to acoustic scattering by a homogeneous sphere or cylinder. In geophysics, effects associated with near-critical reflection are of considerable importance in the theory of head waves.[7-9] For a planar interface, results closely related to a limiting form of those derived here (when the radius of curvature tends to infinity) are known.[10]

In the geometrical-optic approximation to the theory of light scattering by an air bubble in water,[11] the cusp-like singularity of the Fresnel reflectivities is reproduced in the scattering pattern at the critical angle. It is important to distinguish geometrical optics, in which contributions to the intensity from different paths are added incoherently, from the WKB zero-order approximation, in which due account is taken of the phases associated with the corresponding geometrical-optic terms, so that interference effects are included. The WKB approximation, also known as primitive semiclassical approximation in the quantum context, is the analogue of Young's interference theory of the rainbow.[12] It plays

an important role in the present problem, because it allows us to define the *near-critical domain* as the angular neighborhood where the WKB approximation departs significantly from the "exact" Mie results. The departures, due to diffraction, are the new effects that must be accounted for by the theory.

A physical optics approximation,[13,14] constructed by analogy with Airy's theory of the rainbow, predicts a Fresnel-like diffraction pattern in the far field modified by interference with direct transmission. It explains the fine-structure oscillations in terms of interference with rays transmitted along a different path.[5] In the domain of total reflection, not very close to the critical scattering angle, it is in fair agreement with the Mie coarse-structure pattern regarding the locations of maxima and minima; it also predicts the angular spacing of fine-structure modulations. These features agree with measured intensity patterns.[5] In the vicinity of the critical scattering angle, as well as in the partial-reflection domain beyond it, the physical optics approximation does not agree with the Mie results, substantially underestimating the scattered intensity.[5] Detailed comparisons have been hindered by the difficulties associated with removing the contribution from the superimposed (but totally unrelated) fine-structure pattern.

The near-critical region is also excluded from consideration in treatments based on the geometrical theory of diffraction.[15] The physical effects responsible cannot be determined from Mie summations involving a large number of partial-wave terms. Thus, no satisfactory quantitative theory of the new diffraction phenomena in this region is available.

In the present work, we employ CAM (Complex Angular Momentum) theory[16] to deal with near-critical scattering, taking advantage of the physical insights developed in its applications to both classical and quantum scattering problems. Recent developments in CAM theory[17,18] have shown that it can yield extremely accurate asymptotic approximations to exact results.

Here, we do not aim at high accuracy, but rather at a basic understanding of the new diffraction effect. Thus, we develop just the lowest-order transitional asymptotic approximation, keeping only dominant terms and disregarding uniformity. As a consequence, the domain of applicability of the approximations is restricted to large size parameters and to a limited neighborhood of the critical scattering angle. However, the most sizable diffraction effects are confined to this neighborhood, and no difficulty is anticipated in improving the accuracy and extending the domain of validity of the results.

Several shortcomings in the earliest CAM treatment[19] were corrected later,[20-22] yielding preliminary versions of results reported here. These versions have also been employed to derive an asymptotic approximation to the scattering amplitudes at exactly the critical angle.[23-25]

After introducing the CAM representation, we discuss the effective potential concept and its application to the selection and physical interpretation of dominant contributions (Sec. 2). In order to isolate the diffraction effects in near-critical scattering, one must begin by removing the distracting fine-structure modulation. This is accomplished by subtracting out the interfering terms (Sec. 3).

The first relevant contribution, arising from partial reflection, is evaluated in Sec. 4. In Sec. 5, we evaluate the effects due to transmission through the sphere, which yield a relatively minor, but still nonnegligible contribution to diffraction. The most significant contribution, originating from total reflection, is analyzed in Sec. 6.

It turns out that the curvature of the scatterer plays two very different roles in this problem. One is just to spread out the range of angles of incidence; when only this trivial role is taken into account, while neglecting the effects of curvature on reflection amplitudes at the interface, one obtains a "planar limit approximation" (Sec. 6). The results found in this approximation are closely related to those obtained in the total reflection of a divergent beam at a plane interface,[10] including the well-known Goos-Hänchen shift.[26] The spherical

analogue of this shift appears as an angular displacement that may be interpreted as a tunneling effect.

The CAM approximation, defined in Sec. 7, includes the *dynamical* effects of curvature, which modify the interface reflection amplitudes. It contains new diffraction integrals, the Fresnel-Fock and Pearcey-Fock integrals. In the planar limit, in a small neighborhood of the critical angle, the new diffraction contributions are approximated by a function related to Weber parabolic cylinder functions.

Other approximations discussed in Sec. 7 include the WKB approximation; the physical optics approximation; and a modified version of this approximation, with improved features in the domain of partial reflection. Numerical comparisons and plots of the Mie results with all these approximations are presented in Sec. 8. It is found that, in contrast with physical-optics approximations, CAM theory fully accounts for the new diffraction effects in near-critical scattering.

The main conclusions and a physical discussion of the results, including the connections with general semiclassical approximations and catastrophe theory, are given in Sec. 9. Readers who are primarily interested in such general features may proceed directly to this Section.

2. THE CAM REPRESENTATION

2.1. The Mie solution

The Mie scattering amplitudes S_1 (perpendicular polarized) and S_2 (parallel polarized) in the direction θ for the scattering of a linearly polarized plane monochromatic wave with wavenumber k by a homogeneous sphere of radius a and relative refractive index N (assumed real and less than unity in the present work) are given by [27]

$$S_j(\beta,\theta)=\tfrac{1}{2}\sum_{l=1}^{\infty}\left\{\left[1-S_l^{(j)}(\beta)\right]t_l(\cos\theta)+\left[1-S_l^{(i)}(\beta)\right]p_l(\cos\theta)\right\}\qquad (i,j=1,2;\ i\neq j)\qquad (2.1)$$

where $\beta\equiv ka$ is the size parameter; our convention for the time factor is $\exp(-i\omega t)$.

The S-functions $S_l^{(j)}$, associated with magnetic ($j=1$) and electric ($j=2$) multipoles of order l , are given by:

$$S_l^{(j)}(\beta)=-\frac{\zeta_l^{(2)}(\beta)}{\zeta_l^{(1)}(\beta)}\left[\frac{\ln'\zeta_l^{(2)}(\beta)-Ne_j\ln'\psi_l(\alpha)}{\ln'\zeta_l^{(1)}(\beta)-Ne_j\ln'\psi_l(\alpha)}\right]\qquad (2.2)$$

where

$$e_1\equiv 1\,,\qquad e_2\equiv N^{-2}\,,\qquad \alpha\equiv N\beta\qquad (2.3)$$

ψ_l and $\zeta_l^{(1,2)}$ are the Ricatti-Bessel and Ricatti-Hankel functions, respectively, and $\ln'$ denotes the logarithmic derivative.

The angular functions are defined by

$$p_\nu(x)\equiv\frac{P_{\nu-1}(x)-P_{\nu+1}(x)}{1-x^2}\,,\qquad t_\nu(x)\equiv -xp_\nu(x)+(2\nu+1)P_\nu(x)\qquad (2.4)$$

where P_ν is the Legendre function of the first kind (a Legendre polynomial when $\nu=l$ is an integer).

The scattering data are the *polarized intensities*

$$i_j(\beta,\theta) \equiv \left|S_j(\beta,\theta)\right|^2 \qquad (j=1,2) \tag{2.5}$$

and the *phase difference*

$$\delta \equiv \arg S_1 - \arg S_2 \tag{2.6}$$

Instead of (2.5), we shall mainly plot the *gain functions* relative to an isotropic scatterer, given by[12]

$$G_j(\beta,\theta) = 4i_j(\beta,\theta)/\beta^2 \tag{2.7}$$

The G_j are the ratios of the polarized intensities to their limiting geometrical-optic values for scattering by a totally reflecting sphere.

2.2. CAM representation

The first step in the CAM method[28] is to apply to (2.1) the Poisson sum formula

$$\sum_{l=0}^{\infty} f(l+\tfrac{1}{2}) = \sum_{m=-\infty}^{\infty}(-)^m \int_0^{\infty} f(\lambda)\exp(2im\pi\lambda)\,d\lambda \tag{2.8}$$

where the interpolating function $f(\lambda)$ reduces to $f(l+\frac{1}{2})$ at the physical values of the angular momentum λ. This requires adding and subtracting a fictitious $l=0$ term, with

$$p_0(\cos\theta) = t_0(\cos\theta) = \tfrac{1}{2}\sec^2(\theta/2)$$

[cf. (2.4)], so that we get

$$\begin{aligned} S_j(\beta,\theta) = {} & \tfrac{1}{2}\sum_{m=-\infty}^{\infty}(-)^m \int_0^{\infty} d\lambda \exp(2im\pi\lambda) \\ & \times\left\{\left[1-S^{(j)}(\lambda,\beta)\right]t_{\lambda-\frac{1}{2}}(\cos\theta)+\left[1-S^{(i)}(\lambda,\beta)\right]p_{\lambda-\frac{1}{2}}(\cos\theta)\right\} \\ & +\tfrac{1}{2}\sec^2\frac{\theta}{2}\left\{\tfrac{1}{2}\left[S_0^{(1)}(\beta)+S_0^{(2)}(\beta)\right]-1\right\} \qquad (i,j=1,2;\ i\neq j) \end{aligned} \tag{2.9}$$

where

$$S^{(j)}(\lambda,\beta) = -\frac{H_\lambda^{(2)}(\beta)}{H_\lambda^{(1)}(\beta)}\left(\frac{\{2\beta\}-Ne_j\{\alpha\}}{\{1\beta\}-Ne_j\{\alpha\}}\right) \tag{2.10}$$

and $H_\lambda^{(1,2)}$ are the Hankel functions, with

$$\{jz\} \equiv \ln' H_\lambda^{(j)}(z) + \frac{1}{2z}\ , \qquad \{z\} \equiv \ln' J_\lambda(z) + \frac{1}{2z} \tag{2.11}$$

In these expressions, we have employed the relationships among Ricatti-Bessel and Ricatti-Hankel functions and ordinary cylindrical functions.

As discussed in Sec. 1, we want to evaluate only the dominant terms in the asymptotic behavior of S_j for large β and for θ belonging to the near-critical region. Taking into account previous discussions of the CAM method for scattering by a penetrable sphere,[19] this enables us to work with a considerably simplified version of (2.9), through the following steps:

(i) We neglect the fictitious $l=0$ contribution. Since $\left|S_0^{(j)}\right|=1$, this term is $O(1)$ in the near-critical region, in contrast with dominant contributions that are $O(\beta)$ [leading to $G_j = O(1)$ in (2.7)].

- (ii) We keep only the $m=0$ term in (2.9). The dominant contributions[19] will arise from integrals containing stationary-phase points (which are associated with geometrical-optic rays) or from limiting forms of such integrals in the near-critical region. Extra factors $\exp(2im\pi\lambda)$ with $m\neq 0$ remove the stationary-phase points and introduce additional rapid oscillations that render such contributions negligible relative to the dominant ones.

Physically, contributions with $m\neq 0$ are associated with paths taking one or more turns around the origin. While such paths may yield important contributions[16,29] for $N>1$, they give rise only to small correction terms in the present problem.

(iii) It follows from (2.4) and from the asymptotic expansions of the Legendre functions[30] that

$$\left|p_{\lambda-\frac{1}{2}}(\cos\theta)/t_{\lambda-\frac{1}{2}}(\cos\theta)\right| = O\left[\left(|\lambda|\sin\theta\right)^{-1}\right] \qquad (|\lambda|\sin\theta \gg 1) \tag{2.12}$$

It will be seen below that $|\lambda| = O(\alpha)$ for the dominant contributions in the near-critical region, and we assume that both β and α are $\gg 1$. Thus, terms in $p_{\lambda-\frac{1}{2}}$ are $O(\alpha^{-1})$ as compared with those in $t_{\lambda-\frac{1}{2}}$, and will therefore be neglected. This approximation amounts to the neglect of cross-polarization effects,[12] so that only magnetic (electric) multipoles contribute for $j = 1$ ($j = 2$).

For similar reasons, in the last expression of (2.4), we can neglect the first term on the r.h.s. with respect to the second one, employing the approximation

$$t_{\lambda-\frac{1}{2}}(\cos\theta) \approx 2\lambda P_{\lambda-\frac{1}{2}}(\cos\theta) \tag{2.13}$$

(iv) In (2.10), the last terms of (2.11) are $O(\alpha^{-1})$, whereas the first terms, as will be seen below, are $O(1)$. Thus, we may neglect the last terms, employing the approximations[19]

$$\{jz\} \approx \ln' H_\lambda^{(j)}(z) \equiv [jz], \qquad \{z\} \approx \ln' J_\lambda(z) \equiv [z] \tag{2.14}$$

Finally, as a result of (i)-(iv), the CAM representation (2.9) is reduced to the much simpler form

$$S_j(\beta,\theta) \approx \int_0^\infty \left[1 - S^{(j)}(\lambda,\beta)\right] P_{\lambda-\frac{1}{2}}(\cos\theta)\,\lambda\,d\lambda \qquad (j = 1,2) \tag{2.15}$$

where $S^{(j)}$ is given by (2.10), with the approximations (2.14). It is interesting to note that, in this approximation, S_1 is related with the dimensionless amplitude f for scalar scattering by a transparent sphere treated in Ref. 19 by

$$S_1(\beta,\theta) \approx -i\beta f(\beta,\theta) \tag{2.16}$$

so that the results found for S_1 apply also to nonrelativistic quantum scattering by a square potential barrier or to acoustic scattering.

2.3. Localization principle and effective potential

One of the most useful concepts in CAM theory is the *localization principle*,[16] according to which, in the short-wavelength limit, contributions with angular momentum λ are associated with incident rays having an impact parameter

$$b(\lambda) = \lambda/k \tag{2.17}$$

Another basic CAM concept[19] is the *effective potential* $U_{\text{eff}}(\lambda,r)$ for the radial equation, obeyed, in the present case, by the Debye electromagnetic potentials.[31] In terms of the well-known analogy between optics and mechanics, at a given wave number k, a transparent sphere with refractive index $N < 1$ corresponds to a square potential barrier of height $(1-N^2)k^2$ (in units $\hbar = 2m = 1$) extending out to the radius of the sphere $r = a$. The effective potential is the sum of this barrier with the "centrifugal potential" λ^2/r^2 (in the Langer sense).[1] For magnetic polarization, as pointed out above, there is a strict correspondence with quantum scattering; for electric polarization, the boundary conditions at $r = a$ are slightly different, but this does not affect the ensuing qualitative analysis.

As illustrated in Fig. 1(a), the effective potential for this problem is a rounded potential step. In contrast with the situation[32] for $N > 1$, it does not lead to any sharp resonances, which immediately explains why the ripple fluctuations[12,27] that are ubiquitous in Mie cross sections for $N > 1$ are not present for $N < 1$. Also shown in Fig. 1(a) (where λ is fixed) are four different values of k^2, at different heights relative to the potential step: by the localization principle (2.17), they are associated with different impact parameters. The corresponding incident rays are shown in Fig. 1(b).

Situation 1 (Fig. 1), with $0 \le \lambda < \alpha$ [cf. (2.3)], corresponds to angles of incidence θ_1 below the critical angle. The incident ray is refracted into the droplet, where it undergoes multiple internal reflections. The radial turning point (classical distance of closest approach to the center) for an impact parameter b is at $r = b/N$.

Situation 2, with $\lambda = \alpha$, corresponds to incidence at the critical angle θ_c, with impact parameter $b = Na$. The incident ray is totally reflected, but we expect it to generate evanescent waves within the sphere. In terms of the effective potential picture [Fig. 1(a)], this corresponds to a *tunneling* effect. A similar interpretation applies to situation 3, where $\alpha < \lambda < \beta$, with the evanescent wave penetration depth decreasing monotonically as λ increases.

In situation 4, with $\lambda = \beta$, the "energy level" lies at the bottom of the step [Fig. 1(a)], and the incident ray is tangential to the sphere [Fig. 1(b)]. Taking into account the vertical wall in the effective potential at $r = a$, this situation is very similar to that found at $\lambda = \beta$ for an impenetrable sphere[18] and we expect the physical effects to be also very similar: external surface waves ("creeping modes") are launched. The "edge domain"

$$|\lambda - \beta| = O(\beta^{1/3})$$

contributes significantly to diffraction within the penumbra region $0 \leq \theta \lesssim \beta^{-1/3}$; however, for $\theta \gg \beta^{-1/3}$, reflection becomes dominant and this contribution can be neglected. We can also neglect contributions from $\lambda - \beta \gg \beta^{1/3}$, arising from rays that pass outside of the sphere, far from the edge domain.

We conclude that, for the domain of scattering angles of interest (near-critical region), we may cut off the integral (2.15) at $\lambda = \beta$. Furthermore, the resulting contribution from the first term within the square brackets in the integrand, namely,

$$\int_0^\beta P_{\lambda-\frac{1}{2}}(\cos\theta)\,\lambda\,d\lambda$$

gives rise to the classical Airy forward diffraction pattern,[18] which is also negligible in the domain of interest. Finally, we see that, in the near-critical region, (2.15) may be replaced by

$$S_j(\beta,\theta) \simeq -\int_0^\beta S^{(j)}(\lambda,\beta) P_{\lambda-\frac{1}{2}}(\cos\theta)\,\lambda\,d\lambda \qquad (2.18)$$

2.4. Nearside and farside contributions

The asymptotic expansion[30] of $P_\nu(\cos\theta)$ for $|\nu|\sin\theta \gg 1$ shows that it has the character of a standing wave in θ. We may decompose it into running waves by setting[28]

$$P_{\lambda-\frac{1}{2}}(\cos\theta) = Q_{\lambda-\frac{1}{2}}^{(1)}(\cos\theta) + Q_{\lambda-\frac{1}{2}}^{(2)}(\cos\theta) \qquad (2.19)$$

where, for $|\lambda|\sin\theta \gg 1$,

$$Q_{\lambda-\frac{1}{2}}^{(1,2)}(\cos\theta) \simeq \frac{\exp\left\{\mp i\left[\lambda\theta - (\pi/4)\right]\right\}}{(2\pi\lambda\sin\theta)^{1/2}}\left[1 + O\left(|\lambda\sin\theta|^{-1}\right)\right] \qquad (2.20)$$

so that $Q_{\lambda-\frac{1}{2}}^{(1)}$ travels clockwise in θ and $Q_{\lambda-\frac{1}{2}}^{(2)}$ counterclockwise.

Corresponding to this decomposition, (2.18) becomes

$$S_j(\beta,\theta) \simeq S_j^{(-)}(\beta,\theta) + S_j^{(+)}(\beta,\theta) \qquad (2.21)$$

with

$$S_j^{(-,+)}(\beta,\theta) \equiv -\int_0^\beta S^{(j)}(\lambda,\beta) Q_{\lambda-\frac{1}{2}}^{(1,2)}(\cos\theta)\,\lambda\,d\lambda \qquad (2.22)$$

where the superscript $(-)$ is associated with $(^1)$ and $(+)$ with $(^2)$.

In applications of semiclassical scattering to nuclear physics, the $(-)$ component is known as the *nearside amplitude* and the $(+)$ component as the *farside amplitude*.[33] The reason for this nomenclature is that dominant nearside contributions arise from "repulsive" paths, with negative classical deflection angles $\Theta = -\theta$, conventionally represented by incidence on the upper hemisphere (near side), whereas farside contributions arise from "attractive" paths, with positive classical deflection angles, such as $\Theta = \theta$, represented by incidence on the lower hemisphere (far side). Thus, direct reflection at the surface is a typical nearside contribution, whereas Fig. 2 below illustrates a farside contribution.

The diffraction effects of interest in the near-critical region arise entirely from nearside contributions, to be discussed in Secs. 4-8. However, farside contributions cannot be neglected in this region: though appreciably smaller than nearside ones, they interfere with them to produce, in view of the large phase difference, the rapidly-oscillating

modulation of the angular pattern known as "fine structure" (Sec. 1). Examples may be seen in Figs. 3-6 below.

In order to bring out the relevant effects and to allow meaningful comparisons with the numerically summed Mie series, it is essential to subtract out farside contributions, so as to eliminate, as far as possible, their obscuring effect on the pattern of interest. This is the main purpose of the evaluation of farside terms undertaken in the following Section.

3. REMOVAL OF FARSIDE CONTRIBUTIONS

3.1. The Debye expansion

Farside contributions arise from rays transmitted through the sphere after one or more internal reflections.[5] In CAM theory, they are associated with terms in the Debye multiple-internal reflection expansion[19] of the farside amplitude. The Debye expansion of the S-function (2.10) is given by[16,34]

$$S^{(j)}(\lambda,\beta) = S_0^{(j)}(\lambda,\beta) + \sum_{p=1}^{P} S_p^{(j)}(\lambda,\beta) + \Delta S_P^{(j)}(\lambda,\beta), \qquad j = 1,2 \tag{3.1}$$

where P is the order of the last term that one wants to retain and

$$S_0^{(j)}(\lambda,\beta) = \frac{H_\lambda^{(2)}(\beta)}{H_\lambda^{(1)}(\beta)} R_{22}^{(j)}(\lambda,\beta) \tag{3.2}$$

$$S_p^{(j)}(\lambda,\beta) = \frac{H_\lambda^{(2)}(\beta)}{H_\lambda^{(1)}(\beta)} T_{21}^{(j)}(\lambda,\beta) T_{12}^{(j)}(\lambda,\beta) \left[\rho^{(j)}(\lambda,\beta)\right]^{p-1} \frac{H_\lambda^{(1)}(\alpha)}{H_\lambda^{(2)}(\alpha)}, \qquad (p = 1,2,\ldots) \tag{3.3}$$

$$\Delta S_P^{(j)}(\lambda,\beta) = S_{P+1}^{(j)}(\lambda,\beta) \Big/ \left[1 - \rho^{(j)}(\lambda,\beta)\right] \tag{3.4}$$

In the *direct-reflection term* (3.2), $R_{22}^{(j)}$ is the *external spherical reflection coefficient*, given by [cf. (2.11)]

$$R_{22}^{(j)}(\lambda,\beta) = -\frac{\{2\beta\} - Ne_j\{2\alpha\}}{\{1\beta\} - Ne_j\{2\alpha\}} \tag{3.5}$$

In (3.3), we have

$$\rho^{(j)}(\lambda,\beta) = \frac{H_\lambda^{(1)}(\alpha)}{H_\lambda^{(2)}(\alpha)} R_{11}^{(j)}(\lambda,\beta) \tag{3.6}$$

where $R_{11}^{(j)}$ is the *internal spherical reflection coefficient*

$$R_{11}^{(j)}(\lambda,\beta) = -\frac{\{1\beta\} - Ne_j\{1\alpha\}}{\{1\beta\} - Ne_j\{2\alpha\}} \tag{3.7}$$

The inwards and outwards *spherical transmission coefficients* $T_{21}^{(j)}$ and $T_{12}^{(j)}$ in (3.3), respectively, are given by

$$T_{21}^{(j)}(\lambda,\beta) = 1 + R_{22}^{(j)}(\lambda,\beta) \ , \qquad T_{12}^{(j)}(\lambda,\beta) = 1 + R_{11}^{(j)}(\lambda,\beta) \tag{3.8}$$

The Debye term (3.3) is associated with transmission after $(p-1)$ internal reflections, and (3.4) represents the remainder after $(P-1)$ internal reflections.

Substituting (3.1) into (2.22), we finally obtain the Debye expansion of the farside scattering amplitude

$$\begin{aligned} S_j^{(+)}(\beta,\theta) &= -\int_0^{\beta}\left[S_0^{(j)}(\lambda,\beta) + \sum_{p=1}^{P} S_p^{(j)}(\lambda,\beta) + \Delta S_P^{(j)}(\lambda,\beta)\right] Q_{\lambda-\frac{1}{2}}^{(2)}(\cos\theta)\,\lambda\,d\lambda \\ &\equiv S_{j0}^{(+)}(\beta,\theta) + \sum_{p=1}^{P} S_{jp}^{(+)}(\beta,\theta) + \Delta S_{jP}^{(+)}(\beta,\theta) \end{aligned} \tag{3.9}$$

3.2. Evaluation of farside amplitude

We want to evaluate the dominant asymptotic contributions to (3.9) for large values of both β and $\alpha = N\beta$, in a neighborhood of the *critical scattering angle* θ_r,

$$\theta_r = \pi - 2\theta_c = 2\sin^{-1} M \quad , \qquad \theta_c = \sin^{-1} N \tag{3.10}$$

where θ_c is the critical angle of incidence and

$$M \equiv \left(1 - N^2\right)^{1/2} \tag{3.11}$$

Under these conditions, as will appear below, the main contributions arise from values of λ well below α, so that, for all Hankel functions involved in (3.9), we may apply the Debye asymptotic expansion[30]

$$H_{\lambda}^{(1,2)}(x) \sim \left(2/\pi\right)^{1/2}\left(x^2 - \lambda^2\right)^{-1/4} \exp\left\{\pm i\left[\left(x^2 - \lambda^2\right)^{1/2} - \lambda\cos^{-1}(\lambda/x) - (\pi/4)\right]\right\} \tag{3.12}$$

together with the approximation (2.14), that leads to

$$\begin{Bmatrix} R_{22}^{(j)}(\lambda,\beta) \\ R_{11}^{(j)}(\lambda,\beta) \end{Bmatrix} \sim \pm\frac{\left(\beta^2 - \lambda^2\right)^{1/2} - e_j\left(\alpha^2 - \lambda^2\right)^{1/2}}{\left(\beta^2 - \lambda^2\right)^{1/2} + e_j\left(\alpha^2 - \lambda^2\right)^{1/2}} \tag{3.13}$$

where upper and lower signs correspond to the upper and lower reflection coefficient, respectively. We may also employ the asymptotic expansion (2.20) in (3.9).

The dominant contributions to the farside amplitude arise from geometric-optic rays, which, in the λ-plane, are associated with stationary-phase points, i. e., real saddle points.[19] To look for such points in the various terms of (3.9), we set

$$\lambda \equiv \beta\sin w_1 \equiv \alpha\sin w_2 \tag{3.14}$$

with $0 \le w_1 \le \pi/2$ along the path of integration. By the localization principle (2.17), w_1 can be interpreted as the angle of incidence of rays associated with the representation (3.9), while w_2 is the corresponding angle of refraction.

With the above approximations and transformations, the dominant phase factor in the integrand of $S_{j0}^{(+)}$ in (3.9) is found to be [cf. (4.10)]

$$\exp\left\{-2i\beta\left[\cos w_1 - \left(\frac{\pi+\theta}{2} - w_1\right)\sin w_1\right]\right\} \tag{3.15}$$

Differentiating the exponent with respect to w_1, we find that there is no stationary-phase point within the path of integration (direct reflection is associated with repulsive paths, not with attractive ones).

The dominant phase factor in the integrand of $S_{jp}^{(+)}$ is found to be

$$\exp\left\{2i\beta\left[\left(Np\cos w_2 - Np\left(\frac{\pi}{2} - w_2\right)\sin w_2\right) - \cos w_1 + \left(\frac{\pi+\theta}{2} - w_1\right)\sin w_1\right]\right\} \tag{3.16}$$

Differentiating the exponent with respect to w_1, we find that a stationary-phase point $\overline{w}_1 = \theta_{1p}$, $\overline{w}_2 = \theta_{2p}$ must satisfy the simultaneous equations

$$2\theta_{1p} + p\left(\pi - 2\theta_{2p}\right) = \pi + \theta \quad , \qquad \sin\theta_{1p} = N\sin\theta_{2p} \qquad (p = 1,2,\ldots) \tag{3.17}$$

With $N < 1$, these equations have no solutions for $p = 1$: all directly transmitted ray paths are repulsive. But there are solutions for $p > 2$. The lowest-order farside path that contributes, $p = 2$, is illustrated in Fig. 2.

The saddle-point evaluation of $S_{jp}^{(+)}$ yields, as the dominant term,

$$S_{jp}^{(+)}(\beta,\theta) \approx (-i)^{p+1}\beta\left[\frac{Nc_{2p}s_{1p}c_{1p}}{2\sin\theta\left(pc_{1p}-Nc_{2p}\right)}\right]^{1/2}\frac{-4Ne_jc_{2p}c_{1p}}{\left(Ne_jc_{2p}+c_{1p}\right)^2}$$
$$\times\left(\frac{Ne_jc_{2p}-c_{1p}}{Ne_jc_{2p}+c_{1p}}\right)^{p-1}\exp\left[2i\beta\left(Npc_{2p}-c_{1p}\right)\right] \qquad (p=2,3,\ldots) \qquad (3.18)$$

where

$$c_{mp} \equiv \cos\theta_{mp}\ , \qquad s_{mp} \equiv \sin\theta_{mp} \qquad (m=1,2) \qquad (3.19)$$

and θ_{1p} and θ_{2p} , determined by (3.17), are, respectively, the angles of incidence and of refraction of the farside geometrical-optic ray that emerges in the direction θ after $(p-1)$ internal reflections.

The result (3.18) represents the dominant contribution to the *WKB approximation* of $S_{jp}^{(+)}$. Its modulus squared yields the *geometrical-optic* contribution[11] to the intensity from this term. However, the sum of several amplitudes of the form (3.18) goes beyond geometrical optics by taking coherence and interference effects into account.

The square root in (3.18) is the *beam divergence factor* D_p for a multireflected beam[12] and the two factors that follow it represent, respectively, $T_{21}^{(j)}T_{12}^{(j)}$ and $\left(R_{11}^{(j)}\right)^{p-1}$, where $T_{21}^{(j)}$, $T_{12}^{(j)}$ and $R_{11}^{(j)}$ are, respectively, the Fresnel transmission and internal reflection amplitudes at a plane interface[31] associated with the angles θ_{1p} , θ_{2p} and polarization j .The phase factor $(-i)^{p+1}$ represents the cumulative delay arising from the crossing of focal lines.[12]

For $p \gg 1$, we find that

$$\theta_{1p} \approx \theta_c - \frac{N}{8M}\left(\frac{\theta_r+\theta}{p}\right)^2 \ , \qquad \theta_{2p} \approx \frac{\pi}{2} - \left(\frac{\theta_r+\theta}{2p}\right) \qquad (p \gg 1) \qquad (3.20)$$

where θ_c , θ_r and M are defined by (3.10-11). It follows that

$$R_{11}^{(j)} \approx -1 + Ne_j\left[(\theta_r+\theta)/(Mp)\right] \qquad (p \gg 1) \qquad (3.21)$$

so that one approaches total reflection when the number of internal reflections increases. This leads to a relatively low convergence rate of the farside Debye terms for large p .

Indeed, at $\theta = \theta_r$, (3.18)-(3.21) yield

$$S_{jp}^{(+)}(\beta,\theta_r) \approx 2\beta e_j\left(N\theta_r/M\right)^{1/2}\exp\left(-2Ne_j\theta_r/M\right)$$
$$\times\exp\left[2i\beta\left(N\theta_r-M\right)\right]\left(i^{p+1}/p^2\right) \qquad (p \gg 1) \qquad (3.22)$$

which converges only like p^{-2} . Note, however, that successive contributions differ in phase by $\pi/2$, so that corrections to $\left|S_j^{(+)}\right|$ after p terms go like $(p+2)^{-2}$.

The convergence is somewhat faster for polarization 2 (parallel), as may be seen from (3.21) with $e_2 = N^{-2}$. This effect is enhanced, for $N \approx 3/4$, by the accidental proximity between θ_{22} and Brewster's angle, making the number of farside subtractions needed to remove most of the fine-structure oscillations from the Mie amplitudes much smaller for polarization 2 than for polarization 1, as will now be seen.

3.3. Subtracted Mie amplitudes

We define

$$S_j^{(-)}(\beta,\theta|P) \equiv S_j(\beta,\theta) - \sum_{p=2}^{P} S_{jp}^{(+)}(\beta,\theta) \qquad (3.23)$$

where S_j is the "exact" Mie amplitude, given by (2.1), and the subtracted terms are given by (3.18). Note that farside contributions are not removed completely by this subtraction procedure, both because P is finite and because (3.19) contains only the dominant asymptotic farside contribution to the Debye term of order p (e. g., it does not include higher-order WKB corrections). Nevertheless, we refer to (3.23) as the *subtracted Mie amplitude to order* P .

In Fig. 3(a), with $N = 0.75$, we compare the "exact" polarization 1 gain function [cf. (2.7)] G_1, for $\beta = 1{,}000$ and $75° \le \theta \le 90°$, with the subtracted gain functions obtained from (3.23) to orders $P = 2$ (only one term subtracted) and $P = 100$. We see that the fine-structure oscillations in polarization 1 are quite large, and that subtraction of the $p = 2$ farside term alone still leaves a lot of fine-structure "beats" to be removed. With $P = 100$, most of the fine structure has been removed.

Fig. 3(b) shows the effect of "peeling away" successive layers of fine structure from G_1 for $\beta = 10{,}000$ and $78° \le \theta \le 84°$. We see that sizable beats remain even after three subtractions, and a careful comparison between $P = 10$ and $P = 100$ still reveals some differences.

For the polarization 2 gain function G_2, plotted in Fig. 4 for $\beta = 5{,}000$ and $80° \le \theta \le 86°$, we see that the amplitude of fine-structure oscillations is a good deal smaller (because of the proximity to Brewster's angle). Subtraction of the $p = 2$ farside term alone already removes most of the fine structure, as illustrated by the upper curve in Fig. 4 (note the different plot scale), and the main effect of going to $P = 100$ is to introduce some additional smoothing.

Since both S_1 and S_2 contribute to the phase difference δ [cf. (2.6)], one needs to go to large values of P to remove fine structure in this case. This is illustrated in Fig. 5, which shows $\cos\delta$ for $\beta = 100$ and $40° \le \theta \le 130°$, exhibiting large fine-structure oscillations, some of which persist for $P = 2$ (upper curve, with different plotting scale), but are practically eliminated for $P = 100$. The farside subtractions reveal a dip around 106° that was masked by the fine structure oscillations [cf. also Fig. 6(c)].

In Fig. 6, we compare the "exact" Mie results for G_1, G_2 and $\cos\delta$ for $\beta = 1{,}000$ and $65° \le \theta \le 105°$ with their subtracted counterparts to order $P = 100$. We see that the distracting effect of fine structure is indeed removed by the farside subtractions, allowing us to proceed towards our purpose, the explanation of the much broader diffraction pattern around the critical scattering angle that is apparent in these figures.

According to the above discussion, this pattern must arise entirely from the nearside terms $S_j^{(-)}$ in (2.21), so that we now evaluate these terms.

4. THE DIRECT REFLECTION SUBCRITICAL TERM

4.1. Subcritical and supracritical contributions

We split the nearside amplitude [cf. (2.22)] into two parts,

$$S_j^{(-)}(\beta,\theta) = S_j^<(\beta,\theta) + S_j^>(\beta,\theta) \tag{4.1}$$

where

$$S_j^<(\beta,\theta) \equiv -\int_0^\alpha S^{(j)}(\lambda,\beta) Q_{\lambda-\frac{1}{2}}^{(1)}(\cos\theta)\lambda\, d\lambda \tag{4.2}$$

will be called the *subcritical* nearside amplitude and

$$S_j^>(\beta,\theta) \equiv -\int_\alpha^\beta S^{(j)}(\lambda,\beta) Q_{\lambda-\frac{1}{2}}^{(1)}(\cos\theta)\lambda\, d\lambda \tag{4.3}$$

will be called the *supracritical* amplitude. The reason for these names is that, with the substitution (3.14), the subcritical (supracritical) amplitude arises from incident rays with angles of incidence w_1 below (above) the critical angle θ_c [cf. Fig. 1(b)].

The subcritical amplitude is associated with ray paths of the type illustrated in situation 1 in Fig. 1(b), for which it is useful to separate contributions from varying numbers of internal reflections by applying the Debye expansion. Substituting (3.1), with $P = 1$, into (4.2), we find

$$S_j^<(\beta,\theta) = S_{j0}^<(\beta,\theta) + S_{j1}^<(\beta,\theta) + \Delta S_{j1}^<(\beta,\theta) \tag{4.4}$$

where

$$S_{j0}^<(\beta,\theta) = -\int_0^\alpha \frac{H_\lambda^{(2)}(\beta)}{H_\lambda^{(1)}(\beta)} R_{22}^{(j)}(\lambda,\beta) Q_{\lambda-\frac{1}{2}}^{(1)}(\cos\theta)\lambda\, d\lambda \tag{4.5}$$

is the *direct reflection subcritical term*,

$$S_{j1}^<(\beta,\theta) = -\int_0^\alpha \frac{H_\lambda^{(2)}(\beta)}{H_\lambda^{(1)}(\beta)} T_{21}^{(j)}(\lambda,\beta) T_{12}^{(j)}(\lambda,\beta) \frac{H_\lambda^{(1)}(\alpha)}{H_\lambda^{(2)}(\alpha)} Q_{\lambda-\frac{1}{2}}^{(1)}(\cos\theta)\lambda\, d\lambda \tag{4.6}$$

is the *direct transmission subcritical term*, and

$$\Delta S_{j1}^<(\beta,\theta) = -\int_0^\alpha \frac{H_\lambda^{(2)}(\beta)}{H_\lambda^{(1)}(\beta)} T_{21}^{(j)}(\lambda,\beta) T_{12}^{(j)}(\lambda,\beta) \times \left[\frac{\rho^{(j)}(\lambda,\beta)}{1-\rho^{(j)}(\lambda,\beta)}\right] \frac{H_\lambda^{(1)}(\alpha)}{H_\lambda^{(2)}(\alpha)} Q_{\lambda-\frac{1}{2}}^{(1)}(\cos\theta)\lambda\, d\lambda \tag{4.7}$$

is the *remainder subcritical term*.

Each of these terms will be separately discussed. The supracritical amplitude (4.3) is associated with rays that undergo total reflection at the geometrical-optic level [situations 2 to 4 in Fig. 1(b)], for which the Debye expansion is not suitable, so that it requires a different treatment. In the present Section, we discuss the direct reflection subcritical term.

In terms of scattering angles, we must also distinguish between the *domain of partial reflection* $\theta_t < \theta \le \pi$, referred to as PR from now on, and the *domain of total reflection* $0 \le \theta \le \theta_t$, referred to as TR:

$$0 \le \theta \le \theta_t \ (\text{TR}), \qquad \theta_t < \theta \le \pi \ (\text{PR}) \tag{4.8}$$

The deviation from the critical scattering angle θ_t will be measured by the parameter

$$\varepsilon \equiv \tfrac{1}{2}(\theta_t - \theta) \tag{4.9}$$

4.2. The WKB approximation

With the approximations (2.20) and (3.12) and the substitution (3.14), (4.5) becomes

$$S_{j0}^<(\beta,\theta) \approx \frac{e^{-i\pi/4}\beta^{1/2}}{(2\pi\sin\theta)^{1/2}} \int_0^{\theta_t} (\sin w_1)^{1/2} \cos w_1 R_{22}^{(j)} \times \exp\left\{-2i\beta\left[\cos w_1 - \left(\frac{\pi-\theta}{2} - w_1\right)\sin w_1\right]\right\} dw_1 \tag{4.10}$$

where $R_{22}^{(j)}$ is given by (3.5), (3.14). Note that the phase factor in (4.10) differs from that in (3.15) only by the substitution $\theta \to -\theta$.

The integrand of (4.10) has a saddle point at

$$\bar{w}_1 \equiv \theta_1 = (\pi - \theta)/2 \tag{4.11}$$

which lies within the domain of integration if θ is in PR, and outside (beyond θ_c) if θ is in TR [cf. (4.8)]. In either case, assuming that the main contribution to the integral arises from the neighborhood of the saddle point (i. e., from the neighborhood of the upper limit, for θ in TR), we expand the integrand around this point, as one would in the saddle-point method, yielding

$$S_{j0}^{<}(\beta,\theta) \approx \frac{e^{-i\pi/4}}{2\sqrt{\pi}}\beta^{1/2}\left(\sin\frac{\theta}{2}\right)^{1/2}\exp\left(-2i\beta\sin\frac{\theta}{2}\right) \int_{-\bar{w}_1}^{\varepsilon} R_{22}^{(j)}(\lambda,\beta)\exp\left(-i\beta\sin\frac{\theta}{2}v^2\right)dv \qquad (4.12)$$

where ε is given by (4.9), λ is given by (3.14), with

$$w_1 = \bar{w}_1 + v \qquad (4.13)$$

and we have assumed that

$$\beta|v|^3 \ll 1 \qquad (4.14)$$

in the portion of the domain of integration that contributes significantly to the integral.

In the PR domain, sufficiently far from critical scattering, (4.12) should just yield the WKB result associated with the directly reflected geometrical-optic ray. As was done in Sec. (3.2), we may then employ the approximation (3.13) for $R_{22}^{(j)}$. From (4.12), we see that the *range* of the saddle point, i. e., the domain in v that contributes significantly, is

$$|v| = O\left\{\left[\beta\sin(\theta/2)\right]^{-1/2}\right\}$$

In order that the saddle-point method may be applied, the full range of the saddle point (4.11) must be included within the domain of integration in (4.12). This requires

$$\varepsilon < 0 \quad \text{and} \quad |\varepsilon| \gg (M\beta)^{-1/2} \qquad (4.15)$$

where we have employed (3.10).

Assuming the validity of (4.15), the saddle-point evaluation of (4.12) leads to the zero-order WKB result

$$S_{j0}^{<}(\beta,\theta) \approx -\frac{i\beta}{2}\left\{\frac{\sin(\theta/2)-e_j\left[N^2-\cos^2(\theta/2)\right]^{1/2}}{\sin(\theta/2)+e_j\left[N^2-\cos^2(\theta/2)\right]^{1/2}}\right\}\exp\left[-2i\beta\sin(\theta/2)\right] \qquad (4.16)$$

The expression within curly brackets is the Fresnel external reflection amplitude[31] associated with the angle of incidence (4.11). For $j=1$, the result is related by (2.16) with the corresponding result [19] for scalar scattering. The first-order WKB correction $\delta S_{j0}^{<}$ for both the scalar or electromagnetic[34] case satisfies

$$\delta S_{j0}^{<}(\beta,\theta)/S_{j0}^{<}(\beta,\theta) = O\left\{\beta^{-1}\left[N^2-\cos^2(\theta/2)\right]^{-1/2}\right\} \qquad (4.17)$$

This correction does not become very large within the domain (4.15), but it blows up at the critical scattering angle (3.10). Thus, even though the zero-order WKB approximation remains well-behaved as $\theta \to \theta_c$, the divergence of the first-order correction signals the breakdown of this approximation outside of the domain (4.15), arising from the cusp singularity in the Fresnel reflectivities. We now deal with the near-critical domain, where

$$|\varepsilon| = O\left[(M\beta)^{-1/2}\right]$$

From now on, it is therefore assumed that $|\varepsilon| \ll 1$.

4.3. The Fresnel-Fock integral

It follows from (4.9) and (4.11) that, in the λ plane, the saddle point $\bar{\lambda} = \beta\sin\bar{w}_1$ is such that

$$\bar{\lambda} - \alpha = \beta\left[M\sin\varepsilon - N(1-\cos\varepsilon)\right] = M\beta\varepsilon + O(\beta\varepsilon^2) \qquad (4.18)$$

so that the saddle point coincides with the upper limit of integration of (4.12) at the critical scattering angle and is close to the upper limit in the near-critical domain. This invalidates the approximations employed following (4.14) in two ways:

(i) The Debye asymptotic expansion (3.12) that led to (3.13) can no longer be employed to evaluate $\{1\alpha\}$ and $\{2\alpha\}$ in (3.7) [cf. (2.14)]. Physically, this means that

the effects of the curvature of the spherical surface become important, so that the reflectivities can no longer be approximated by their planar-interface Fresnel limits. Correcting the reflectivities eliminates the cusp singularity and the divergence at the critical angle.

(ii) Although the dominant contributions to (4.12) still arise from the neighborhood of the saddle point (in view not only of the usual saddle-point arguments, but also of the sharp peaking of the reflectivities at the critical angle), the saddle-point method is no longer directly applicable, because part of the range of the saddle point lies outside the range of integration.

The most thorough procedure to deal with point (i) would be to employ the uniform asymptotic expansions of the cylindrical functions[18]. However, our goal is to find the lowest-order approximation that will allow us to explain the new diffraction effects in the near-critical region. Thus, we sacrifice uniformity and high accuracy, by employing a transitional asymptotic approximation to the cylindrical functions: the Schöbe approximation, which, to lowest order,[19] is

$$H_\lambda^{(1,2)}(x) \approx 2\exp(\mp i\pi/3)(2/x)^{1/6}\mathrm{Ai}\left[\exp(\pm 2i\pi/3)(2/x)^{1/3}(\lambda - x)\right], \quad |\lambda - x| = O\left(x^{1/3}\right) \quad (4.19)$$

where Ai denotes the Airy function. Applying this to $\{2\alpha\}$ in (3.5) [but still employing (3.12) for $\{1\beta\}$ and $\{2\beta\}$], we find

$$R_{22}^{(j)}(\lambda,\beta) \approx \frac{1+\gamma'\Psi_j[N;\gamma'(\lambda-\alpha)]}{1-\gamma'\Psi_j[N;\gamma'(\lambda-\alpha)]} \quad (4.20)$$

where

$$\gamma' \equiv (2/\alpha)^{1/3} \quad (4.21)$$

and we have introduced the new notation

$$\Psi_j[N;X] \equiv e^{-i\pi/6}\left(Ne_j/M\right)\ln' \mathrm{Ai}\left(e^{-2i\pi/3}X\right) \quad (4.22)$$

Within the domain of applicability of the Schöbe approximation, according to (4.20), the deviation of $\left|R_{22}^{(j)}\right|$ from unity (total reflection) remains $O(\gamma')$.

Replacing ν by

$$u \equiv \left[\beta\sin(\theta/2)\right]^{1/3}\nu \quad (4.23)$$

in (4.13), and taking (4.14) into account, we find that, in (4.20),

$$\gamma'(\lambda-\alpha) \approx \gamma'\left\{\beta\left[\cos(\theta/2)-N\right]+\left[\beta\sin(\theta/2)\right]^{1/3}u-\tfrac{1}{2}\cot(\theta/2)u^2\right\}$$

For $\theta \sim \theta_t$, by (4.14) and (4.22), we have

$$\gamma'|u|^2 \sim \left(\beta^{1/3}|\nu|\right)^2 \ll 1$$

so that the last term of the above expression may be neglected. Thus, substituting these results into (4.12):[35]

$$S_{j0}^{<}(\beta,\theta) \approx \frac{e^{-i\pi/4}}{2\sqrt{\pi}}\beta\exp\left(-2i\beta\sin\frac{\theta}{2}\right)\int_{-\infty}^{X=0}\left(\frac{1+\gamma'\Psi_j[N;X]}{1-\gamma'\Psi_j[N;X]}\right)\exp\left(-iu^2\right)du \quad (4.24)$$

where the lower limit has been replaced by $-\infty$ and

$$X \equiv \gamma'\left\{\beta\left[\cos(\theta/2)-N\right]+\left[\beta\sin(\theta/2)\right]^{1/3}u\right\} \quad (4.25)$$

If the deviation ε from the critical scattering angle (4.9) satisfies $|\varepsilon| \ll 1$, we have

$$X \approx \gamma'\left(M\beta\varepsilon - \tfrac{1}{2}N\beta\varepsilon^2 + \sqrt{M\beta}u\right)$$

As will appear below, $|\varepsilon| = O\left(\beta^{-1/3}\right)$ in the near-critical region, so that $\gamma'\beta\varepsilon^2 \ll 1$ can be neglected in this expression. Thus,

$$X \approx \gamma'\sqrt{M\beta}\left(\sqrt{M\beta}\varepsilon + u\right) \quad (4.26)$$

so that the upper limit of integration in (4.24) corresponds approximately to $u = -\sqrt{M\beta}\varepsilon$.

The integral in (4.24) resembles a Fresnel integral, except for the first factor in the integrand, arising from (4.20), which is similar to that appearing in Fock-type functions.[28] We therefore call (4.24) a *Fresnel-Fock integral*. For its numerical evaluation (see Appendix B), it is convenient to proceed as follows:

(i) In PR, where the stationary-phase (saddle) point $u = 0$ falls within the domain of integration, we deform the path of integration to go from $e^{3i\pi/4}\infty$ to the origin (this deformation is allowed), then from the origin to w along the real axis [where $u = w$ is the upper limit]. Along the first part of the path, the integrand has the fast Gaussian decay characteristic of a steepest-descent path.

The second part is a definite integral along a piece of a stationary-phase path, so that it has an oscillatory (Fresnel-like) character, but w remains of order unity within the near-critical region, so that the number of oscillations is small. It is interesting to note that a similar mixed steepest-descent-plus-stationary-phase path was useful in CAM approximations to near-forward diffraction.[18]

(ii) In TR, where the upper limit w is negative, the path is deformed onto a straight line from $e^{3i\pi/4}\infty$ to w, parallel to the steepest-descent path. The integrand is still dominated by Gaussian-like decay at large $|u|$; there is also some oscillation, but this is rapidly damped by the Gaussian factor.

4.4. Discussion

The following physical effects are incorporated into (4.24):

(a) The Fresnel-like character associated with the existence of a stationary-phase point within the domain of integration (PR) or outside it, but close to its edge (TR);

(b) The incomplete character of the Fresnel-like integral, since only part of the range of the stationary-phase point falls within the domain of integration (the tail end of the range, in TR);

(c) The deviation of the spherical reflection coefficient $R_{22}^{(j)}$ from its limiting Fresnel value for a plane interface, due to the effect of curvature. These features are missing in the WKB approximation, as was discussed at the beginning of Sec. 4.3. Although (4.24) will not match very smoothly with the WKB approximation outside of the

near-critical domain (because we did not apply uniform asymptotic approximations), we can employ it to estimate the angular width of this domain.

In the PR region, by (4.26), we require

$$|\varepsilon| \gg (M\beta)^{-1/4} \tag{4.27}$$

in order for a substantial part of the range of the stationary-phase point $u = 0$ of (4.24) to be included within the domain of integration. This agrees with (4.15).

In the TR domain, since (4.24) resembles an incomplete Fresnel integral, we expect $|S_{j0}^{<}|$ to fall off roughly like

$$\left(\sqrt{M\beta}\varepsilon\right)^{-1} \text{ for } \varepsilon \geq (M\beta)^{-1/4}.$$

Deviations from the WKB approximation should therefore be small when (4.27) holds. We conclude that the angular width of the domain where diffraction effects are significant (near-critical domain), for the direct-reflection subcritical contribution, must be of the order of a few times $(M\beta)^{-1/4}$.

5. TRANSMITTED SUBCRITICAL CONTRIBUTIONS

5.1. Direct transmission subcritical term: WKB approximation

The direct transmission subcritical term is given by (4.6). At the geometrical-optic level, it gives rise to two angular domains:[19] an illuminated region, $\theta < \theta_t$ that coincides with TR, singly covered by directly transmitted rays; and a shadow region, $\theta > \theta_t$ that coincides with PR. For this term, the near-critical domain is a typical *Fock-type transition*,[16] associated with the disappearance of one real ray.

Well within the illuminated region TR, one may apply the WKB approximation, treating $S_{j1}^{<}$ like $S_{j1}^{(+)}$ in Sec. (3.2), i. e., employing (2.20) and (3.12). Thus, the saddle point is given by (3.17) for $p = 1$, with $\theta \to -\theta$ (because $Q_{\lambda-\frac{1}{2}}^{(2)} \to Q_{\lambda-\frac{1}{2}}^{(1)}$), yielding

$$\bar{\lambda} = \alpha\left[1 - 2N\cos(\theta/2) + N^2\right]^{-1/2}\sin(\theta/2) \tag{5.1}$$

provided that $\gamma'\left(\alpha - \bar{\lambda}\right) \gg 1$, in order that (3.12) with $x = \alpha$ may be employed. From (4.9) and (5.1), we find that, for $\varepsilon \ll 1$, this condition is equivalent to

$$\varepsilon \gg \gamma' \tag{5.2}$$

The saddle-point evaluation of (4.6) yields, as its dominant term, the zero-order WKB approximation

$$S_{j1}^{<}(\beta,\theta) \approx -i\beta\left[\frac{Nc_2 s_1 c_1}{2\sin\theta(c_1 - Nc_2)}\right]^{1/2}\frac{4Ne_j c_2 c_1}{\left(Ne_j c_2 + c_1\right)^2}\exp\left[-2i\beta(c_1 - Nc_2)\right], \quad \theta_t - \theta \gg \gamma' \tag{5.3}$$

where

$$c_m \equiv \cos\theta_m \ , \qquad s_m \equiv \sin\theta_m \qquad (m = 1,2) \ , \tag{5.4}$$

and θ_1 and θ_2 are related to θ by

$$\tan\theta_1 = N\sin(\theta/2)/\left[1 - N\cos(\theta/2)\right], \quad \theta_2 = \sin^{-1}(\sin\theta_1/N) \tag{5.5}$$

allowing us[19] to express (5.3) directly in terms of θ. The expression within square brackets in (5.3) is the beam divergence[12] factor D_1 and the following factor is the product of the internal and external Fresnel transmission amplitudes, so that, by (3.8) and (3.13), the WKB result may be rewritten as

$$S_{j1}^{<}(\beta,\theta) \approx -i\beta\sqrt{D_1}\left(1 - r_j^2\right)\exp\left[-2i\beta(c_1 - Nc_2)\right], \quad \theta_t - \theta \gg \gamma' \tag{5.6}$$

We note that (5.3), if continued to the shadow boundary $\theta = \theta_t$, would vanish there.

The first-order WKB correction,[19] similarly to (4.17), would blow up if continued to the critical scattering angle; the condition for it to remain small is equivalent to (5.2), namely, $\theta_t - \theta \gg \gamma'$.

5.2. Fock-type approximation

According to the above discussion, the near-critical domain where diffraction effects are significant for the direct transmission subcritical term should be given by

$$\varepsilon = O(\gamma') \tag{5.7}$$

Since the saddle point (5.1) would approach $\bar{\lambda} = \alpha$ for $\theta \to \theta_t$, we expect that the main contribution to (4.6) in this region will arise from the domain $\gamma'|\lambda - \alpha| = O(1)$, where the Schöbe approximation (4.19) may be applied for $x = \alpha$.

Thus [cf. (4.12)], (4.6) becomes

$$S_{j1}^{<}(\beta,\theta) \approx \frac{e^{-i\pi/4}\beta^{1/2}}{(2\pi\sin\theta)^{1/2}}\int_0^{\theta_t}(\sin w_1)^{1/2}\cos w_1\, T_{21}^{(j)}\frac{H_\lambda^{(1)}(\alpha)}{H_\lambda^{(2)}(\alpha)}T_{12}^{(j)}$$
$$\times\exp\left\{-2i\beta\left[\cos w_1 - \left(\frac{\pi - \theta}{2} - w_1\right)\sin w_1\right]\right\}dw_1 \tag{5.8}$$

where, by (3.8) and (4.20),

$$T_{21}^{(j)}(\lambda,\beta) = 1 + R_{22}^{(j)}(\lambda,\beta) = \frac{2}{1 - \gamma'\Psi_j\left[N;\gamma'(\lambda - \alpha)\right]} \tag{5.9}$$

with $\lambda = \beta \sin w_1$.

By (3.7) and (3.8),

$$\frac{H_\lambda^{(1)}(\alpha)}{H_\lambda^{(2)}(\alpha)} T_{12}^{(j)}(\lambda,\beta) = \frac{4iNe_j}{\pi\alpha\left[H_\lambda^{(2)}(\alpha)\right]^2\left(\{1\beta\} - Ne_j\{2\alpha\}\right)} \tag{5.10}$$

where we have employed the Wronskian[30] of $H_\lambda^{(1)}$, $H_\lambda^{(2)}$. Again in the Schöbe approximation, this becomes

$$\frac{H_\lambda^{(1)}(\alpha)}{H_\lambda^{(2)}(\alpha)} T_{12}^{(j)}(\lambda,\beta) \approx \frac{e^{-2i\pi/3} Ne_j\gamma'}{2\pi M\left\{1 - \gamma'\Psi_j\left[N;\gamma'(\lambda-\alpha)\right]\right\}\mathrm{Ai}^2\left[e^{-2i\pi/3}\gamma'(\lambda-\alpha)\right]} \tag{5.11}$$

Since the main contribution to (5.8) in the domain (5.7) arises from the neighborhood of the upper limit where the Schöbe approximation is valid, we expand the integrand around this point, setting

$$w_1 \equiv \theta_c - \zeta\ , \qquad \zeta = O(\gamma'^2) \tag{5.12}$$

so that (5.8) becomes, with the above approximations,

$$S_{j1}^{<}(\beta,\theta) = -e^{i\pi/12}\frac{N^{1/4}e_j}{\pi M}\left(\frac{\beta}{2\pi\sin\theta}\right)^{1/4}\exp\left[-2i\beta(M - N\varepsilon)\right] \times \int_0^{t_0} \frac{\exp\left[-2i(\varepsilon/\gamma')t\right]dt}{\mathrm{Ai}^2\left(e^{i\pi/3}t\right)\left[1 - e^{-i\pi/6}\left(Ne_j/M\right)\gamma'\ln'\mathrm{Ai}\left(e^{i\pi/3}t\right)\right]^2} \tag{5.13}$$

where we have set

$$t \equiv M\gamma'\beta\zeta \tag{5.14}$$

and $t_0 \gg 1$ is the boundary of the domain that yields significant contributions.

In order to convert (5.13) into an integral with fast-decreasing integrand, we rotate the path of integration to the straight line $t = e^{i\pi/3}x$. This is allowed, because the path stays away from the Regge-Debye poles[19] [roots of the integrand denominator in (5.13)]. The final result is

$$S_{j1}^{<}(\beta,\theta) = e^{-7i\pi/12}\frac{N^{1/4}e_j}{\pi M}\left(\frac{\beta}{2\pi\sin\theta}\right)^{1/4}\exp\left[-2i\beta(M - N\varepsilon)\right] \times \int_0^{-} \frac{\exp\left[2e^{-i\pi/6}(\varepsilon/\gamma')x\right]}{\mathrm{Ai}^2\left(e^{2i\pi/3}x\right)}dx \tag{5.15}$$

where we have neglected the $O(\gamma')$ correction in the denominator of (5.13) and, in view of the fast decrease of the integrand [dominated by a factor[30] $\exp\left(-\frac{4}{3}x^{3/2}\right)$ for $x \gg 1$], the upper limit has been extended to infinity. Since the result is valid within the domain (5.7), no significant contributions arise from $x \gg 1$, in agreement with the assumptions made in the derivation.

The integral in (5.15) is an incomplete Fock-type function [cf. reference 19, eq. (5.85)]. The integrand decays exponentially with ε in the shadow region PR ($\varepsilon < 0$) and grows exponentially with ε in the illuminated region TR ($\varepsilon > 0$), where the exponent, however, is limited by (5.7) to values of order unity. Thus, (5.15) interpolates smoothly (but not uniformly) between the illuminated and shadow regions associated with the disappearance of the directly transmitted ray, as is typical for Fock-type transitions.[16]

Comparing (5.15) with (4.24), we see that the direct transmission contribution in the near-critical region is $O\left(\beta^{-1/4}\right)$ times smaller than that of direct reflection, which has the typical $O(\beta)$ magnitude associated with geometrical-optic terms. This suppression effect has a simple explanation.The zero-order WKB approximation goes to zero like $(\cos\theta_2)^{1/2}$ as $\theta_2 \to \pi/2$ ($\varepsilon \to 0$). A factor $\cos\theta_2$ arises from $T_{12}^{(j)}$ in the Fresnel (plane interface) approximation, and an additional factor $(\cos\theta_2)^{1/2}$ arises from the beam divergence factor D_1 in (5.3). However, for a curved surface, $T_{12}^{(j)}$ does not vanish as $\theta_2 \to \pi/2$: we see from (5.11) that it becomes $O(\gamma')$, so that the $(\cos\theta_2)^{1/2}$ behavior is changed by the curvature into a behavior like $\gamma'^{1/4} = O\left(\beta^{-1/4}\right)$, exactly the suppression factor found.

5.3. The remainder term

The remainder subcritical term (4.7) differs from (4.6) by the additional integrand factor

$$\Delta_j(\lambda,\beta) \equiv \rho_j(\lambda,\beta)/\left[1-\rho_j(\lambda,\beta)\right] \tag{5.16}$$

where ρ_j is given by (3.6). In the Debye expansion (3.1), within the near-critical domain (5.7), a term of order $p \geq 2$, in the WKB approximation, would have a saddle point $\overline{\lambda}_p$ approaching $\lambda = \alpha$ more and more closely as p increases [cf. (3.20) with $\theta \to -\theta$], so that $\lambda = \alpha$ is an accumulation point of saddle points for the Debye terms. It follows that, within the near-critical region, the dominant contributions to (4.7) should still arise from the neighborhood of $\lambda = \alpha$.

We see from (3.6) that ρ_j contains the internal spherical reflection coefficient $R_{11}^{(j)}$, which decays relatively rapidly as the internal angle of incidence

$$w_2 = \sin^{-1}(\lambda/\alpha)$$

decreases from its limiting value $\pi/2$. Also, within the domain of validity of the Schöbe approximation, along the same path of integration[36] that led to (5.15), we find that (5.16) contributes another fast-decaying factor [cf. (3.6)]

$$H_\lambda^{(1)}(\alpha)/H_\lambda^{(2)}(\alpha) \approx e^{-2i\pi/3}\,\mathrm{Ai}(x)/\mathrm{Ai}\left(e^{2i\pi/3}x\right) \tag{5.17}$$

which decays like $\exp\left(-\frac{4}{3}x^{3/2}\right)$ for $x \gg 1$.

For both of these reasons, we expect that the contribution from the remainder term (4.7) is substantially smaller than that from $S_{j1}^{<}$, given by (5.15). Numerical estimates confirm this expectation. Since the contribution from $S_{j1}^{<}$ is already $O\left(\beta^{-1/2}\right)$ times smaller than that from direct reflection, and as we are retaining only the lowest-order dominant contributions, we shall neglect the remainder term (4.7) within the near-critical region.

6. THE SUPRACRITICAL AMPLITUDE

6.1. The WKB approximation

The supracritical amplitude $S_j^{>}$ is given by (4.3), with $S^{(j)}$ defined by (2.10). Comparing these expressions with (4.5), we see that the only differences with respect to the direct reflection subcritical term are in the limits of integration and in the replacement of $R_{22}^{(j)}$ by

$$R^{(j)}(\lambda,\beta) \equiv -\frac{\{2\beta\}-Ne_j\{\alpha\}}{\{1\beta\}-Ne_j\{\alpha\}} \equiv \exp\left[2i\phi_j(\lambda,\beta)\right] \tag{6.1}$$

which, for real λ, is a pure phase factor. Thus, (4.10) is replaced by

$$S_j^{>}(\beta,\theta) \approx \frac{e^{-i\pi/4}\beta^{1/2}}{(2\pi\sin\theta)^{1/2}}\int_{\theta_c}^{\pi/2} dw_1\,(\sin w_1)^{1/2}\cos w_1$$
$$\times\exp\left\{-2i\beta\left[\cos w_1-\left(\frac{\pi-\theta}{2}-w_1\right)\sin w_1\right]+2i\phi_j\right\} \tag{6.2}$$

If we can treat ϕ_j as a slowly-varying phase, the integrand still has a stationary-phase point (saddle point) at [cf. (4.9), (4.11)]

$$\overline{w}_1 \equiv \theta_1 = (\pi-\theta)/2 = \theta_c + \varepsilon \tag{6.3}$$

However, in contrast with (5.10), this point lies within the domain of integration if θ is in TR, and outside if θ is in PR. The range of the saddle point is still given by

$$|\delta w_1| = O\left\{\left[\beta\sin(\theta/2)\right]^{-1/2}\right\}$$

(cf. Sec. 4.2). In order for it to be included well within the domain of integration in (6.2), we must have

$$\varepsilon \gg (M\beta)^{-1/2} \tag{6.4}$$

With $|\varepsilon| \ll 1$, (6.3) yields

$$\overline{\lambda} - \alpha \approx M\beta\varepsilon$$

so that, when (6.4) holds, one can generally apply the Debye asymptotic approximation (3.12) to evaluate (6.1), with the following results:

$$R^{(j)}(\lambda,\beta) \approx \frac{(\beta^2-\lambda^2)^{1/2} - ie_j(\lambda^2-\alpha^2)^{1/2}}{(\beta^2-\lambda^2)^{1/2} + ie_j(\lambda^2-\alpha^2)^{1/2}} \tag{6.5}$$

$$\phi_j \approx -\tan^{-1}\left(e_j\sqrt{\sin^2 w_1 - N^2}/\cos w_1\right) \tag{6.6}$$

We see that (6.5) is the continuation of (3.13) to $\lambda > \alpha$, with

$$(\alpha^2-\lambda^2)^{1/2} \to i(\lambda^2-\alpha^2)^{1/2}$$

With $\lambda = \beta\sin w_1$, (6.5) is just the Fresnel reflection amplitude at a plane interface in the total reflection domain, and (6.6) is the well-known phase shift associated with total reflection,[31] for an angle of incidence w_1.

Under these conditions, applying the saddle-point method to (6.2) yields the zero-order WKB approximation

$$S_j^>(\beta,\theta) \approx -\frac{i\beta}{2}\exp\left[-i\delta_j(\theta)\right]\exp\left(-2i\beta\sin\frac{\theta}{2}\right) \tag{6.7}$$

where

$$\tan\left[\frac{\delta_j(\theta)}{2}\right] = e_j\frac{\sqrt{\cos^2(\theta/2)-N^2}}{\sin(\theta/2)} \tag{6.8}$$

This result is the continuation of (4.16) to the TR region, and it has the same physical interpretation.

6.2. The Pearcey-Fock integral

In the near-critical domain, the saddle point (6.3) is close to the lower limit of integration of (6.2), and the WKB approximation breaks down for the same two reasons discussed in Sec. 4.3 (but interchanging PR and TR).

We expand the integrand of (6.2) around the saddle point (6.3), just as was done for (4.12), with the same notation (4.13) and the same assumption that (4.14) holds in the relevant portion of the domain of integration. The result is

$$S_j^>(\beta,\theta) \approx \frac{e^{-i\pi/4}}{2\sqrt{\pi}}\beta^{1/2}\left(\sin\frac{\theta}{2}\right)^{1/2}\exp\left(-2i\beta\sin\frac{\theta}{2}\right)$$
$$\int_{-\varepsilon}^{\varepsilon} R^{(j)}(\lambda,\beta)\exp\left(-i\beta\sin\frac{\theta}{2}v^2\right)dv \tag{6.9}$$

where $R^{(j)}$ is given by (6.1).

Employing the Schöbe approximation (4.19) to evaluate $\{\alpha\}$, and retaining the Debye approximation (3.12) for $\{1\beta\}$ and $\{2\beta\}$, we find [cf. (4.20)]

$$R^{(j)}(\lambda,\beta) \approx \frac{1+i\gamma'\Phi_j[N;\gamma'(\lambda-\alpha)]}{1-i\gamma'\Phi_j[N;\gamma'(\lambda-\alpha)]} \tag{6.10}$$

where [cf. (4.22)]

$$\Phi_j[N;X] \equiv \left(Ne_j/M\right)\ln' \mathrm{Ai}(X) \tag{6.11}$$

Again with the change of variable (4.23) and with the same approximations that led to (4.24), we find that (6.9) becomes

$$S_j^>(\beta,\theta) \approx \frac{e^{-i\pi/4}}{2\sqrt{\pi}}\beta\exp\left(-2i\beta\sin\frac{\theta}{2}\right)\int_{X=0}^{\infty}\left(\frac{1+i\gamma'\Phi_j[N;X]}{1-i\gamma'\Phi_j[N;X]}\right)\exp\left(-iu^2\right)du \tag{6.12}$$

where X is still given by (4.25) and the upper limit

$$\left[\beta\sin(\theta/2)\right]^{1/2}\theta \sim \sqrt{M\beta}\theta_t \gg 1$$

has been replaced by ∞. In terms of the phase angle ϕ_j defined in (6.1), this approximation to $R^{(j)}$ corresponds to

$$\phi_j \approx \tan^{-1}\left[\left(Ne_j/M\right)\gamma'\ln' \mathrm{Ai}(X)\right] \tag{6.13}$$

The result (6.12) is the counterpart of (4.24), and its numerical evaluation (Appendix B) follows a procedure entirely similar to that outlined at the end of Sec. 4.3, with the roles of PR and TR interchanged:

(i) In TR, where $u=0$ lies within the domain of integration, we integrate first along the real interval $[w,0]$, where

$$u=w\equiv\left[N-\cos(\theta/2)\right]\left[\beta/\sin(\theta/2)\right]^{1/3}<0$$

is the lower limit of integration in (6.12), and then from $u=0$ to $e^{-i\pi/4}\infty$, an allowed path deformation. This combines a piece of stationary-phase path having few integrand oscillations with a steepest-descent path having Gaussian decay, leading to fast numerical convergence.

(ii) In PR, the path is rotated onto a straight line from w (now >0) to $e^{-i\pi/4}\infty$, parallel to the steepest-descent path, leading to Gaussian decay of the integrand (with a few superposed oscillations) and again fast convergence.

To discuss the physical interpretation of (6.12), it is convenient at first to introduce additional (more restrictive) approximations. Since $\gamma'\ll 1$ and it is assumed in (6.10) that the main contribution comes from $X=O(1)$, we may employ the further approximation

$$\phi_j\approx\left(Ne_j/M\right)\gamma'\ln'\mathrm{Ai}(X)$$

With the new change of variable

$$u+\left[\beta\sin(\theta/2)\right]^{1/3}\varepsilon=\zeta \tag{6.14}$$

and the additional assumption

$$|\varepsilon|\ll\gamma' \tag{6.15}$$

(which allows us to neglect terms of orders $\gamma'\beta\varepsilon^2$ and $\beta\varepsilon^3$), (6.12) becomes

$$S_j^>(\beta,\theta)\approx\frac{e^{-i\pi/4}}{2\sqrt{\pi}}\beta\exp\left[-2i\beta(M-N\varepsilon)\right]$$
$$\times\int_0^\infty\exp\left\{-i\left[\zeta^2-2\varepsilon\sqrt{\beta\sin\frac{\theta}{2}}\zeta-2\frac{Ne_j\gamma'}{M}\ln'\mathrm{Ai}\left(\gamma'\sqrt{\beta\sin\frac{\theta}{2}}\zeta\right)\right]\right\}d\zeta \tag{6.16}$$

In view of (6.15), we can make the additional approximation $\sin(\theta/2)\approx M$ within the square roots, yielding[37]

$$S_j^>(\beta,\theta)\approx\frac{e^{-i\pi/4}}{2\sqrt{\pi}}\beta\exp\left[-2i\beta(M-N\varepsilon)\right]$$
$$\times\int_0^\infty\exp\left\{-i\left[\zeta^2-x\zeta-\frac{y^{1/2}}{2^{1/2}}e_j\ln'\mathrm{Ai}\left(2^{1/2}\frac{\zeta}{y^{1/2}}\right)\right]\right\}d\zeta \tag{6.17}$$

where we have introduced the notations

$$x(\beta,\varepsilon)\equiv 2(M\beta)^{1/2}\varepsilon \tag{6.18}$$

$$y(\beta)\equiv(4/M)^{1/2}N^{1/2}\beta^{-1/2} \tag{6.19}$$

The reasons for these notations will become apparent later.

The integral in (6.12), as well as its simplified version (6.17), is a new type of diffraction integral. We call it a *Pearcey-Fock integral* (the justification for this name is given below). To clarify its physical interpretation, we consider the behavior of (6.17) in a limiting situation, the *planar reflection limit*.

6.3. Planar reflection limit and Goos-Hänchen shift

If β is so large that

$$\beta^{-1/2}\ll 1 \tag{6.20}$$

(6.19) implies that $y\ll 1$, so that, apart from a very small portion of the range of integration, the argument of the Airy function in (6.17) is $\gg 1$. In that case,[30]

$$\ln'\mathrm{Ai}(z)\approx-\sqrt{z}\quad,\qquad\left(|z|\gg 1,\ |\arg z|<\pi\right) \tag{6.21}$$

so that [neglecting the contribution from the domain where (6.21) does not hold] (6.17) becomes

$$S_j^>(\beta,\theta)\approx\frac{e^{-i\pi/4}}{2\sqrt{\pi}}\beta\exp\left[-2i\beta(M-N\varepsilon)\right]$$
$$\times\int_0^\infty\exp\left[-i\left(\zeta^2-x\zeta+e_jy\sqrt{\zeta}\right)\right]d\zeta \tag{6.22}$$

From (6.10), we see that (6.21) amounts to the approximation

$$R^{(j)}(\lambda,\beta) \approx \exp\left[-2ie_j \frac{N}{M}\sqrt{\frac{2}{\alpha}(\lambda-\alpha)}\right] \tag{6.23}$$

and, with $(\lambda-\alpha)/\alpha \ll 1$, this is equivalent to (6.5-6). Thus, (6.22) corresponds to the replacement of the true spherical reflection coefficients by those associated with a plane interface at the corresponding angle of incidence w_t in (6.2). In this "planar reflection limit", the curvature of the spherical surface is taken into account only through the spread in the angles of incidence w_t that contribute to the result.

With the change of variable $\zeta = t^2$, we find[37]

$$S_j^>(\beta,\theta) \approx \frac{e^{-i\pi/4}}{2\sqrt{\pi}}\beta \exp[-2i\beta(M-N\varepsilon)] \times \int_0^\infty \exp\left[-i\left(t^4 - xt^2 + e_j y t\right)\right] t\,dt \tag{6.24}$$

The *Pearcey integral* $P(x,y)$ is defined by[38-40]

$$P(x,y) \equiv \int_{-\infty}^{\infty} \exp\left[i\left(t^4 + xt^2 + yt\right)\right] dt \tag{6.25}$$

which explains the choice of notations in (6.18-19). We may rewrite (6.25) as

$$P(x,y) = \wp(x,y) + \wp(x,-y) \tag{6.26}$$

where we have defined the "half-range Pearcey integral"

$$\wp(x,y) \equiv \int_0^\infty \exp\left[i\left(t^4 + xt^2 + yt\right)\right] dt \tag{6.27}$$

In terms of this function, (6.24) becomes

$$S_j^>(\beta,\theta) \approx \frac{e^{-i\pi/4}}{2\sqrt{\pi}}\beta \exp[-2i\beta(M-N\varepsilon)] \frac{\partial \wp^*}{\partial y}\left(-x, e_j y\right) \tag{6.28}$$

where the star denotes the complex conjugate.

Pearcey's integral (6.25) is the diffraction integral associated with the *cusp catastrophe*,[41] a caustic resulting from confluences of up to three stationary-phase points. In the present situation, only one stationary-phase point is relevant. From (6.24), we find the stationary-phase condition

$$\bar{t}^2 = \frac{x}{2} - \frac{e_j y}{4\bar{t}} \tag{6.29}$$

This can be solved by iteration, if the last term is a small correction. The result is, in terms of the w_t variable [cf. (4.13),(4.23), (6.3)]

$$\overline{w}_t \equiv \theta_t = \theta_c + \frac{\bar{t}^2}{(M\beta)^{1/2}} = \theta_c + \left[1 - \frac{(N/2)^{1/4} e_j}{(M\varepsilon)^{1/4}\beta}\right]\varepsilon \tag{6.30}$$

It follows that, in this approximation, the relationship between the angle of incidence θ_t and the direction of observation θ is

$$\theta = \pi - 2\theta_t - \delta\theta_j^{GH} \tag{6.31}$$

where

$$\delta\theta_j^{GH}(\varepsilon) = -\frac{(2N)^{1/4} e_j}{M^{1/4}\beta\varepsilon^{1/4}} \tag{6.32}$$

represents an additional angular displacement undergone by the reflected ray (stationary-phase path), as compared with the geometrically reflected ray (Fig. 7). This displacement corresponds to the well-known *Goos-Hänchen shift* at total reflection.[26,42] Indeed, one can readily verify that Artmann's expression[43] for the linear shift

$$\delta x_j^{GH} = \frac{2e_j \tan\theta_t}{k\sqrt{\sin^2\theta_t - N^2}} \tag{6.33}$$

reduces to $a\left|\delta\theta_j^{GH}\right|$ when $\theta_t = \theta_c + \varepsilon$, $|\varepsilon| \ll 1$. Physically, this shift arises from the tunneling of light into the optically rarer medium (situation 3 in Sec. 2.3 and Fig. 1), as an evanescent wave. The linear shift is of the same order of magnitude as the penetration depth.

The condition that the last term of (6.29) should represent a small correction, assumed in the derivation of (6.32), amounts to

$$\varepsilon \gg N^{1/2}/\left(M\beta^{1/2}\right) \tag{6.34}$$

which, by (6.32), is equivalent to

$$\left|\delta\theta_j^{GH}\right| \ll \varepsilon$$

i. e., the angular shift must be much smaller than the deviation from the critical scattering angle. This condition is violated as θ approaches the critical angle θ_t .

To check that the displacement of the stationary phase point (6.30) from its geometrical-optic value (6.3) causes an angular displacement of the whole pattern, we computed the stationary-phase approximation to (6.28) in the TR region $\varepsilon > 0$. We indeed found a Fresnel-like pattern, with an angular displacement given by $\frac{5}{4}\delta\theta_j^{GH}(\varepsilon)$ at each ε satisfying (6.34).

It should be stressed that the above discussion is based upon the planar reflection limit, in which the only effect of surface curvature is to spread the range of angles of incidence. The dynamical effect of curvature, which changes the reflection amplitudes from their planar Fresnel values (6.23) to the spherical ones (6.10), is not included. Thus, for a more accurate quantitative expression, one should go back to (6.12).

7. APPROXIMATIONS TO THE NEARSIDE AMPLITUDE

7.1. CAM and WKB approximations

The lowest-order, transitional *CAM approximation* to the nearside amplitude is [cf. (4.1), (4.4)]

$$S_{j,\mathrm{CAM}}^{(-)}(\beta,\theta) \simeq S_{j0}^{<}(\beta,\theta) + S_{j1}^{<}(\beta,\theta) + S_j^{>}(\beta,\theta) \tag{7.1}$$

where $S_{j0}^{<}$ is given by (4.24), $S_{j1}^{<}$ by (5.15), and $S_j^{>}$ by (6.12). What is the expected domain of validity of these approximations?

To begin with, use of the lowest-order asymptotic approximations requires that size parameters be restricted to large values. It has been assumed throughout that $\gamma' \ll 1$; thus, the numerical comparisons in Sec. 8 will be performed for $\beta \geq 10^3$.

For the Fresnel-Fock integral (4.24), according to the discussion given in Sec. 4.4, the angular domain of validity should be

$$|\varepsilon| \leq O\left[(M\beta)^{-\frac{1}{2}}\right]$$

It is convenient to introduce the parameter

$$\eta \equiv \sqrt{\frac{2\pi}{M\beta}} \tag{7.2}$$

as a measure of the *width of the near-critical region*. In terms of η , the expected domain of validity of (4.24) is given by

$$|\varepsilon/\eta| = O(1) \tag{7.3}$$

For the direct transmission contribution (5.15), in the approximations that lead from (5.8) to (5.13), terms of order $|\varepsilon/\gamma'|$ are neglected compared with unity, so that one should have $|\varepsilon| \ll \gamma'$. Within the range of size parameters we treat, this condition is still compatible with (7.3). Actually, the accuracy of (5.15) is somewhat lower than that of the

other two CAM terms in (7.1) [comparable to that of (6.17) as an approximation to (6.12)]; but this need not concern us because, in the near-critical region, direct transmission is suppressed by a factor $O(\beta^{-1/6})$ compared to direct reflection, as we saw in Sec. 5.2.

Finally, for (6.12), the approximations are essentially the same as those employed in (4.24), so that the domain of applicability is again (7.3). Thus, *the CAM approximation may be applied for* $|\varepsilon/\eta| = O(1)$. Within the somewhat more restricted domain $|\varepsilon| \ll \gamma'$, one may replace (6.12) by (6.17), with some loss in accuracy.[44]

The (lowest-order) *WKB approximation* to the total nearside amplitude is given by

$$\begin{aligned} S^{(-)}_{j,\mathrm{WKB}}(\beta,\theta) &\approx S^{>}_{j}(\beta,\theta) + S^{<}_{j1}(\beta,\theta) \ , \qquad \theta \le \theta_t \\ &\approx S^{<}_{j0}(\beta,\theta) \ , \qquad\qquad\quad \theta \ge \theta_t \end{aligned} \tag{7.4}$$

where $S^{<}_{j0}$ is given by (4.16), $S^{<}_{j1}$ by (5.3), and $S^{>}_{j}$ by (6.7). According to (4.15), (6.4) and (5.2) [which, as noted above, is consistent with (6.4)], a necessary condition for the validity of the WKB approximation is

$$|\varepsilon| \gg \eta \tag{7.5}$$

One should remember, however, that the neglect of higher-order internally multireflected nearside terms (Sec. 5.3) is justified only in the near-critical region; if one goes much beyond this region , the WKB contribution from these terms also has to be included.

According to the above discussion, the domains of applicability of the CAM approximation and the WKB approximation are mutually exclusive and roughly complementary. However, we cannot expect a smooth matching between them, because of the *transitional* character of the present (lowest-order) CAM approximation. A smooth match and an extended domain of validity would require a *uniform* CAM approximation (possible improvements are discussed in Sec. 9).

It is useful to extrapolate the WKB approximation (7.4) all the way to $\varepsilon = 0$. As was noted at the end of Sec. 5.1, the direct transmission contribution to (7.4) vanishes at $\theta = \theta_t$, and it is readily seen that (4.16) and (6.7) approach a common limit, so that this extrapolated zero-order WKB approximation is continuous at θ_t . The geometrical-optic cusp (discontinuous derivative) at θ_t , however, is preserved.

7.2. Asymptotic near-critical behavior in the planar reflection limit

The planar reflection limit of the CAM approximation, in which the spherical reflection coefficients are replaced by the Fresnel ones, was employed in Sec. 6.3 to discuss the physical interpretation of the Pearcey-Fock integral. In the present section and in the following one, we apply it both to the supracritical and the subcritical reflection amplitudes. The motivation is twofold: (i) For very large β and very small $|\varepsilon|$, the resulting approximation is simpler than the CAM approximation and reasonably accurate; (ii) For smaller β or larger $|\varepsilon|$, though the errors get large, the qualitative behavior remains similar to that of the CAM approximation and is much simpler to discuss, giving considerable insight into the structure and behavior of the various CAM terms.

The combined reflection amplitude in the CAM approximation, given by the sum of (4.24) and (6.12), can be written as

$$\begin{aligned} S^{<}_{j0} + S^{>}_{j} = {} & \frac{e^{-i\pi/4}}{2\sqrt{\pi}}\beta \exp\left(-2i\beta\sin\frac{\theta}{2}\right) \\ & \times\left[\int_{-\infty}^{0} e^{-i(v+w)^2} R^{(j)}_{22}(v)\,dv + \int_{0}^{\infty} e^{-i(v+w)^2} R^{(j)}(v)\,dv\right] \end{aligned} \tag{7.6}$$

where we have set $u = v + w$, with [see the comments on numerical evaluation following (4.26) and (6.12)]

$$w \equiv \left[N - \cos(\theta/2)\right]\left[\beta/\sin(\theta/2)\right]^{1/4} \tag{7.7}$$

and $R^{(j)}_{22}$ and $R^{(j)}$ are respectively given by (4.20) and (6.10), where

$$X = \gamma'\left[\beta\sin(\theta/2)\right]^{1/4} v \tag{7.8}$$

Note that $v = -w$ is the position of the WKB stationary-phase point, and that

$$w = -\sqrt{M\beta\varepsilon}$$

for small enough $|s|$ [see (7.25)].

We now assume that β is very large [condition (6.20) is satisfied], so that we may employ (6.21) over essentially the whole relevant range of integration in (7.6). This amounts to taking the planar limit of the spherical reflection coefficients, yielding

$$S_{j0}^{<}+S_j^{>}\approx\frac{e^{-i\pi/4}}{2\sqrt{\pi}}\beta\exp\left(-2i\beta\sin\frac{\theta}{2}\right)\times\left[\int_{e^{3\pi i/4}\infty}^{0}e^{-i(v+w)^2}\left(\frac{1-|\sigma_j|}{1+|\sigma_j|}\right)dv+\int_{0}^{e^{-i\pi/4}\infty}e^{-i(v+w)^2}\left(\frac{1-i\sigma_j}{1+i\sigma_j}\right)dv\right] \tag{7.9}$$

where

$$\sigma_j(v)\equiv e_j\frac{\sqrt{2N}}{M}\left[\frac{\sin(\theta/2)}{\beta}\right]^{1/4}\sqrt{v} \tag{7.10}$$

and where we have rotated the paths of integration so that they are parallel to the steepest-descent paths, leading to a Gaussian-like decay of the integrands for large $|v|$.

The expressions within the parentheses in the integrands of (7.9) are approximations to the Fresnel reflection amplitudes near critical incidence [somewhat more accurate than (6.23)]. Note that the below-critical amplitude is obtained from the above-critical one by the replacement

$$\sqrt{v}\to-i\sqrt{|v|}\qquad(v<0) \tag{7.11}$$

In a small neighborhood of the critical scattering angle, the results are only affected by the behavior of these Fresnel amplitudes close to critical incidence, where the reflectivities are close to unity, so that

$$\frac{1-i\sigma_j}{1+i\sigma_j}=1-2i\sigma_j-2\sigma_j^2+O\left(|\sigma_j|^3\right),\qquad(|\sigma_j|\ll 1) \tag{7.12}$$

with a corresponding expansion for the other integrand in (7.9). Note that (7.12) preserves unitarity to second order in $|\sigma_j|$. Since the dominant contributions to the integrals in (7.9) arise from a neighborhood of the saddle point $v=-w$, the condition for applying (7.12) is

$$|\sigma_j(-w)|=e_j(2N|\epsilon|/M)^{1/4}\ll 1 \tag{7.13}$$

which restricts its validity to a few degrees from the critical scattering angle for polarization 1 and an even narrower domain for polarization 2. But we do obtain the planar-limit asymptotic behavior within the domain previously excluded by condition (6.34).

Substituting into (7.9) the expansion (7.12) and its analogue for the other integrand, the first and third terms of the expansion give rise to readily evaluated Gaussian integrals, and we find

$$S_{j0}^{<}+S_j^{>}\approx-\frac{i\beta}{2}\exp\left(-2i\beta\sin\frac{\theta}{2}\right)\times\left\{1-2^{1/4}\frac{\sqrt{N}}{M}e_jP(w)\left[\frac{\sin(\theta/2)}{\beta}\right]^{1/4}+\frac{4N}{M^2}e_j^2w(\theta)\left[\frac{\sin(\theta/2)}{\beta}\right]^{1/2}\right\} \tag{7.14}$$

where

$$P(w)\equiv\frac{e^{i\pi/4}}{\sqrt{\pi}}\left[\int_{-\infty}^{0}e^{-i(v+w)^2}\sqrt{|v|}\,dv+i\int_{0}^{\infty}e^{-i(v+w)^2}\sqrt{v}\,dv\right] \tag{7.15}$$

in which the paths of integration have again been shifted back to the real axis.

It will be useful to evaluate separately the contributions from subcritical and supracritical reflection. To order $\beta^{-1/4}$, they are, respectively:

$$S_{j0}^{<}(\beta,\theta)\approx-\frac{i\beta}{2}\exp\left(-2i\beta\sin\frac{\theta}{2}\right)\frac{e^{i\pi/4}}{\sqrt{\pi}}\times\left\{\int_{-\infty}^{0}e^{-i(v+w)^2}dv-2^{1/2}\frac{\sqrt{N}}{M}e_j\left[\frac{\sin(\theta/2)}{\beta}\right]^{1/4}\int_{-\infty}^{0}e^{-i(v+w)^2}\sqrt{|v|}dv+\cdots\right\} \tag{7.16}$$

and

$$S_j^{>}(\beta,\theta)\approx-\frac{i\beta}{2}\exp\left(-2i\beta\sin\frac{\theta}{2}\right)\frac{e^{i\pi/4}}{\sqrt{\pi}}\times\left\{\int_{0}^{\infty}e^{-i(v+w)^2}dv-2^{1/4}i\frac{\sqrt{N}}{M}e_j\left[\frac{\sin(\theta/2)}{\beta}\right]^{1/4}\int_{0}^{\infty}e^{-i(v+w)^2}\sqrt{v}dv+\cdots\right\} \tag{7.17}$$

The first terms within curly brackets are Fresnel integrals. The second ones can be evaluated in terms of the Weber parabolic cylinder function $D_\nu(z)$ (see Appendix A).

According to Eq.(A1), the results are

$$S_{j0}^{<}(\beta,\theta)\approx-\frac{i\beta}{2}\exp\left(-2i\beta\sin\frac{\theta}{2}\right)\left\{\frac{e^{i\pi/4}}{\sqrt{2}}\left[F*\left(\sqrt{\tfrac{2}{\pi}}w\right)-F*(-\infty)\right]\right.$$
$$\left.-e^{-i\pi/8}e_j\frac{\sqrt{N}}{M}\left[\frac{\sin(\theta/2)}{2\beta}\right]^{1/4}e^{-iw^2/2}D_{-1/2}\left(-\sqrt{2}\,e^{i\pi/4}w\right)+\cdots\right\} \qquad (7.18)$$

and

$$S_j^{>}(\beta,\theta)\approx-\frac{i\beta}{2}\exp\left(-2i\beta\sin\frac{\theta}{2}\right)\left\{\frac{e^{i\pi/4}}{\sqrt{2}}\left[F*(\infty)-F*\left(\sqrt{\tfrac{2}{\pi}}w\right)\right]\right.$$
$$\left.-e^{-i\pi/8}e_j\frac{\sqrt{N}}{M}\left[\frac{\sin(\theta/2)}{2\beta}\right]^{1/4}ie^{-iw^2/2}D_{-1/2}\left(\sqrt{2}\,e^{i\pi/4}w\right)+\cdots\right\} \qquad (7.19)$$

where $F(z)$ denotes the Fresnel integral.[3]

Adding up these results and using Eq.(A2), we recover the first term within curly brackets in (7.14) and we get, for the second one,

$$P(w)=2^{-1/4}e^{i\pi/8}\exp\left(-iw^2/2\right)D_{1/2}\left(\sqrt{2}\,e^{-i\pi/4}w\right) \qquad (7.20)$$

The cancellation between the w-dependent Fresnel integrals in the first terms of (7.18) and (7.19) should be noted.

The corresponding expansion for the direct transmission subcritical contribution (5.15) is obtained by expanding the exponential in the integrand into powers of ε/γ' and integrating term by term, with the help of the integrals

$$\int_0^\infty\frac{dx}{\mathrm{Ai}^2\left(e^{2i\pi/3}x\right)}=2\pi e^{i\pi/6} \qquad (7.21)$$

and (evaluated numerically)

$$m_0\equiv\frac{e^{-i\pi/3}}{\pi}\int_0^\infty\frac{x\,dx}{\mathrm{Ai}^2\left(e^{2i\pi/3}x\right)}\approx1.23599-0.369444i \qquad (7.22)$$

The result is

$$S_{j1}^{<}(\beta,\theta)\approx e^{-5i\pi/12}\frac{Ne_j}{M^{1/2}\sqrt{\pi\beta}}\exp\left(-2i\beta\sin\frac{\theta}{2}\right)e^{-iw^2}\left[1+m_0\frac{\varepsilon}{\gamma'}+O\left(\frac{\varepsilon^2}{\gamma'^2}\right)\right] \qquad (7.23)$$

Substituting (7.14) and (7.23) into (7.1), we finally get the *planar limit approximation* to $S_j^{(-)}$ in the immediate vicinity of the critical angle

$$S_{j,\mathrm{PL}}^{(-)}(\beta,\theta)\approx-\frac{i\beta}{2}\exp\left(-2i\beta\sin\frac{\theta}{2}\right)\left\{1-2^{1/4}\frac{\sqrt{N}}{M}e_jP(w)\left[\frac{\sin(\theta/2)}{\beta}\right]^{1/4}\right.$$
$$\left.+\frac{4N}{M^2}e_j^2w\left[\frac{\sin(\theta/2)}{\beta}\right]^{1/4}+\frac{2}{\sqrt{\pi}}e^{i\pi/12}\frac{Ne_j}{M^{1/2}}\frac{e^{-iw^2}}{\beta^{1/2}}\left(1+m_0\frac{\varepsilon}{\gamma'}\right)\right\} \qquad (7.24)$$

According to (7.7) and (4.9),

$$w=-\sqrt{M\beta}\varepsilon\left[1+O\left(\varepsilon^2\right)\right]\approx-\sqrt{2\pi}\,\varepsilon/\eta \qquad (7.25)$$

which should be at most of order unity within the domain of applicability of (7.24).

For $|w|\ll1$, we can apply the power series expansion[30] of $D_{1/2}$ to obtain

$$e^{-i\pi/8}P(w)=\frac{\sqrt{\pi}}{\Gamma\left(\frac{1}{4}\right)}\left[1+\frac{i}{2}w^2+O\left(w^4\right)\right]+\frac{\Gamma\left(\frac{1}{4}\right)}{2\sqrt{\pi}}e^{-i\pi/4}\left[w-\frac{i}{6}w^3+O\left(w^5\right)\right] \qquad (7.26)$$

In particular, at the critical scattering angle ($w=0$), (7.24) yields

$$S_{j,\mathrm{PL}}^{(-)}(\beta,\theta_t)\approx-\frac{i\beta}{2}e^{-2iM\beta}\left[1-\frac{2^{1/4}\sqrt{\pi}}{\Gamma\left(\frac{1}{4}\right)}e^{i\pi/8}\frac{\sqrt{N}}{M}e_j\left(\frac{M}{\beta}\right)^{1/4}+\frac{2}{\sqrt{\pi}}e^{i\pi/12}\frac{Ne_j}{M^{1/2}\beta^{1/2}}\right] \qquad (7.27)$$

which differs from previous results[23-25] in the coefficient of $\beta^{-1/2}$. For $N=0.75$, this expression leads to values for G_1 and G_2 that agree with those obtained from the CAM approximation (7.1), for $1{,}000\le\beta\le10{,}000$, within better than 1.5% and 0.5%, respectively.

7.3. Discussion of planar limit approximation

Although the planar limit approximation (7.24) is reasonably accurate only for very large β and for small deviations from the critical angle [cf. (7.13)] such that $|w|$ remains

of order unity, it is nevertheless instructive to employ it to show the qualitative behavior of the solution[45] even though extrapolating it to $|w| \gg 1$.

The asymptotic behavior of $P(w)$ for $|w| \gg 1$ follows from Eqs.(A3)-(A5):

$$P(w) \approx \sqrt{w}\left[1+\frac{i}{16w^2}+O\left(w^{-4}\right)\right] \quad , \qquad w \gg 1 \tag{7.28}$$

$$P(w) \approx i\sqrt{|w|}\left[1-\frac{e^{-iw^2}}{2^{1/2}w^2}+\frac{i}{16w^2}+O\left(w^{-4}\right)\right] \quad , \qquad w \ll -1 \tag{7.29}$$

The dominant term in each of these expressions agrees with the result of applying the stationary phase method to (7.15). The continuation of the $w>0$ expression through the branch cut corresponds to the choice

$$\sqrt{w} \to i\sqrt{|w|} \qquad (w<0) \tag{7.30}$$

The function $|P(w)|$ is plotted in Fig. 8, together with $\sqrt{|w|}$, its asymptotic limit for $|w| \gg 1$. This limit is approached monotonically and quite rapidly for $w>0$, whereas the approach is oscillatory and slower for $w<0$, in agreement with (7.28-29). Also plotted is the magnitude of the first term within curly brackets in (7.19). This well-known Fresnel pattern may be thought of as the "Fresnel transform" of the Heaviside step function, whereas, according to (7.15), the function $P(w)$ is the "Fresnel transform" of the square root function, with its branches defined by (7.30).

Substituting the asymptotic expansions (7.28-29), as well as (7.25), into (7.24), we find, in the partial reflection domain,

$$S_{j,\mathrm{PL}}^{(-)}(\beta,\theta) \approx -\frac{i\beta}{2}\exp\left(-2i\beta\sin\frac{\theta}{2}\right)\left\{1-2^{1/2}e_j\sqrt{\frac{N}{M}|\varepsilon|}+4\frac{N}{M}e_j^2|\varepsilon| \right.$$
$$\left. +\frac{2}{\sqrt{\pi}}e^{i\pi/12}\frac{Ne_j}{M^{1/2}\beta^{1/2}}\left(1-m_0\frac{|\varepsilon|}{\gamma'}\right)e^{-iM\beta\varepsilon^2}+\cdots\right\} \quad , \ \varepsilon<0 \ \ (\mathrm{PR}) \tag{7.31}$$

The first three terms within curly brackets in (7.31) represent the expansion of the Fresnel external reflection amplitude at the geometrical-optic angle of incidence, up to second order in the small parameter σ_j [cf. (7.12)]. Thus, they are equivalent, to this order, to the WKB approximation (7.4); the fourth term (Fock direct transmission penumbra contribution) adds a small $O\left(\beta^{-1/2}\right)$ oscillatory correction.

Similarly, in the total reflection domain, we find

$$S_{j,\mathrm{PL}}^{(-)}(\beta,\theta) \approx -\frac{i\beta}{2}\exp\left(-2i\beta\sin\frac{\theta}{2}\right)\left\{1-2^{1/2}ie_j\sqrt{\frac{N}{M}\varepsilon}-4\frac{N}{M}e_j^2\varepsilon+ie_j\sqrt{N}\frac{e^{-iM\beta\varepsilon^2}}{\beta(M\varepsilon)^{1/2}} \right.$$
$$\left. +\frac{2}{\sqrt{\pi}}e^{i\pi/12}\frac{Ne_j}{M^{1/2}\beta^{1/2}}\left(1+m_0\frac{\varepsilon}{\gamma'}\right)e^{-iM\beta\varepsilon^2}+\cdots\right\} \qquad \varepsilon>0 \quad (\mathrm{TR}) \tag{7.32}$$

The first three terms within curly brackets again represent the Fresnel total reflection amplitude (unimodular to second order in the expansion parameter) at the geometrical-optic angle of incidence, expanded as in (7.12); those terms are equivalent to the WKB approximation (6.7). The fourth term, arising from the oscillatory term in (7.29), gives oscillations (diffraction fringes) around the WKB pattern. For the polarized intensities or gain functions, the oscillations have phase $M\beta\varepsilon^2$ (up to an additive constant) and amplitude envelope

$$A_{j,\mathrm{PL}} \approx \pm\frac{2e_j\sqrt{N}}{M^{1/2}\beta^{1/2}|w|^{1/2}} \tag{7.33}$$

where $|w|$ is of order unity in the domain under consideration [see (7.25)].The direct transmission contribution (last term within curly brackets) is also oscillatory, with similar phase but much smaller amplitude. Because of its scaling factor $\beta^{-1/2}$, the diffraction oscillation remains sizable up to very large values of β .

The qualitative conclusions from (7.31-32) are that, *in PR, the nearside amplitude should rapidly tend towards the WKB approximation. In TR, the nearside amplitude should exhibit diffraction oscillations around the WKB value, approaching it much more slowly than in PR. The phase of the oscillations should be governed by the Fresnel parameter* $M\beta\varepsilon^2$ *, and their envelope should be approximately given by* (7.33)*, scaling like* $\beta^{-1/2}$ *, and with* $\approx N^{-2}$ *times larger magnitude for polarization 2.*

These conclusions are already in qualitative agreement with the patterns illustrated in Fig. 6 (for detailed comparisons, see Sec.8). In view of the asymptotic extrapolation, (7.31-32) cannot be expected to be quantitatively accurate.

Now consider the contributions from direct (partial) and total reflection (7.18-19) to the total nearside amplitude. Beginning with the TR angular domain, and applying the asymptotic expansions of the Fresnel integral[30] and of the parabolic cylinder function $D_{-\frac{1}{2}}$ [Eqs.(A3-5)], we find

$$S_j^>(\beta,\theta)\approx -\frac{i\beta}{2}\exp\left(-2i\beta\sin\frac{\theta}{2}\right)\left\{1-2^{\frac{1}{2}}ie_j\sqrt{\frac{N}{m}}\varepsilon+ie_j\frac{\sqrt{N}}{2}\frac{e^{-iM\beta\varepsilon^2}}{\beta(M\varepsilon)^{\frac{1}{2}}}+\frac{e^{-i\pi/4}}{2\sqrt{\pi}}\frac{e^{-iM\beta\varepsilon^2}}{\sqrt{M\beta\varepsilon}}+O(\varepsilon)\right\} \qquad \text{(in TR)} \qquad (7.34)$$

$$S_{j0}^<(\beta,\theta)\approx -\frac{i\beta}{2}\exp\left(-2i\beta\sin\frac{\theta}{2}\right)\left\{ie_j\frac{\sqrt{N}}{2}\frac{e^{-iM\beta\varepsilon^2}}{\beta(M\varepsilon)^{\frac{1}{2}}}-\frac{e^{-i\pi/4}}{2\sqrt{\pi}}\frac{e^{-iM\beta\varepsilon^2}}{\sqrt{M\beta\varepsilon}}+O(\varepsilon)\right\} \qquad \text{(in TR)} \qquad (7.35)$$

These show that the dominant oscillatory term in (7.32) arises in equal measure from direct (partial) and total reflection contributions. However, the last terms of (7.34-35) contain a much larger oscillation, arising from the Fresnel integrals in (7.18-19), with a size-independent amplitude that scales like $1/w$, in contrast with (7.33). These terms, which originate from the cutoff that separates subcritical and supracritical contributions, cancel each other exactly when (7.34) and (7.35) are added, to give (7.32).

Similarly, in the PR angular domain, we find

$$S_{j0}^<(\beta,\theta)\approx -\frac{i\beta}{2}\exp\left(-2i\beta\sin\frac{\theta}{2}\right)\left\{1-2^{\frac{1}{2}}e_j\sqrt{\frac{N}{m}|\varepsilon|}+e_j\frac{\sqrt{N}}{2}\frac{e^{-iM\beta\varepsilon^2}}{\beta(M|\varepsilon|)^{\frac{1}{2}}}-\frac{e^{-i\pi/4}}{2\sqrt{\pi}}\frac{e^{-iM\beta\varepsilon^2}}{\sqrt{M\beta|\varepsilon|}}+O(|\varepsilon|)\right\} \qquad \text{(in PR)} \qquad (7.36)$$

$$S_j^>(\beta,\theta)\approx -\frac{i\beta}{2}\exp\left(-2i\beta\sin\frac{\theta}{2}\right)\left\{-e_j\frac{\sqrt{N}}{2}\frac{e^{-iM\beta\varepsilon^2}}{\beta(M|\varepsilon|)^{\frac{1}{2}}}+\frac{e^{-i\pi/4}}{2\sqrt{\pi}}\frac{e^{-iM\beta\varepsilon^2}}{\sqrt{M\beta|\varepsilon|}}+O(|\varepsilon|)\right\} \qquad \text{(in PR)} \qquad (7.37)$$

When these two contributions are added, *both* types of oscillatory terms, that found in (7.32) as well as the much larger Fresnel oscillations, cancel out, leaving only the WKB terms in (7.31) [the small oscillatory correction in (7.31) arises entirely from direct transmission].

As will be seen in Sec. 8, these qualitative features of the reflection amplitudes in the planar limit approximation remain valid for the corresponding terms in the CAM approximation.

7.4. Physical optics approximations

A Physical Optics Approximation (POA) to near-critical scattering was derived by Marston and Kingsbury[13,14] by a procedure reminiscent of Airy's theory of the rainbow.[12] The contribution from reflection, in the TR region, is found to be

$$S_{j,\mathrm{POA}}^{(-),\mathrm{R}}(\beta,\theta)=\frac{\beta}{2}\frac{\exp(i\gamma_{0j})}{\sqrt{2}}\left[F\left(\sqrt{\frac{M\beta}{2\pi}}\sin 2\varepsilon\right)-F(-\infty)\right] \qquad \text{(in TR)} \qquad (7.38)$$

where the superscript R denotes reflection, γ_{0j} is a phase[14] and F is the Fresnel integral function. The only other contribution included is that from direct transmission:

$$S_{j,\mathrm{POA}}^{(-),\mathrm{T}}(\beta,\theta)=\beta\sqrt{D_1}\left(1-r_j^2\right)\exp\left[i\left(\frac{\pi}{4}+\gamma_{1j}\right)\right]H(\varepsilon) \qquad (7.39)$$

where the superscript T denotes transmission, r_j and D_1 are the expressions in (5.6), and γ_{1j} is another phase.[14] The Heaviside step function $H(\varepsilon)$ restricts the contribution to the TR region, in agreement with geometrical optics.

Although well-defined expressions are obtained for the phases γ_{0j} and γ_{1j}, Marston and Kingsbury found[14] that the agreement with Mie theory is significantly improved by replacing $(\gamma_{0j}-\gamma_{1j})$, in the TR region, by the *WKB phase difference* between the total reflection and transmission contributions

$$\gamma_{0j}-\gamma_{1j}\to\left[-\delta_j(\theta)-2\beta\sin(\theta/2)\right]-\left[-2\beta(c_1-Nc_2)\right] \tag{7.40}$$

where the first square bracket contains the phase arising from the last two phase factors in (6.7) and the second one is the phase of the last phase factor in (5.3). This still leaves an overall phase factor undetermined, as well as the question of how to extend the reflection contribution to the PR region.

Langley and Marston[5] choose an overall phase factor such that the transmission contribution (7.39) is just the WKB approximation (5.3). They extend the reflection contribution (7.38) to the PR region by just omitting the total reflection phase shift $-\delta_j$ from (7.40) (which is equivalent to taking the Fresnel reflectivities at the critical angle). With these adjustments, the POA becomes[5]

$$S_{j,\mathrm{POA}}^{(-)}(\beta,\theta)=S_{j,\mathrm{POA}}^{(-),\mathrm{R}}(\beta,\theta)+S_{j,\mathrm{POA}}^{(-),\mathrm{T}}(\beta,\theta) \tag{7.41}$$

where

$$S_{j,\mathrm{POA}}^{(-),\mathrm{R}}(\beta,\theta)=-\frac{i\beta}{2}\exp\left(-2i\beta\sin\frac{\theta}{2}\right)\exp\left[-iH(\varepsilon)\delta_j(\theta)\right]\times\frac{e^{-i\pi/4}}{\sqrt{2}}\left[F\left(\sqrt{\frac{M\beta}{2\pi}}\sin 2\varepsilon\right)-F(-\infty)\right] \tag{7.42}$$

$$S_{j,\mathrm{POA}}^{(-),\mathrm{T}}(\beta,\theta)=-i\beta\sqrt{D_1}\left(1-r_j^{\,2}\right)\exp\left[-2i\beta(c_1-Nc_2)\right]H(\varepsilon) \tag{7.43}$$

To establish a connection between the contribution from total reflection in POA and CAM, let us apply the planar reflection approximation (6.21) to (6.16):

$$S_j^{>}(\beta,\theta)=\frac{e^{-i\pi/4}}{2\sqrt{\pi}}\beta\exp\left[-2i\beta(M-N\varepsilon)\right]\times\int_0^{\infty}\exp\left\{-i\left[\zeta^2-2\varepsilon\sqrt{\beta\sin\frac{\theta}{2}}\zeta+\frac{2^{1/4}\sqrt{N}e_j}{M^{1/4}\beta^{1/4}}\sqrt{\zeta}\right]\right\}d\zeta \tag{7.44}$$

where $O(\varepsilon^2)$ corrections to the last term in the integrand phase have been neglected.

In the TR region, we now apply Marston and Kingsbury's assumption that the square root term in the integrand phase can be treated as slowly-varying and taken at the stationary-phase point of the remainder of the phase,

$$\bar{\zeta}=\left[\beta\sin(\theta/2)\right]^{1/4}\varepsilon$$

By (6.14), (4.23) and (4.13), $\bar{\zeta}$ is just the geometrical-optic stationary phase point. In the PR region, the stationary phase point falls outside of the range of integration; thus, the dominant contribution to the integral[46] arises from the endpoint $\zeta=0$ in (7.42), so that the square root term is taken at this point. The result is

$$S_{j,\mathrm{MPOA}}^{>}(\beta,\theta)\approx-\frac{i\beta}{2}\exp\left(-2i\beta\sin\frac{\theta}{2}\right)\exp\left[-iH(\varepsilon)\delta_j(\theta)\right]\times\frac{e^{i\pi/4}}{\sqrt{2}}\left[F*\left(\sqrt{\frac{2}{\pi}}\beta\sin\frac{\theta}{2}\,\varepsilon\right)-F*(-\infty)\right] \tag{7.45}$$

where MPOA stands for "modified physical optics approximation"; δ_j is the total reflection Fresnel phase shift (6.8); and $O(\beta\varepsilon^3)$ terms in the phase have been neglected, consistent with the approximations made in (6.16).

Comparing (7.45) with the POA result (7.42), we find only two significant differences: the contribution from the Fresnel integral terms is complex conjugated and, in their argument, there is the substitution

$$\sqrt{M\beta}\sin(2\varepsilon)\to\sqrt{\beta\sin(\theta/2)}(2\varepsilon) \tag{7.46}$$

While the arguments (7.46) agree for small $|\varepsilon/\eta|$, they differ greatly for larger values of $|\varepsilon/\eta|$: the MPOA result (7.45) approaches the WKB result (6.7), while the POA result (7.42) does not.[47]

We will try to improve the POA by treating in a symmetric way the contribution from the direct reflection subcritical term, which is neglected in the POA. Starting from (4.12), and employing the Fresnel approximation (3.13) to $R_{22}^{(j)}$, we again treat this expression as slowly-varying (neglecting its rapid variation near the critical angle). Thus,

we evaluate it at the geometrical-optic stationary phase point (4.11) in the PR region, and at the endpoint (critical incidence, where $R_{22}^{(j)} = 1$) in the TR region. The result is

$$S_{j0,\mathrm{MPOA}}^{<}(\beta,\theta) = -\frac{i\beta}{2}\exp\left(-2i\beta\sin\frac{\theta}{2}\right) \times\left\{H(\varepsilon)+\left[\frac{\sin(\theta/2)-e_j\sqrt{N^2-\cos^2(\theta/2)}}{\sin(\theta/2)+e_j\sqrt{N^2-\cos^2(\theta/2)}}\right]H(-\varepsilon)\right\} \times\frac{e^{i\pi/4}}{\sqrt{2}}\left[F*\left(-\sqrt{\frac{2}{\pi}}\beta\sin\frac{\theta}{2}\,\varepsilon\right)-F*(-\infty)\right] \qquad (7.47)$$

In (7.47) we define $H(0)\equiv 1/2$ so that the expression within curly brackets becomes 1 at the critical angle. Again, this result approaches the WKB approximation (4.16) for $\varepsilon<0$, $|\varepsilon/\eta|\gg 1$.

Taking the WKB approximation to the direct transmission contribution, as in the POA, the MPOA is defined by

$$S_{j,\mathrm{MPOA}}^{(-)}(\beta,\theta) = S_{j,\mathrm{MPOA}}^{>}(\beta,\theta)+S_{j0,\mathrm{MPOA}}^{<}(\beta,\theta)+S_{j,\mathrm{POA}}^{(-),\mathrm{T}}(\beta,\theta) \qquad (7.48)$$

where the first two terms are respectively given by (7.45) and (7.47), and the third one by (7.43).

A qualitative discussion of the physical optics approximations in the near-critical region, along lines similar to Sec. 7.3, can readily be given. At the critical angle θ_t , it follows from (7.41) that

$$S_{j,\mathrm{POA}}^{(-)}(\beta,\theta_t) = -\frac{i\beta}{4}e^{-2iM\beta} \qquad (7.49)$$

which differs by a factor of 1/2 from the dominant term in (7.27). The reason is the omission of subcritical reflection (which contributes an equal amount at θ_t). Taking into account the correction terms in (7.27), we find that the POA gain functions should be well below the corresponding CAM ones at (and near) the critical angle, the difference increasing with β and being smaller for polarization 2.

For larger deviations from the critical angle, there is a close similarity between (7.42) and the Fresnel-integral terms in (7.18), apart from complex conjugation [note that $F(-w) = -F(w)$ and that the arguments of the Fresnel functions are approximately the same for $|\varepsilon| \ll 1$]. Thus, the departure of (7.42) from the WKB approximation in the TR region has the same large-amplitude Fresnel oscillatory character as the last term in (7.34). In (7.32), this term was cancelled by the subcritical reflection contribution, but the POA misses this important cancellation.

The POA intensity oscillations in the TR region have an envelope with amplitude

$$A_{\mathrm{POA}} \approx \pm 1/\left(\sqrt{\pi}|w|\right)$$

A_{POA} is not only larger than (7.33), but also size-and-polarization independent, and it decreases more slowly with the distance from the critical angle. Since the stationary phase point in the POA is the geometrical-optic one, the POA pattern should also be displaced from the true one by the Goos-Hänchen shift. The differences should be smaller for polarization 2, and should get worse as β increases. The POA (=WKB) contribution from direct transmission (7.43) grows like $\varepsilon^{\frac{1}{2}}$ and has the same Fresnel oscillatory character, so that it eventually becomes dominant at larger deviations from the critical angle.

In the PR region, only (7.42) contributes to the POA, and the contribution is again similar to the Fresnel (last) term in (7.37), giving rise to a polarization-independent term that decays like w^{-2} . Unlike (7.31),this does not approach the WKB result, so the POA fails completely in the PR region; this is not surprising in view of its omission of subcritical reflection.

For the MPOA, (7.45)-(7.48) yield, at the critical angle,

$$S_{j,\mathrm{MPOA}}^{(-)}(\beta,\theta_t) = -\frac{i\beta}{2}e^{-2iM\beta} = S_{j,\mathrm{WKB}}^{(-)}(\beta,\theta_t) \qquad (7.50)$$

where the last equality follows from (7.4), and the contributions are evenly split between subcritical and supracritical reflection. Since the correction terms in (7.27) are not included, the MPOA gain functions will have values above the corresponding CAM ones; thus CAM

is bracketed between the POA and the MPOA. Since the WKB approximation is expected to fail near the critical angle, so also should the MPOA.

For larger deviations from the critical angle, the Fresnel terms in (7.45) and (7.47) are almost identical to those in (7.19) and (7.18), respectively. However, while one of the contributions is multiplied by a Fresnel reflection amplitude, the other one has a coefficient unity, so that there is no cancellation of Fresnel-like oscillatory terms. In the TR region, the behavior of the MPOA resembles that of the POA, but, unlike the POA, it does approach the WKB result at large values of ε.

The main advantage of the MPOA over the POA is that it also approaches the WKB result for large $|\varepsilon|$ in the PR region, because it includes the subcritical contribution (7.47). However, the approach is oscillatory rather than monotonic, because of the non-cancellation between the asymptotic Fresnel "tails" arising from (7.45) and (7.47).

8. NUMERICAL COMPARISONS

In the present Section, we compare numerically summed Mie results (see Appendix B for computational procedures) with the various approximations defined in Sec. 7. We always take $N = 0.75$ and subtract farside contributions out to order $P = 100$.

8.1. The WKB approximation

Comparisons with the WKB approximation (7.4) are useful because it contains the interference effects among all contributing terms, evaluated at the level of geometrical optics. The main omitted physical effect is diffraction, so that this comparison helps define the angular domains where significant diffraction effects (deviations from WKB results) occur. Small deviations, of course, may be attributed to omitted higher-order WKB corrections. Furthermore, far enough from the critical scattering angle, neglected higher-order Debye contributions (beyond direct transmission) must be taken into account.

Although the domain of validity of the WKB approximation was estimated to be given by (7.5), we shall extrapolate it all the way to the critical angle ($\varepsilon = 0$); as was mentioned following (7.4), it will then exhibit a cusp at $\varepsilon = 0$, inherited from geometrical optics.

In Fig. 9, the nearside Mie results for $\beta = 5{,}000$ are compared with the corresponding WKB results. The cusp in the WKB data at $\theta = \theta_r$ is quite apparent. Note that $G_{1,\mathrm{WKB}}(\beta, \theta_r) = G_{2,\mathrm{WKB}}(\beta, \theta_r) = 1$, in agreement with (7.50), and that $\theta = \theta_r - \eta$ is approximately the position of the first peak in the gain functions, which gives another interpretation of the parameter η.

We see that our estimate $|\theta-\theta_t| \gg 2\eta$ for the domain of validity of the WKB approximation [(4.9), (7.5)] appears to be well verified. Indeed, as anticipated in the qualitative discussion in Sec. 7.3, the WKB approximation very rapidly approaches the Mie solution on the PR side, within a distance η of the critical angle; while the approach is considerably slower and oscillatory on the TR side, where one needs to go to an angular distance at least 4-5 times η for a reasonable merge.

The growth in the amplitude of oscillation as one goes further away from θ_t arises from interference between reflection and transmission, as was first pointed out by Marston and Kingsbury.[14] This requires, at large enough distances from θ_t on the TR side, the inclusion of higher-order near-side transmitted Debye components, which we have not taken into account. Thus, we restrict the comparisons to the first few oscillations, where most of the diffraction contributions are concentrated.

In conclusion, we see that the diffraction effects that need to be explained in the near-critical region occur within a distance of order η from θ_t on the PR side, and within a distance of a few times η, covering the first few oscillations, on the TR side.

8.2. The physical optics approximations

We now compare the subtracted Mie results with the POA [eq. (7.41)] and the MPOA [eq. (7.48)]. Figure 10 shows this comparison for $\beta = 5{,}000$.

The geometrical-optic cusp at θ_t persists in the MPOA. It is not present in the POA for G_1 and G_2, but it is present in the POA for $\cos\delta$. These breaks in slope all arise from the Heaviside step functions in (7.41) and (7.48), where one must remember that (7.43) is $O(\varepsilon^{1/2})$ as $\varepsilon \downarrow 0$.

As expected (Sec. 7.4), the POA, because of its neglect of subcritical reflection, fails completely in the PR region; it has much larger errors than the WKB result, which it

does not approach at large angles, except for $\cos\delta$, which is = 1 both for (7.42) and (4.16). In the TR region, again, the POA phase difference is chosen to be identical with the WKB one, so that they lead to the same results for $\cos\delta$ [Figs. 9(c) and 10(c)]. For both G_1 and G_2, the POA is better than the WKB approximation for the first and second peaks of oscillation, but gets worse for the other peaks [Figs. 9(a,b) and 10(a,b)].

While the inclusion of subcritical reflection in the MPOA lets it approach the WKB result in the PR region, the approach is oscillatory, in agreement with the discussion in Sec. 7.4. Thus, although it is distinctly better than the POA in this region (except for $\cos\delta$, which is affected by the oscillations), it is worse than the WKB approximation. In the TR region, the MPOA is generally better than the POA for G_1, but without much of an advantage. For G_2, the POA tends to be better than the MPOA, except for some of the peaks at large ϵ. Finally, for $\cos\delta$, the MPOA is slightly better, but the advantages are small.

In conclusion, little advantage is gained by going over from the POA to the MPOA. In accounting for diffraction, both physical optics approximations improve on WKB just in the region between the top of the first peak and the second one, but the errors are still considerable.

8.3. The CAM approximation

Comparisons between the Mie results and the CAM approximation (7.1) will be made for $\beta = 1{,}000$ and $\beta = 10{,}000$. Since we have only developed the lowest-order CAM approximation, employing transitional (non-uniform) asymptotic approximations and assuming that $\gamma' \ll 1$, the lowest value of β for which it is reasonable to make comparisons is $\beta = 1{,}000$. The planar limit approximations of Sec. 7.2 begin to be applicable around $\beta = 10{,}000$, in a very restricted neighborhood of θ_t.

The results for $\beta = 1{,}000$ are shown in Fig.11. The POA and WKB approximations are also shown. Between $\theta_t - \eta$ and $\theta_t + \eta$, the CAM approximation provides a much better fit to G_1 and $\cos\delta$ than the other approximations. For G_2, this is also true, except that the POA, on the TR side, approaches comparable accuracy towards $\theta_t - \eta$.

For $\theta > \theta_t + 2\eta$ on the PR side, the CAM results for G_1 and G_2 are less accurate than the WKB approximation, showing small residual traces of oscillatory behavior. The CAM results for $\cos\delta$ also show some oscillation, followed by a dip near 95°. It can be verified that the Mie results for $\cos\delta$ show a similar dip (absent from the POA and the WKB approximation) about 10° further on (cf. also Fig. 5).

For $\theta < \theta_t - \eta$ on the TR side, the accuracy of the CAM approximation tends to deteriorate and to become comparable to (or worse than) that of the other approximations. Thus, at $\beta = 1{,}000$, the CAM approximation accounts well for the diffraction effects within a band of width about 2η centered on θ_t, but it is not a significant improvement on the other approximations at greater deviations from the critical angle.

The corresponding results for $\beta = 10{,}000$ are shown in Fig. 12. At this higher value of β, both the quality of the CAM fit and its range are considerably improved. For G_1 [Fig. 12(a)], the differences between the CAM approximation and the Mie result are of the same order as the residual fluctuations in the Mie data, not eliminated by the subtraction procedure, except at the high end of the angular range shown, where traces of oscillation are still present in CAM. Essentially all diffraction effects (departures from the WKB approximation) are accounted for. The same holds for G_2 [Fig. 12(b)], with slightly larger deviations at large distances from the critical angle. Note, by comparison with Fig. 11, that the POA errors become worse as β increases, in agreement with the qualitative discussion given in Sec. 7.4.

For $\cos\delta$ [Fig. 12(c)], the CAM fit is excellent on the PR side. It appears to have somewhat larger deviations in the TR region, but the corresponding relative errors are small [the vertical scale in Fig. 12(c) has a large displacement from the origin].

We conclude that, *at $\beta = 10{,}000$, the lowest-order CAM approximation already accounts very well for the diffraction effects in near-critical scattering.*

8.4. Discussion of individual contributions

In order to relate the results with the qualitative discussions given in Secs. 7.3-7.4, it is instructive to plot separately the contributions from the various terms in the CAM and POA approximations. So as to bring out the role of interference effects, one should plot amplitudes rather than intensities, so that we define

$$g_j(\beta,\theta) = \sqrt{G_j(\beta,\theta)} \qquad (j = 1,2) \tag{8.1}$$

and we denote the corresponding CAM contributions by PR (partial reflection), DT (direct transmission), and TR (total reflection), respectively associated with the magnitudes of (4.24), (5.15), and (6.12). Similarly, for the POA, we denote by R (reflection) and T (transmission) the contributions to (8.1) respectively associated with the magnitudes of (7.42) and (7.43).

All these contributions, for $\beta = 1{,}000$, are plotted in Fig. 13(a) (for polarization 1) and in Fig. 13(b) (for polarization 2). The leftward displacement of the TR curves with respect to the R ones is immediately noticeable in these figures. This is a consequence of the *spherical Goos-Hänchen angular shift* discussed in Sec. 6.3, or, equivalently, of the *tunneling of light within the bubble*.

According to (6.32), the shift should be $e_2/e_1 = N^{-2} = 16/9 \approx 1.8$ times larger for polarization 2, and a comparison between Figs. 13(b) and 13(a) shows that this relationship is approximately satisfied. Numerical tests of (6.32) at points satisfying

condition (6.34) also show consistency. In fact, one can only expect an order-of-magnitude agreement, for several reasons: (6.32) was derived by comparing two stationary-phase approximations in the planar limit, which requires large β and small ϵ, tending to get into conflict with (6.34); the CAM result is not a stationary-phase approximation; and the POA result also differs slightly from that considered in Sec. 6.3 for the stationary-phase comparison.

The POA transmission contribution (curve T), equivalent to an extrapolated WKB approximation, also differs considerably from the CAM result (curve DT), although they tend to merge in the TR region at large ϵ [the CAM Fock result (5.15) rejoins the WKB result, though not uniformly]. In particular, the CAM transmission contribution has a tail extending into the PR region, where the POA contribution is identically zero.The contribution from partial reflection (curve DR), neglected in the POA, not only is dominant in the PR region, but also has an appreciable tail extending into the TR region.

Let us now connect the CAM curves with the qualitative discussion of individual contributions given in Sec. 7.3. The crossover between the TR and DR curves occurs near $\theta = \theta_t$, where they give comparable contributions. In the TR region, the amplitude of oscillation of the TR curve is reduced by interference with the tail of the PR curve (Fresnel terms). This cancellation of dominant Fresnel contributions is more noticeable in the PR region, where the oscillations of the DR curve about its mean are removed by interference with a TR tail of the same magnitude. The cancellation is practically complete at the far end of the curves in Fig. 13(b), leading to a strong enhancement of the DT contribution.

Fig. 14 shows corresponding results at $\beta = 10{,}000$. The Goos-Hänchen shift is a good deal smaller, as expected from its inverse dependence with β in (6.32). It shows all the qualitative and semi-quantitative features already discussed in connection with Fig. 13. The Fresnel-like oscillations about the mean in curves TR and DR, which cancel out through interference between the corresponding amplitudes, leaving only the considerably smaller "parabolic-cylinder-like" oscillations on the TR side (Sec. 7.3), can be seen quite

clearly (the envelope of the damped oscillations in the DR curve should be compared with the tail of the TR curve).

9. CONCLUSION

We have developed, in lowest order of approximation, the CAM theory of near-critical Mie scattering. Already in this order, in spite of the transitional nature of the asymptotic approximations employed, CAM theory accounts for the new diffraction effects that are observed and, for the first time, explains their physical origin. In terms of the effective potential, they arise from a small neighborhood of the edge of the curved potential step shown in Fig. 1(a) (situation 2).

The lowest-order CAM approximation developed in this paper has several limitations: its accuracy becomes high only at large values of β (several thousand), and it does not merge smoothly with the WKB approximations at large deviations from the critical scattering angle, restricting its angular domain of applicability. These limitations are not inherent but are merely due to focusing on the dominant contributions, neglecting correction terms and employing various simplifying approximations, including the use of transitional asymptotic expansions. However, it is known[17,32] that CAM theory, with the help of uniform approximations, is capable of yielding extremely accurate and uniformly valid results, with domains of applicability that extend all the way to size parameters of order unity. Thus, if required, it offers well-defined procedures for improving the accuracy and domain of validity of the results.

The theory as developed to this order would apply with only minor modifications to a variety of other problems involving near-critical scattering at a curved interface. As was pointed out following (2.16), it applies to nonrelativistic quantum scattering by a square potential barrier, as well as to acoustic scattering from a homogeneous sphere. In seismology, analogous diffraction effects must occur in the generation of head waves[7-9] at a curved interface.

With trivial changes, the theory also applies to near-critical scattering by a homogeneous circular cylinder. In the electromagnetic problem, for instance, the partial-wave scattering amplitude coefficients differ from the Mie coefficients only by the replacement of Ricatti-Bessel functions by ordinary Bessel functions,[27] and of Legendre functions by trigonometric ones, which agrees with the asymptotic approximations we have employed.[48] Thus, the diffraction effect is structurally stable, remaining basically unaffected by the change from spherical to cylindrical geometry; indeed, experimental observations[2,6] were made in light scattering from cylindrical "bubbles".

Initial attempts at interpretation[2] tried to correlate the effect with the rainbow, which is also structurally stable, treating it as a "reciprocal rainbow". In terms of this "analogy", the geometrical-optic treatment[11] would correspond to the Descartes theory of the rainbow and the WKB approximation to Young's interference theory[12]; the POA would be the counterpart of the Airy theory.

However, the analogy is misleading: near-critical scattering is a new diffraction effect, entirely different from rainbow scattering. At the geometrical-optic level, a rainbow is a caustic direction, with an infinite discontinuity in the intensity, whereas in near-critical scattering the intensity remains continuous: the critical scattering angle corresponds to an infinite discontinuity in the *slope* of the intensity, which we propose to call a *weak caustic*. The weaker nature of the singularity leads to a better behavior of the WKB approximation. Indeed, while the zero-order ("primitive semiclassical") WKB approximation cannot be employed in the rainbow region, where it diverges at the rainbow angle,[29] it is well-behaved in the near-critical region, where it reproduces the geometrical-optic cusp at the critical angle. It is only the first-order WKB correction that diverges at the critical angle.

The diffraction effects in rainbow scattering[29] are spread over an angular domain of order $\beta^{-2/3}$ and include: an intensity enhancement of order $\beta^{1/3}$; diffractive changes in supernumerary interference oscillations on the bright side; and tunneling into the dark side. In near-critical scattering, diffraction effects spread over a broader angular domain, of order

$\beta^{-1/4}$ [cf. (7.2)]. There is no overall intensity enhancement. The diffractive changes in interference oscillations on the total reflection side (where tunneling is very important) and to the intensity decay on the partial reflection side scale like $\beta^{-1/4}$, so that they remain appreciable up to very large values of β.

Although direct transmission gives a nonnegligible contribution, the new diffraction effect arises basically from "a peculiar kind of reflection", to paraphrase Thomas Young's picture of edge diffraction.[3] The new diffraction integral associated with the effect is the combination of the Fresnel-Fock and Pearcey-Fock integrals.

The curvature of the interface produces two very different types of effects:

(i) It spreads the range of angles of incidence. If only this relatively trivial effect is taken into account, and the surface is replaced by its tangent plane at the point of incidence to evaluate the reflection coefficients, the problem is mapped into that of a divergent beam incident on a plane interface, corresponding to the planar reflection limit. In this limit, the new diffraction effects are described (as corrections to the WKB results) by the function $P(w)$, related to the parabolic cylinder functions by (7.20), and defined by (7.15) as the Fresnel transform of the square root function. Similar functions are found in the treatment of near-critical reflection of spherical waves at a plane interface.[10] The plot of $|P(w)|$ in Fig. 8 already shows some basic qualitative features of the new diffraction corrections. The failure of physical optics approximations stems from their attempt to describe the results in terms of the usual Fresnel pattern, the Fresnel transform of the Heaviside step function: as we have seen, subcritical and supracritical Fresnel contributions cancel each other exactly. The planar limit approximation is quantitatively useful only for very large size parameters and very small deviations from the critical angle.

(ii) A much deeper effect of curvature is manifested, in the effective potential, through the inertial (centrifugal) barrier, which also plays a crucial role in edge diffraction.[17,18,32] This is responsible for the difference between the planar and spherical reflection coefficients, giving rise to the Fock-type effects. The effective potential for near-

critical incidence, i. e., around situation 2 in Fig. 1(a), may be approximated by a linearly rising potential step, which explains the appearance of Airy functions in the new diffraction integrals. Taking into account these dynamical effects of curvature leads to a considerable improvement in accuracy and extension of the domain of validity of the approximations. The next step beyond the transitional Fock-type theory takes into account the curvature of the potential step and leads to the uniform approximation, that should further improve the accuracy and extend the range of applicability of the CAM theory. Thus, the planar reflection limit, the present transitional CAM approximation and a uniform CAM approximation provide successively better and broader approximations.

In terms of the short-wave asymptotics of Huygens-Fresnel-type integral representations of wave fields, of the type

$$f(\beta,\varepsilon)=\int A(\lambda,\varepsilon)\exp\left[i\beta\Phi(\lambda,\varepsilon)\right]d\lambda \tag{9.1}$$

where β is large and both the "amplitude" A and the "phase" Φ depend on one or more control parameters ε, rainbows are associated with the *fold catastrophe*,[41] where Φ is a cubic polynomial such that the ordinary saddle-point method cannot be applied. The corresponding catastrophe diffraction integral[41] is the Airy function.

In spite of the appearance of functions related to Pearcey's integral (6.25), connected with the cusp catastrophe (the next one in the hierarchy[41]), near-critical scattering does not arise from this catastrophe. What breaks down in the saddle-point method has to do with the amplitude A rather than with the exponent Φ in (9.1). In the saddle-point method, it is assumed[48] that A is single-valued and holomorphic within the range of integration. It is this assumption that breaks down in near-critical scattering. In the planar limit, A goes through a *branch cut* within the domain of the saddle point: see (7.11) and the remarks following (6.6). In the exact CAM representation, there is no branch cut, but A is *piecewise analytic*, i. e., it is represented by *two different analytic functions* in different parts of the range of integration: in the subcritical range, it is given by the first

term (3.2) of the Debye expansion (3.1) [cf. (4.5)], involving the spherical reflection coefficient $R_{22}^{(j)}$, while in the supracritical range it is given by the full S-function [cf. (4.2)], involving the total spherical reflection coefficient $R^{(j)}$

The generalized Goos-Hänchen shift, whose presence and relevance are obvious in Figs. 13 and 14, is a direct manifestation of tunneling. Thus, the CAM treatment of near-critical scattering from a curved interface reveals the important role of tunneling in this new diffraction effect in semiclassical scattering, as has already been found in forward diffraction, rainbow scattering, glory scattering and orbiting,[32] i. e., in all semiclassical diffraction effects known so far.

Well-documented and tested Fortran programs for doing the computations reported herein are available from the third author on IBM or Macintosh diskettes.

ACKNOWLEDGMENTS

It is a pleasure to thank Professor P. L. Marston for useful correspondence and for sending us several papers in advance of publication. Part of this work was done while the second author held a National Research Council-NASA Resident Research Associateship. This work was supported by the Brazilian agencies CAPES, CNPq, FAPESP and FINEP.

APPENDIX A. THE PARABOLIC CYLINDER FUNCTION

The Weber parabolic cylinder function (in Whittaker s notation) $D_\nu(z)$ has the integral representation[49]

$$D_\nu(z)=\frac{\exp(-z^2/4)}{\Gamma(-\nu)}\int_0^\infty t^{-\nu-1}\exp\left(-\frac{1}{2}t^2-zt\right)dt \quad , \quad \mathrm{Re}\,\nu<0 \tag{A1}$$

where Γ is Euler's Gamma function. It satisfies the relationship[49]

$$\sqrt{2\pi}D_\nu(iz)=\Gamma(\nu+1)\left[e^{-i\pi\nu/2}D_{-\nu-1}(z)+e^{i\pi\nu/2}D_{-\nu-1}(-z)\right] \tag{A2}$$

For $|z|\gg 1$, $|z|\gg|\nu|$, its asymptotic expansion is given by[49]

$$D_\nu(z)\approx e^{-z^2/4}z^\nu\left[1-\frac{\nu(\nu-1)}{2z^2}+O\left(z^{-4}\right)\right] \quad , \quad |\arg z|<3\pi/4 \tag{A3}$$

$$D_\nu(z)\approx e^{-z^2/4}z^\nu\left[1-\frac{\nu(\nu-1)}{2z^2}+O\left(z^{-4}\right)\right]-\frac{\sqrt{2\pi}}{\Gamma(-\nu)}e^{i\pi\nu}$$
$$\times e^{z^2/4}z^{-\nu-1}\left[1+\frac{(\nu+1)(\nu+2)}{2z^2}+O\left(z^{-4}\right)\right] \quad , \quad \pi/4<\arg z<5\pi/4 \tag{A4}$$

$$D_\nu(z)\approx e^{-z^2/4}z^\nu\left[1-\frac{\nu(\nu-1)}{2z^2}+O\left(z^{-4}\right)\right]-\frac{\sqrt{2\pi}}{\Gamma(-\nu)}e^{-i\pi\nu}$$
$$\times e^{z^2/4}z^{-\nu-1}\left[1+\frac{(\nu+1)(\nu+2)}{2z^2}+O\left(z^{-4}\right)\right] \quad , \quad -5\pi/4<\arg z<-\pi/4 \tag{A5}$$

APPENDIX B. COMPUTATIONAL CONSIDERATIONS

All computations reported here were carried out in 14-digit precision, and all quantities were computed to an accuracy of at least 6 significant digits.

B1. Mie Theory

In preparation for this study, it was necessary to extend the Mie scattering algorithms of Wiscombe[50] to the case of refractive index less than unity. Considerable care was exercised to do this correctly, because there is danger of severe numerical ill-conditioning due to the large size parameters and consequently long (up to 10,000 terms) Mie series involved. The main concern was the recurrence for the Bessel function ratio $A_n(N\beta)$, since this is by far the most important place where the refractive index N affects the Mie algorithm. It was found that, contrary to the $N > 1$ situation, it was *never* possible to use up-recurrence for A_n; doing so led to disastrous errors. A_n always had to be computed by down-recurrence.

The only other issue in the Mie algorithm was the number of terms to take in the Mie series. The formula used in Wiscombe[50] was fitted to the $N > 1$ case but was found to be entirely satisfactory for $N < 1$ also. Adding 5% more terms than required by this formula had no effect. Using 10% fewer terms, on the other hand, had a big effect, indicating considerable cancellation among the first 90% of the terms (at least near the critical angle) and thus a preponderant influence of the terms in the tail end of the Mie series.

Before devising the method of subtracting the farside contributions, we tried averaging the Mie results over narrow angular bins to tame the Mie fluctuations, but this

was highly unsatisfactory. In general, we have found that such filters (even very sophisticated ones) are of little value in smoothing Mie curves; the Mie fluctuations are very strange (appearing almost fractal in that there is structure within structure) and are definitely not of the sort which are susceptible to traditional smoothing algorithms.

B2. CAM calculations

The main concerns in computing the CAM approximation are: (a) replacing infinite upper limits in some integrals with finite values; (b) computing Airy functions Ai and Ai′ of complex argument; (c) doing the integrals by numerical quadrature.

B2.1. Upper Limits

The evaluation of the Fresnel-Fock integral (4.24) and the Pearcey-Fock integral (6.12) is performed according to the procedure defined following (4.26) and (6.13), so that [including the incomplete Fock-type function (5.15)] all CAM integrals with infinite upper limits have rapidly decreasing integrands—in some cases monotonically decreasing ones, in other cases oscillatory with a monotonically decreasing envelope.

Since the monotonic decrease is at least exponential [in fact, faster than exponential: with power 3/2 for (5.15) and Gaussian for (4.24) and (6.12)], it is possible just to use finite rather than infinite upper limits without having to add in an estimate of the residual, as long as large enough upper limits are used. Our criterion was that doubling the value of the upper limit should not affect the computed value of the integral to 6 significant digits.

Regarding the finite pieces of stationary-phase integrals that contribute to (4.24) and (6.12), as was pointed out following (4.26) and (6.13), the integrands, though oscillatory, only go through a small number of oscillations when θ is in the near-critical region.

B2.2. Airy functions

It is difficult to find algorithms for computing Ai(z) and Ai′(z) for complex z. Algorithms for real z, based on Chebyshev polynomial fits (e.g. Prince[51]), are easy to

find but not extensible. Sophisticated algorithms for Bessel functions of complex argument (including Airy functions) have been developed by Amos.[52] However, Amos computes Airy functions in terms of I and K Bessel functions of fractional order. To us, this seemed excessively complicated and wasteful of computer time, because the Airy functions are entire functions without branch cuts and have simple power and asymptotic series representations. We developed fast routines based entirely on these series. (Our experience contradicts Schulten et al.,[53] who claim that the power and asymptotic series are too limited in range and slowly converging to be useful for moderate values of z).

The power series for both Ai and Ai′ take the form (Reference 30, Eq. 10.4.2):

$$c_1 f(z) - c_2 g(z)$$

where both $f(z)$ and $g(z)$ are power series. This becomes increasingly ill-conditioned as $|z|$ increases: either because the subtraction causes loss of significant digits (e.g. on the positive real axis); or because $f(z)$ and $g(z)$ contain large nearly-cancelling terms (e.g. on the negative real axis). But by using 14-digit precision and allowing a loss of up to 7 significant digits in the computation, it is possible to reach up to $|z| = 5.4$ using no more than 23 terms (all 14 digits are lost for $|z| \geq 8$). The number of terms necessary was fitted as a linear function of $|z|$ ($4.75 + 3.3\,|z|$ for Ai and $5.0 + 3.35\,|z|$ for Ai′); this allows a more accurate and efficient summation using a Horner's Rule factorization.

For $|z| > 5.4$ the Airy asymptotic series give equivalent precision (6 digits or more) to the power series in 20 or less terms. The simpler asymptotic series (Reference 30, Eq. 10.4.59) is used for almost all z; however, it is not valid on the negative real axis, so very near that axis [when $\mathrm{Re}(z) < -0.998\,|z|$] the more complicated series 10.4.60 is used instead. The series is stopped when the final term added is below 10^{-8} times the leading term, provided that the series is decreasing at this point (which is always the case for $|z| > 5$). In no case is the asymptotic series summed to where the terms start to increase, which occurs roughly at term number $= 2|\zeta|$ where $\zeta = 2/3\, z^{3/2}$. The number of terms necessary is gotten from an empirical function of $|\zeta|$ so that a Horner factorization can be used, as for the power series.

The accuracy of our routines falls from ≥ 10 significant digits to roughly 7 digits as $|z|$ increases from zero, or decreases from large values, toward 5.4. The only error condition occurs for very large $|z|$, when the exponential in the asymptotic form may overflow.

We checked our routines for Ai(z) and Ai′(z) against the routines of Prince[51] for real z; along rays $\arg(z) = \pi/3$ and $2\pi/3$, where Ai(z) and Ai′(z) can be expressed in terms of Airy functions of real argument using Reference 30, Eq. 10.4.9, with $z = r$ and $z = r\,e^{\pm i\pi}$ (r real); against Table VII of Schulten, et.al.[53] for $|z| = 6$ and $\arg(z)$ from 0 to π in steps of $\pi/6$; and against old tables of Harvard University[54] and Woodward et al.[55]

B2.3. Quadrature

The integrals were calculated using the Kronrod-Patterson method involving a sequence of interleaving 1, 3, 7, 15, 31, 63, 127 and 255-point extended Gauss-type quadrature formulae.[56] Since each successive formula employs all points used by its predecessor, no integrand values are wasted when the order of the integration formula is increased; this is a considerable merit when the integrands are as complicated as in CAM approximations. Convergence is defined to occur when the relative differences between the magnitudes of two successive formulae are less than 10^{-6}. It was never necessary to go beyond the 255-point formula, and usually convergence occurred much earlier in the sequence. Since it is the magnitude of the integral whose convergence is tested, it is possible for the real or imaginary part separately to be poorly converged, if one of them is orders of magnitude smaller than the other one; in practice, this did not prove to be a problem.

B3. Transcendental equation solution

According to (3.17), the following transcendental equation must be solved in the computation of the p-th term of the farside sum:

$$f_p(\theta_{1p}) \equiv \sin\theta_{1p} - N\cos\left[(2\theta_{1p} - \theta - \pi)/(2p)\right] = 0 \qquad \text{(B1)}$$

Fig. 15 shows f_p for $\theta = 80°$ and various values of p. The curves converge rather quickly to $f_\infty(\theta_{1p}) = \sin\theta_{1p} - N$ as the single root approaches $\sin^{-1} N$. An examination of many such curves for different N and θ showed always this same behavior: between 0 and the critical angle there is always a monotone increase and a single root, and the curves always converge rather quickly to f_∞ as p increases.

The asymptotic approximation (3.20) to the root θ_{1p} turns out to be excellent even for low values of p. Empirically, it always exceeds the true root. Typically it is high by 20–30% for $p = 2$; a few per cent for $p = 3$; and around 1% or less for $p = 4$. By $p = 30$ or thereabouts, (3.20) is good to 5-6 significant digits. Empirically, (3.20) converges monotonically to the true root as p increases, so we stop solving the transcendental equation as soon as (3.20) agrees with the root to 6 significant digits; (3.20) is then used for the root for all larger values of p.

We routinely take terms up to $p = 100$ in the far-side sum (to ensure convergence to roughly 4 significant digits) and evaluate this sum at 100's to 1000's of angles θ; thus the transcendental equation needs to be solved 10^4–10^5 times in a typical computation. This clearly made manual inspection of each solution impossible, so a safe root-finder with guaranteed convergence was essential.

Our first choice for such a root-finder was the routine RTSAFE from Press et al..[57] RTSAFE requires the root to be bracketed. It uses Newton's Method except when the Newton step is either too large or would place the next guess for the root outside the brackets; then it reverts to the bisection method. Typically, RTSAFE required 5-6

iterations (independent of p) to converge the root to 6 significant digits. 0 and $\pi/2$ were used as the root brackets because it can easily be shown that

$$f_p(0) < 0 \quad \text{and} \quad f_p(\pi/2) > 0.$$

The critical angle was also tried as the upper root bound in place of $\pi/2$, but this actually inhibits convergence by forcing more non-Newton steps.

We were able to reduce the number of root-finding iterations required to 2-3 by making two changes to RTSAFE: first, allowing the input of an initial guess [which we took to be (3.20)]; and second, using Regula Falsi instead of bisection (Regula Falsi converges faster). This is almost a best-possible result.

B4. Fresnel Integrals

The Fresnel integral $F(x) = C(x) + iS(x)$ occurs in the POA and MPOA results (7.41) and (7.48). The computation of this function would not be remarkable, except that the approximate fits given in Eqs. 7.3.32 and 7.3.33 of Reference 30 and employed in References 5 and 14 have serious problems for small x. We discovered this in trying to reconcile differences between our implementation of the POA formulas and some published numbers.

Although it proved harder than expected to find Fresnel integral routines among the usual mathematical libraries—in particular IMSL has none—we did find them in the well-known NAG library (see Cowell[58]). When we compared the NAG values with the fit proposed in Reference 30, we found serious errors in $S(x)$ for $x < 0.4$: 4% at $x = 0.32$, 25% at $x = 0.22$, and growing catastrophically large for $x < 0.2$. Even where the fits based on Reference 30 were good, their errors were never smaller than a few tenths of a percent; this hardly seems sufficient for present-day computations.

References and notes

*Permanent address: Departamento de Física, Pontifícia Universidade Católica, Rio de Janeiro, RJ 22452, Brazil.

1. M. V. Berry and K. E. Mount, Rep. Prog. Phys. **35**, 315 (1972).
2. C. Pulfrich, Ann. Phys. Chem. (Leipzig) **33**, 209 (1888).
3. A. Sommerfeld, *Optics* (Academic, New York, 1954).
4. G. Mie, Ann. Phys. (Leipzig) **25**, 377 (1908).
5. D. S. Langley and P. L. Marston, Appl. Opt. **23**, 1044 (1984).
6. P. L. Marston, J. L. Johnson, S. P. Love and B. L. Brim, J. Opt. Soc. Am. **73**, 1658 (1983).
7. V. Cerveny and R. Ravindra, *Theory of Seismic Head Waves* (University of Toronto Press, 1971).
8. A. Ben-Menahem and S. J. Singh, *Seismic Waves and Sources* (Springer, Berlin, 1981).
9. A. Hanyga, ed., *Seismic Wave Propagation in the Earth* (Elsevier, Amsterdam, 1985).
10. L. M. Brekhovskii, *Waves in Layered Media* (Academic, New York, 1960).
11. G. E. Davis, J. Opt. Soc. Am. **45**, 572 (1955).
12. H. C. van de Hulst, *Light Scattering by Small Particles* (Wiley, New York, 1957).
13. P. L. Marston, J. Opt. Soc. Am. **69**, 1205 (1979); **70**, 353 (E) (1980).
14. P. L. Marston and D. L. Kingsbury, J. Opt. Soc. Am. **71**, 192 , 917 (E) (1981).
15. D. Ludwig, J. Math. Phys. **11**, 1617 (1970).
16. H. M. Nussenzveig, J. Opt. Soc. Am. **69**, 1068 (1979), and references therein.
17. H. M. Nussenzveig and W. J. Wiscombe, Phys. Rev. Lett. **59**, 1667 (1987).
18. H. M. Nussenzveig, J. Phys. A **21**, 81 (1988).
19. H. M. Nussenzveig, J. Math. Phys. **10**, 82 (1969).
20. N. Fiedler-Ferrari, Ph. D. thesis, University of São Paulo (1983).

21. H. M. Nussenzveig, Rev. Bras. Fis., special issue, 302 (1984).
22. N. Fiedler-Ferrari and H. M. Nussenzveig, Part. Charact. **4**, 147 (1987).
23. C. E. Dean, Ph. D. thesis, Washington State University (1989).
24. P. L. Marston, W. P. Arnott, S. M. Baumer, C. E. Dean and B. T. Unger, in *Proc. III Intern. Coll. on Drops and Bubbles*, ed. T. G. Wang (AIP Conference Proceedings, 1989).
25. C. E. Dean and P. L.Marston, private communication.
26. F. Goos and H. Hänchen, Ann. Phys. Lpz. (6) **1**, 333 (1947).
27. C. F. Bohren and D. R. Huffman, *Absorption and Scattering of Light by Small Particles* (Wiley, New York, 1983).
28. H. M. Nussenzveig, Ann. Phys. (N.Y.) **34**, 23 (1965).
29. H. M. Nussenzveig, J. Math. Phys. **10**, 125 (1969).
30. M. Abramowitz and I. A. Stegun, eds., *Handbook of Mathematical Functions* (National Bureau of Standards, Washington, 1964).
31. M. Born and E. Wolf, *Principles of Optics* (Pergamon, London, 1959).
32. H. M. Nussenzveig, Comments At. Mol. Phys. **23**, 175 (1989).
33. D. M. Brink, *Semi-classical Methods for Nucleus-Nucleus Scattering* (Cambridge University Press, 1985), and references therein.
34. V. Khare, Ph. D. thesis (University of Rochester, 1975, available from University Microfilms, Inc.).
35. This result is given in references 20 and 22 with an overall minus sign missing. We thank Professor P. L. Marston for bringing this misprint to our attention.
36. Note that the extra factor (5.16) does not prevent deformation into this path, because no zeros of its denominator (Regge poles) are located in the fourth quadrant of the λ-plane.[19]

37. This differs from the corresponding expression in references 20 and 22 by a factor $(\sin\theta/\sin\theta_i)^{1/2}$, which can be taken as unity within the present approximation.

38. T. Pearcey, Phil. Mag. **37**, 311 (1947).

39. J. N. L. Connor and D. Farrelly, J. Chem. Phys. **75**, 2831 (1981).

40. J. N. L. Connor and P. L. Curtis, J. Phys. A **15**, 1179 (1982).

41. M. V. Berry, in *Progress in Optics*, ed. E. Wolf (North-Holland, Amsterdam, 1980), vol. 18, 259.

42. H. K. V. Lötsch, Optik **32**, 116; 189; 299; 553 (1971), and references therein.

43. K. Artmann, Ann. Phys.Lpz.(6) **2**, 87 (1948).

44. This was done in references 20 and 22.

45. A numerical comparison between (7.24) and (7.1) for $\beta = 10{,}000$ confirms their similarity in qualitative behavior, as well as the accuracy of (7.24) in a small angular neighborhood of the critical scattering angle.

46. F. W. J. Olver, *Asymptotics and Special Functions* (Academic, New York, 1974).

47. The WKB result was approached in the original version[13] of the POA, where the argument of the Fresnel integral was $\sqrt{2M\beta/\pi\epsilon}$.

48. The denominator $(\lambda \sin\theta)^{1/2}$ in (2.20) is "slowly-varying" in the near-critical domain and introduces only minor modifications.

49 W. Magnus, F. Oberhettinger and R. P. Soni, *Formulas and Theorems for the Special Functions of Mathematical Physics*, 3rd ed. (Springer, New York, 1966).

50. W. J. Wiscombe, Appl. Opt. **19**, 1505 (1980).

51. P. J. Prince, ACM Trans. Math. Soft. **1**, 372 (1975).

52. D. Amos, ACM Trans. Math. Soft. **12**, 265 (1986).

53. Z. Schulten, D. Anderson and R, Gordon, J. Comput. Phys. **31**, 60 (1979).

54. Harvard University, Staff of the Computation Laboratory, *Tables of the modified Hankel functions of order one-third and of their derivatives* (Harvard University Press, Cambridge, Mass.,1945).

55. P. Woodward, A. Woodward, R. Hensman, H. Davies and N. Gamble, *Phil. Mag.* **37**, 236 (1946).

56. T. Patterson, Commun. Assoc. for Comput. Mach. **16**, 694 (1973).

57 W. Press, B. Flannery, S. Teukolsky and W. Vettering, *Numerical Recipes: the Art of Scientific Computing* (Cambridge University Press, 1986), Ch. 9.

58. W. Cowell, ed., *Sources and Development of Mathematical Software* (Prentice-Hall, Englewood Cliffs, New Jersey, 1984), Ch. 14.

Figure captions

Fig. 1: (a) The effective potential $U_{\text{eff}}(\lambda,r)=(\lambda^2/r^2)+(1-N^2)k^2H(a-r)$, where H is the Heaviside step function. Four different levels for k^2 , corresponding to different impact parameters, are shown. (b) Ray paths associated with the four situations in (a). 1: subcritical incidence; 2: critical incidence; 3: supracritical incidence; 4: edge incidence.

Fig. 2: Lowest-order ($p=2$) farside ray path, with $2\theta_1+2(\pi-2\theta_2)=\pi+\theta$.

Fig. 3: (a) Comparison of exact polarization 1 gain function G_1(Mie) with subtracted gain functions to orders $P=2$ and $P=100$, for $N=0.75$, $\beta=1{,}000$. (b) Effect on G_1(Mie) of increasing number of subtractions, for $N=0.75$, $\beta=10{,}000$. To avoid overlap, the curves have been offset by varying amounts.

Fig. 4: Same as Fig. 3(a) for polarization 2, with $\beta=5{,}000$. The curve for $P=2$ is plotted at a different scale (indicated on the right) to facilitate the comparison.

Fig. 5: Same as Fig. 3(a) for the cosine of the phase difference , with $\beta=100$. For $P=2$, a different scale (indicated on the right) is employed, to facilitate the comparison.

Fig. 6: Exact and subtracted ($P=100$) scattering data, with $N=0.75$ and $\beta=1{,}000$. (a) G_1 ; (b) G_2 ; (c) $\cos\delta$.

Fig. 7: An incident ray AB with $\theta_i>\theta_c$ is not geometrically reflected as the ray BE : instead, it tunnels into the sphere and travels the additional arc BC (associated with the Goos-Hänchen angular displacement $\delta\theta_j^{\text{GH}}$) before reemerging at the angle of reflection θ_i (ray CD).

Fig. 8: The function $|P(w)|$ and its asymptotic limit $\sqrt{|w|}$. A Fresnel diffraction pattern is shown for comparison.

Fig. 9: Comparison between subtracted Mie results to order $P=100$ and the WKB approximation, for $N=0.75$, $\beta=5{,}000$. The angular width parameter η is defined by (7.2). (a) $G_1(\beta,\theta)$; (b) $G_2(\beta,\theta)$; (c) $\cos\delta(\beta,\theta)$.

Fig. 10: Comparison between subtracted Mie results to order $P=100$ and the POA and MPOA, for $N=0.75$, $\beta=5{,}000$. (a) $G_1(\beta,\theta)$; (b) $G_2(\beta,\theta)$; (c) $\cos\delta(\beta,\theta)$.

Fig. 11: Comparison between subtracted Mie results to order $P=100$ and the CAM approximation, for $N=0.75$, $\beta=1{,}000$. The POA and the WKB approximations are also shown. (a) $G_1(\beta,\theta)$; (b) $G_2(\beta,\theta)$; (c) $\cos\delta(\beta,\theta)$.

Fig. 12: Same as Fig. 11, for $\beta=10{,}000$.

Fig. 13: Contributions to $g_j(\beta,\theta)=\sqrt{G_j(\beta,\theta)}$, for the CAM approximation, from partial reflection (PR), direct transmission (DT) and total reflection (TR), and, for the POA, from reflection (R) and transmission (T), for $\beta=1{,}000$.(a) for $j=1$; (b) for $j=2$.

Fig. 14: Same as Fig. 13, for $\beta=10{,}000$.

Fig. 15: Plots of $f_p(\theta_{i_p})$, defined by Eq. (B1), for $N = 0.75$, $\theta = 80°$ and various values of p . For $p \to \infty$, the single zero of this function approaches $\theta_c = \sin^{-1} N$.

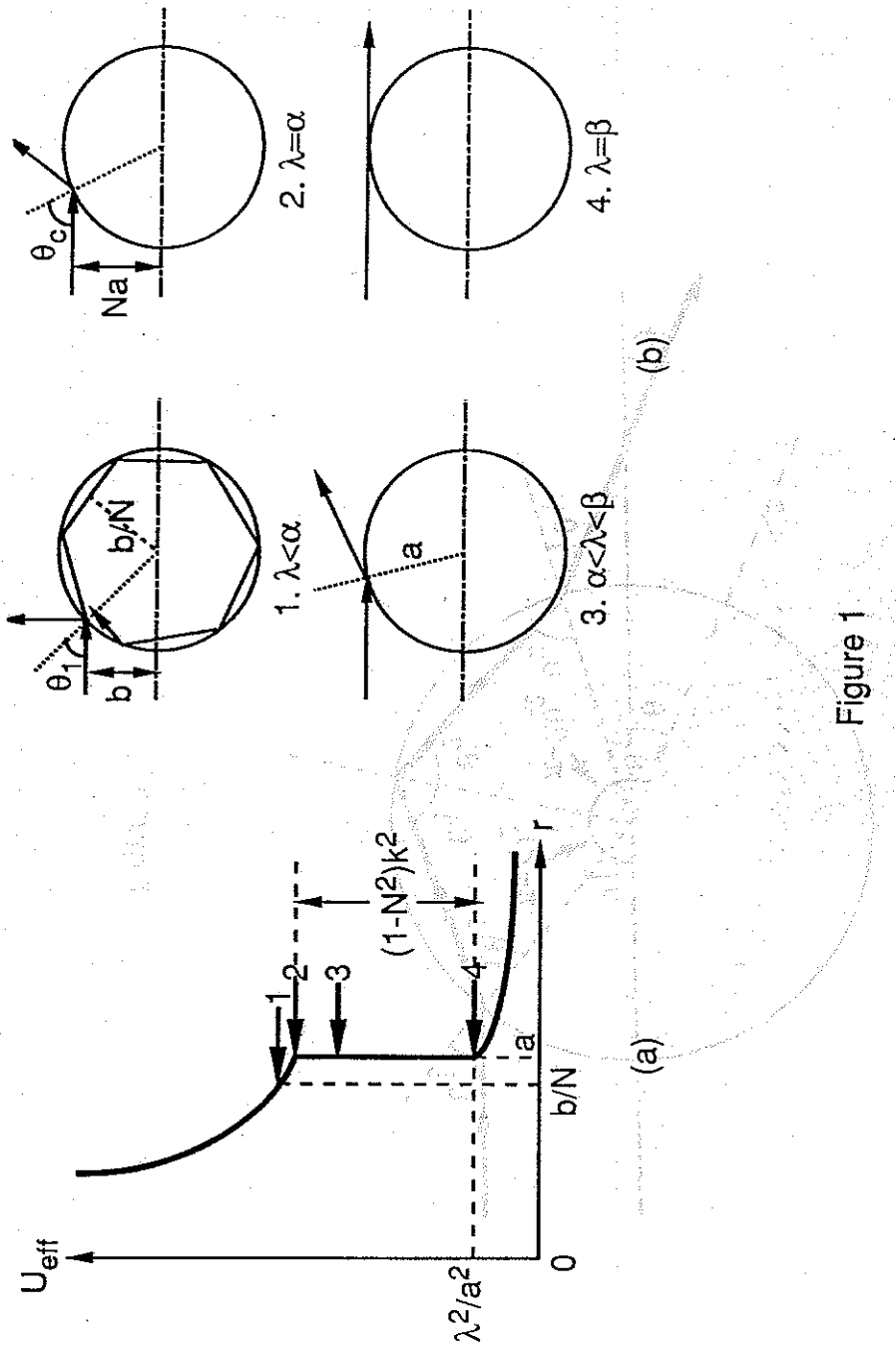

Figure 1

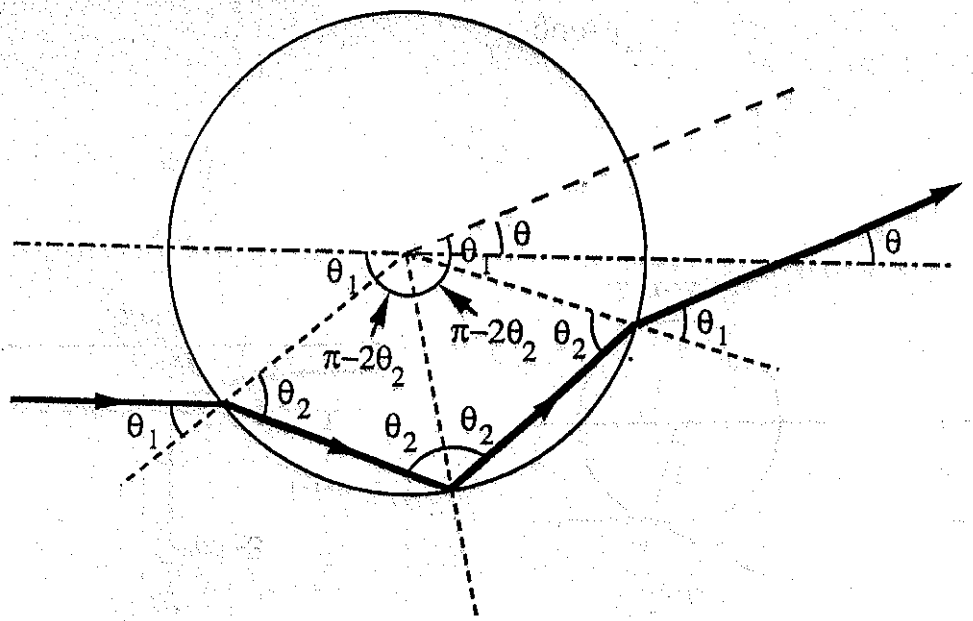

Figure 2

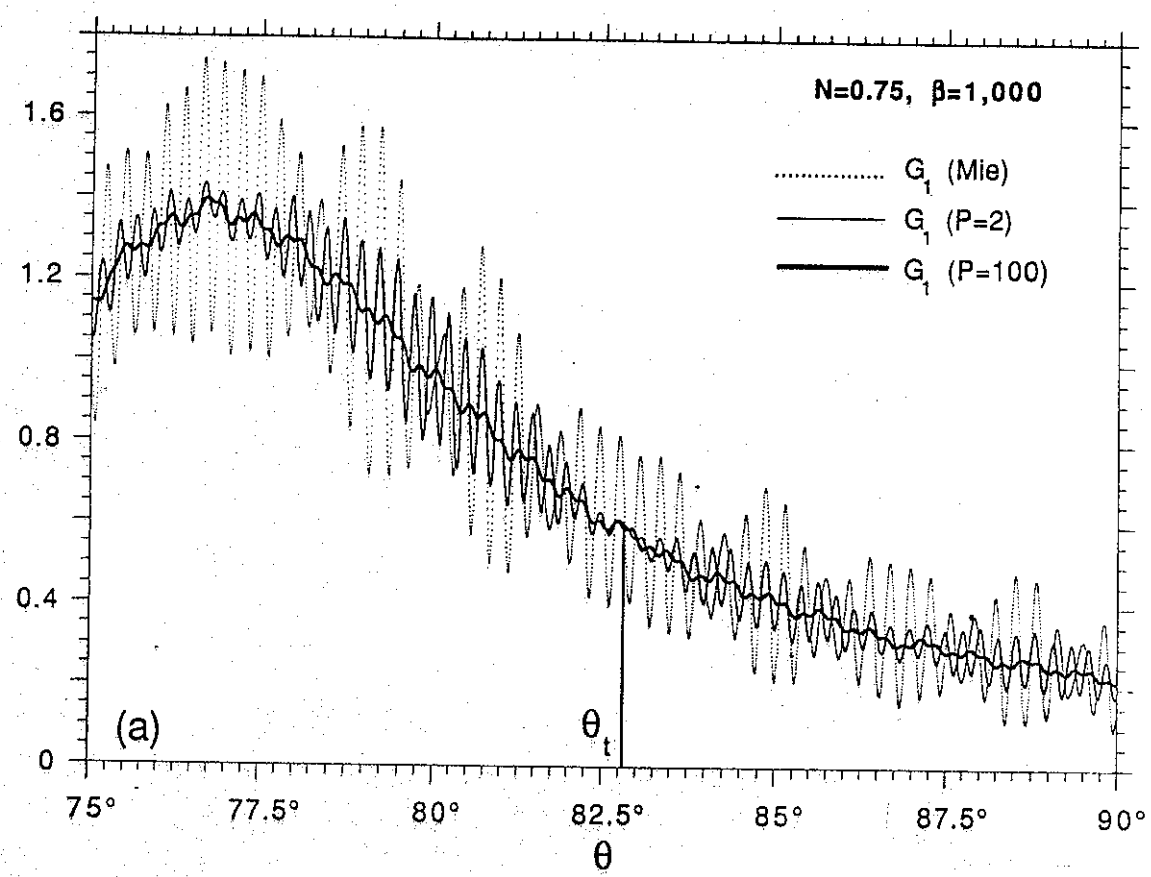

Figure 3(a)

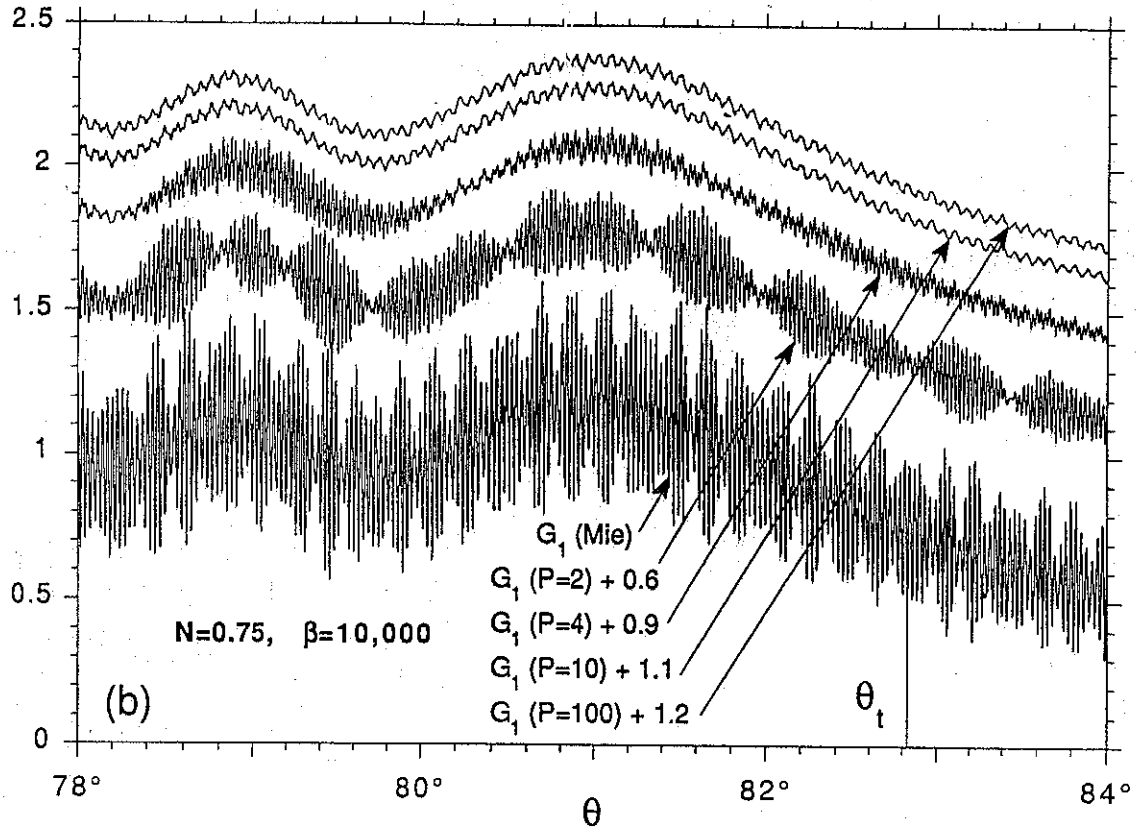

Figure 3(b)

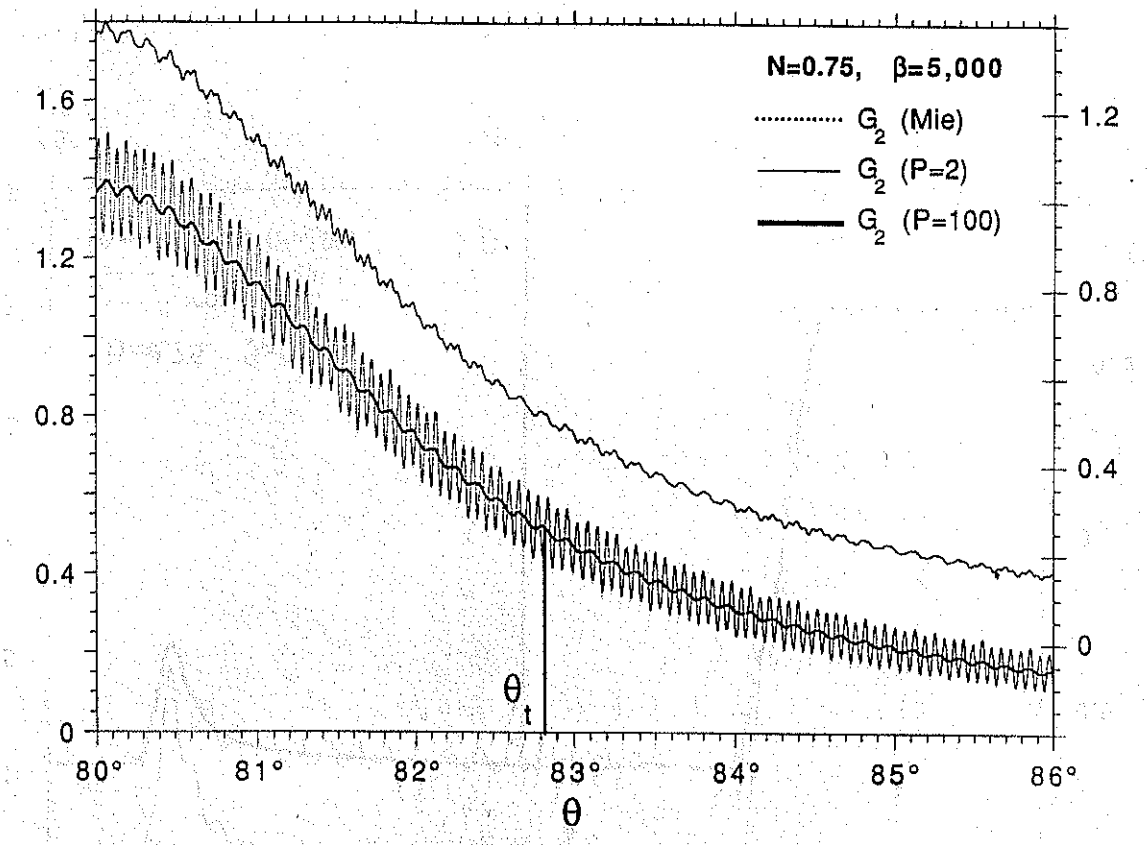

Figure 4

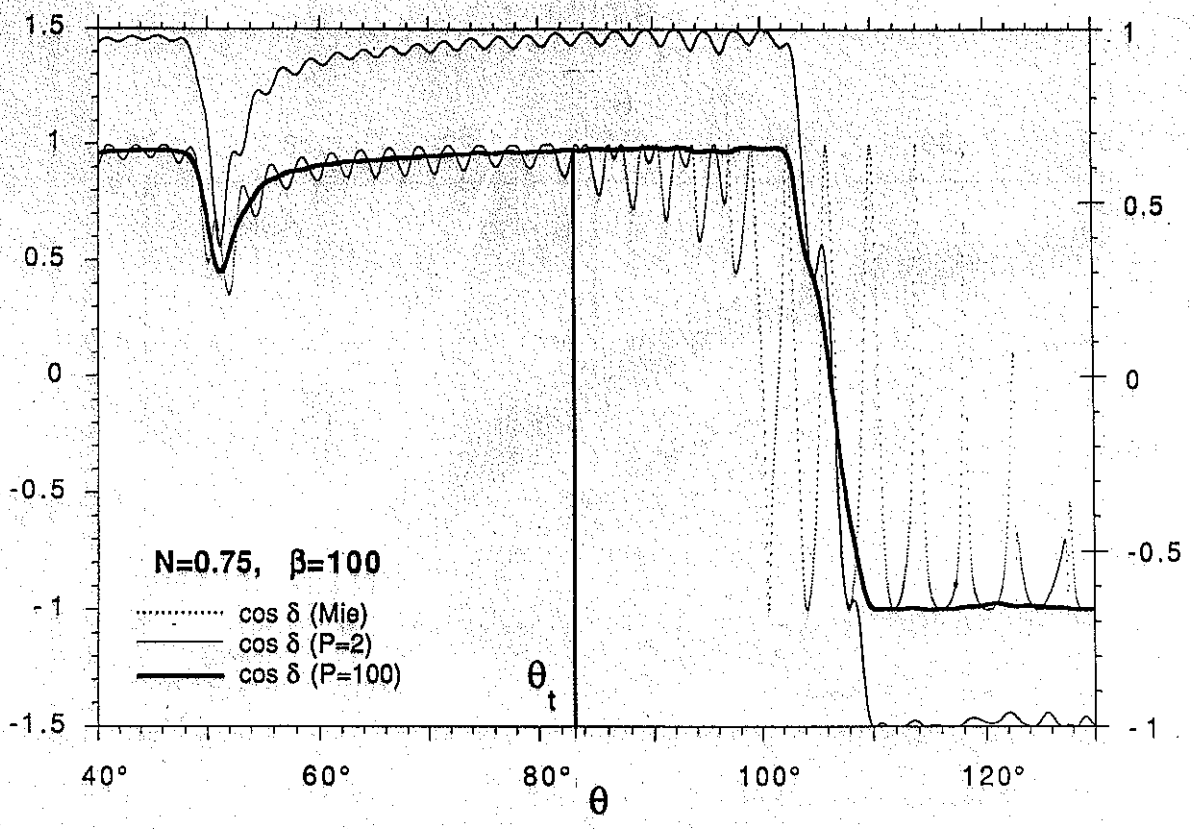

Figure 5

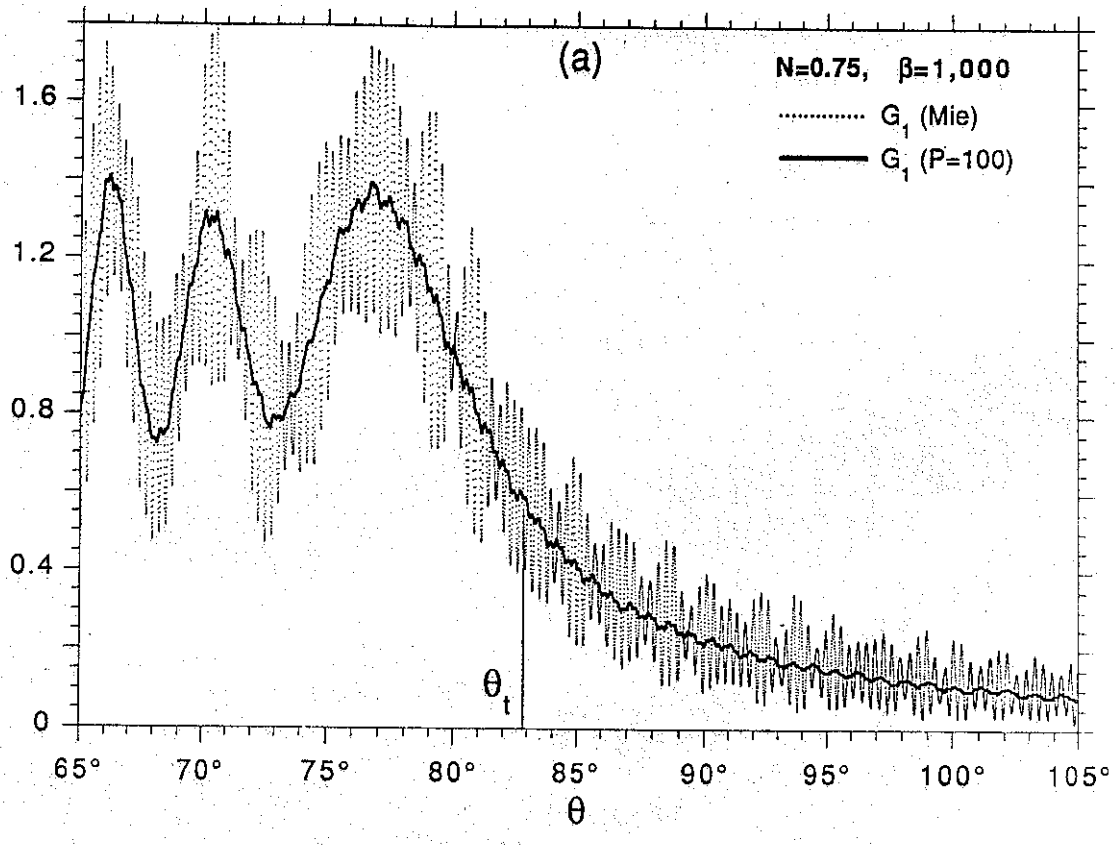

Figure 6(a)

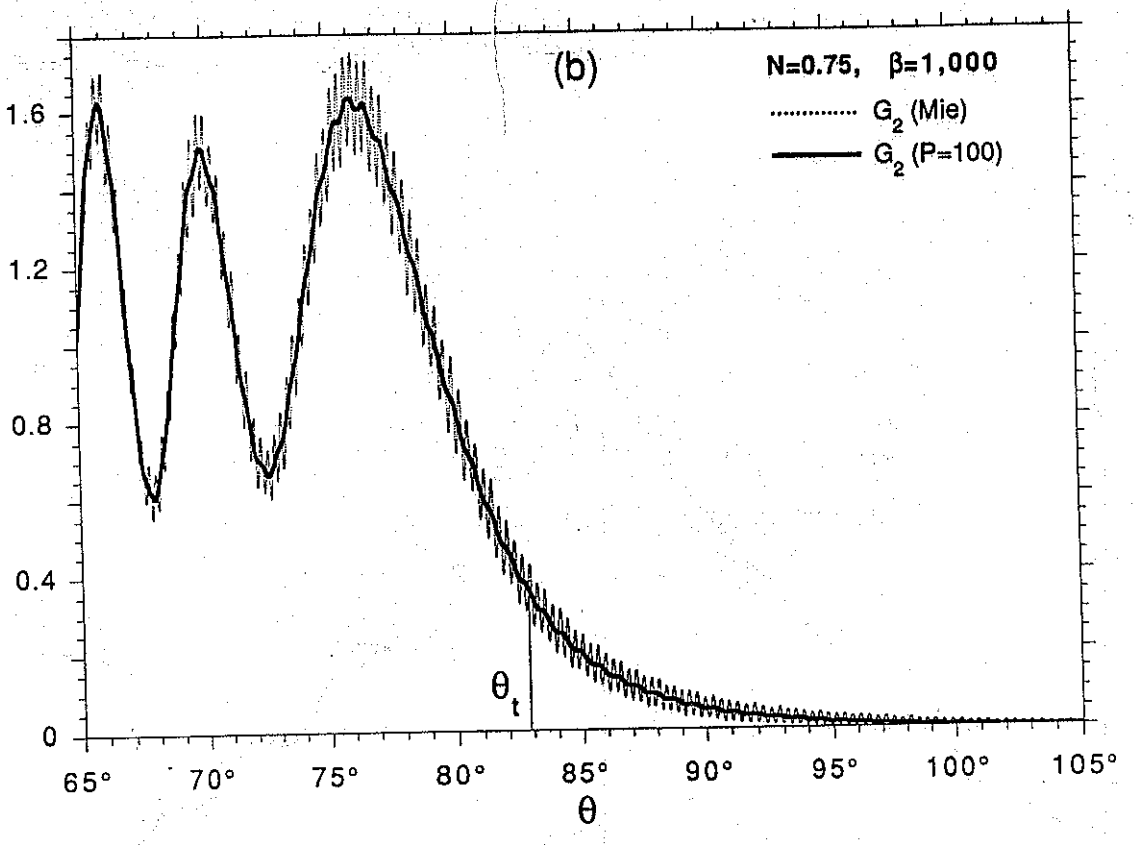

Figure 6(b)

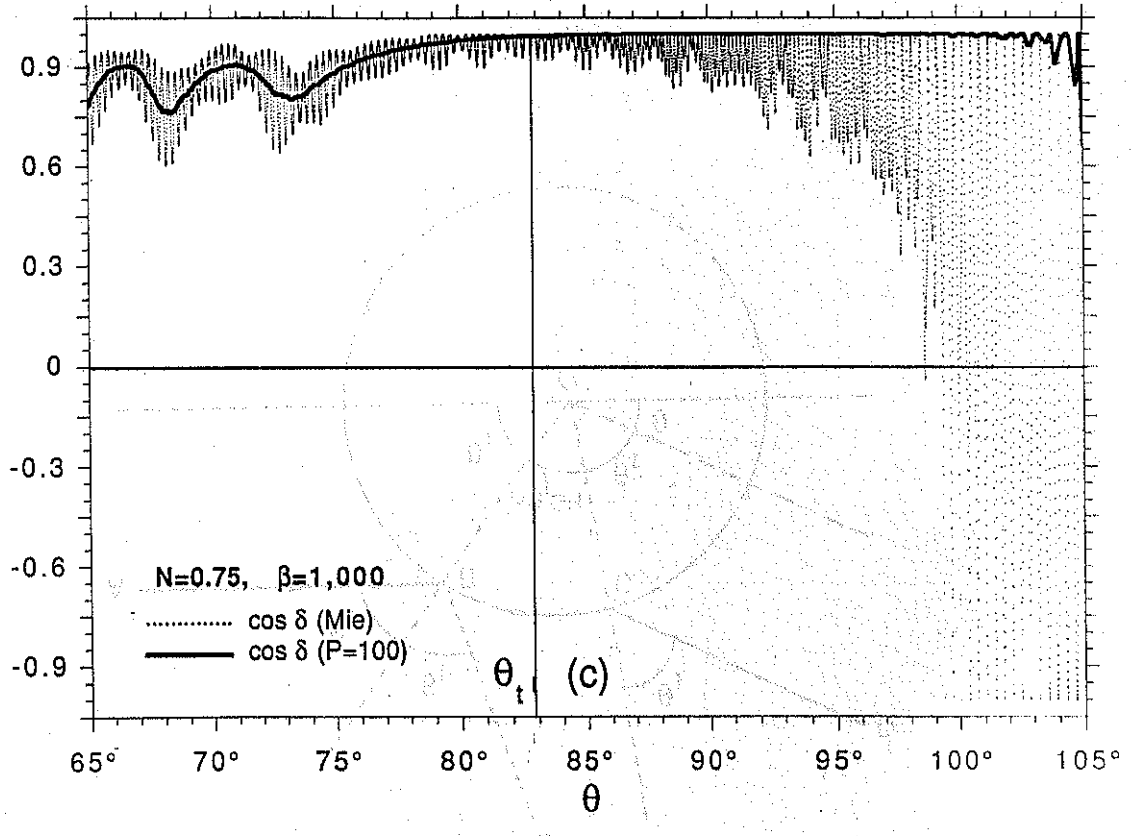

Figure 6(c)

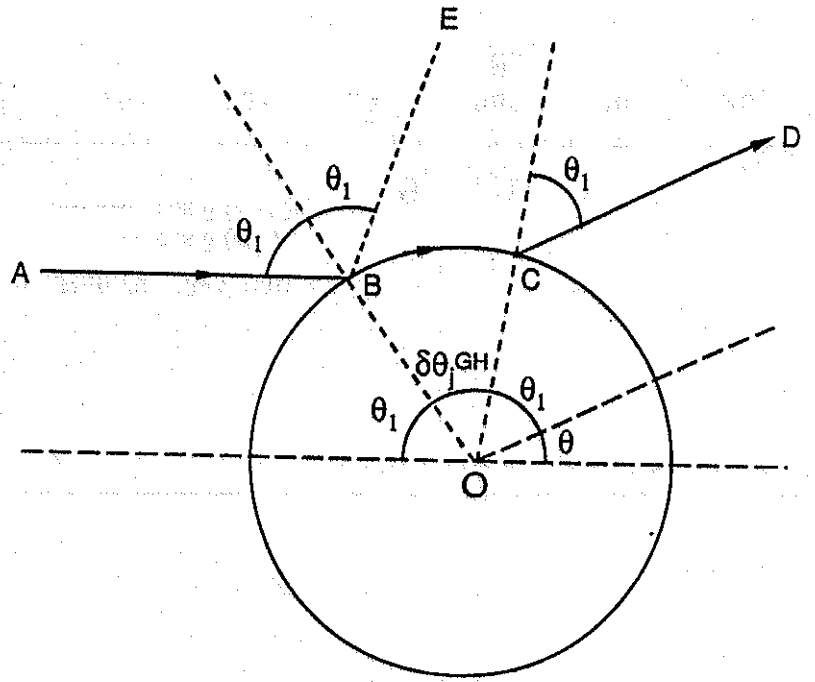

Figure 7

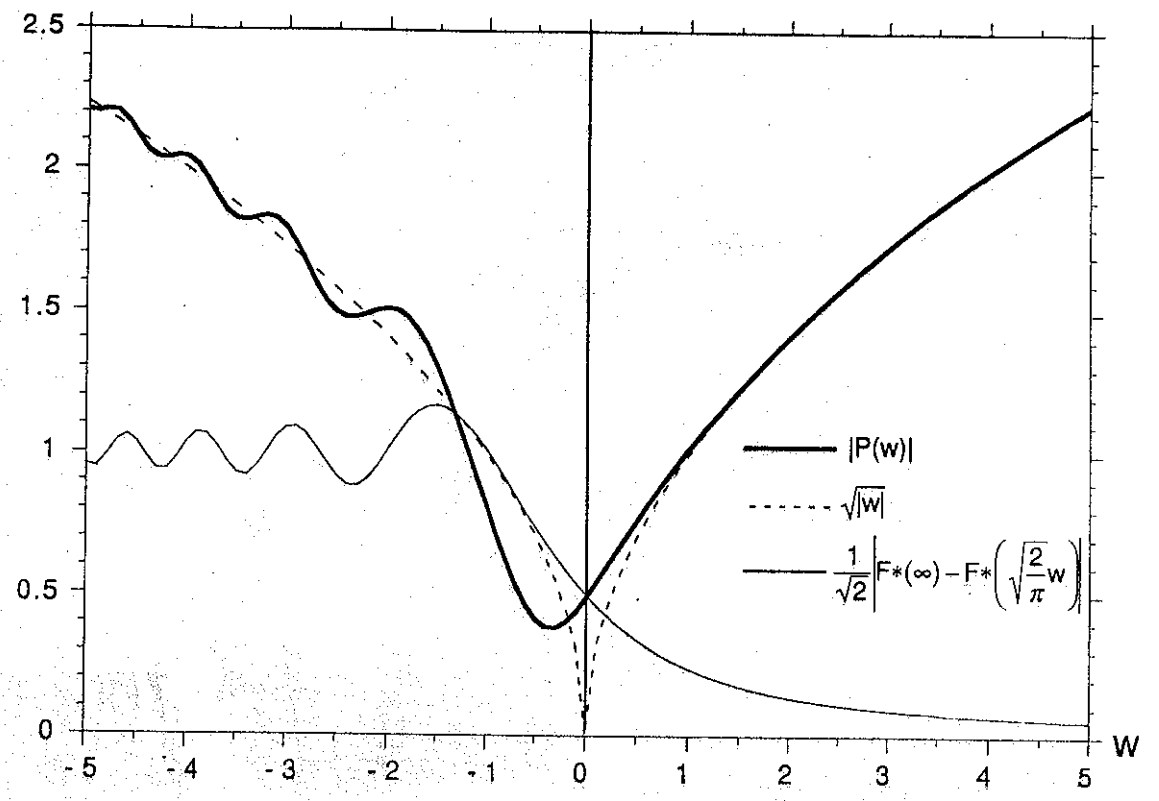

Figure 8

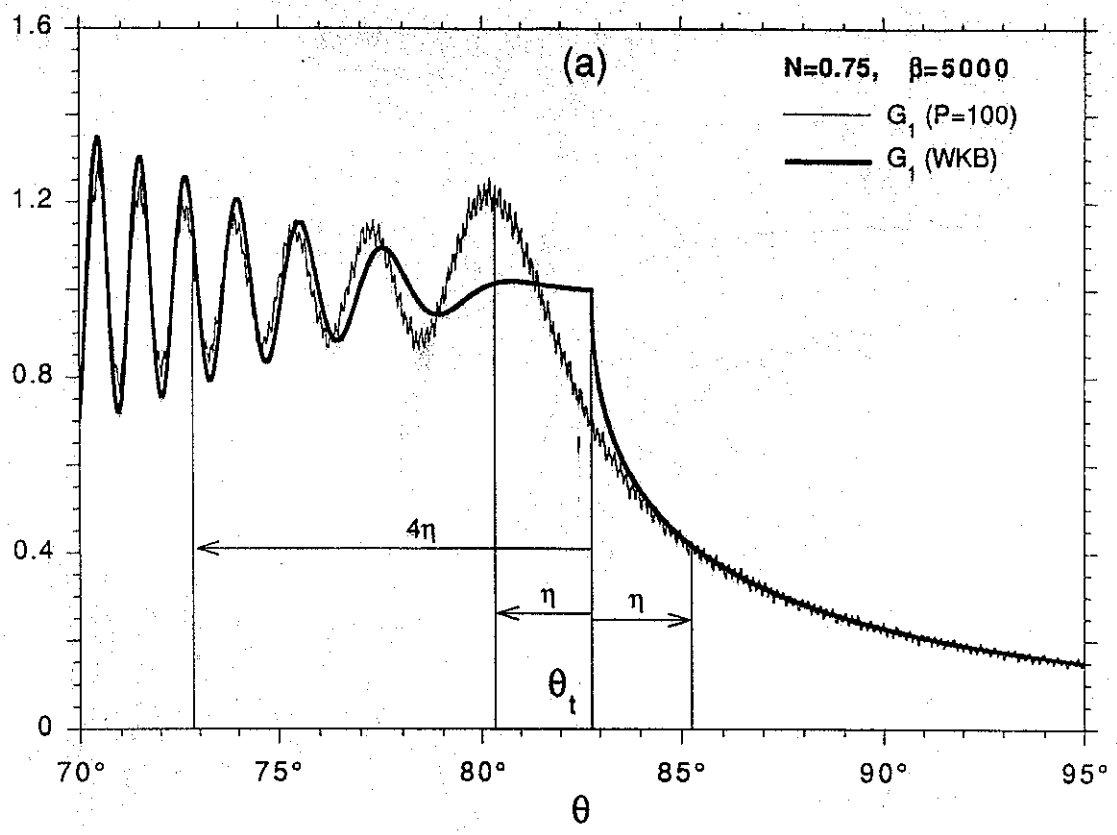

Figure 9(a)

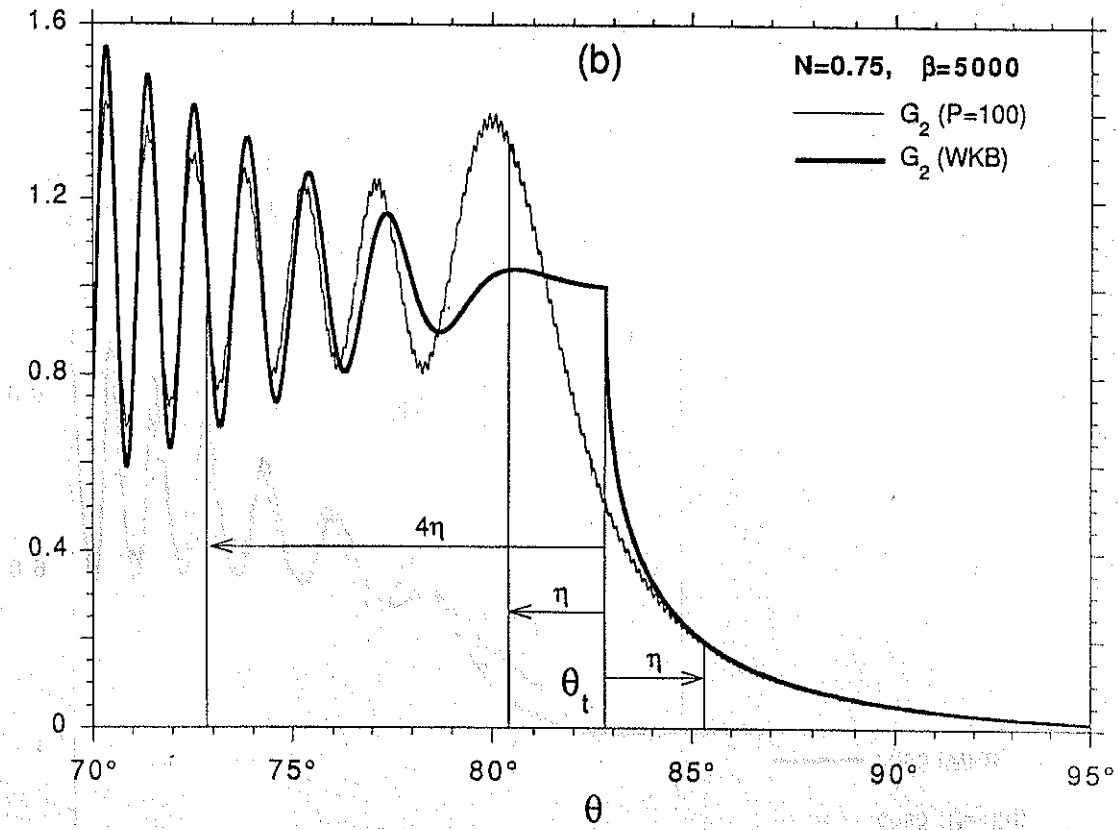

Figure 9(b)

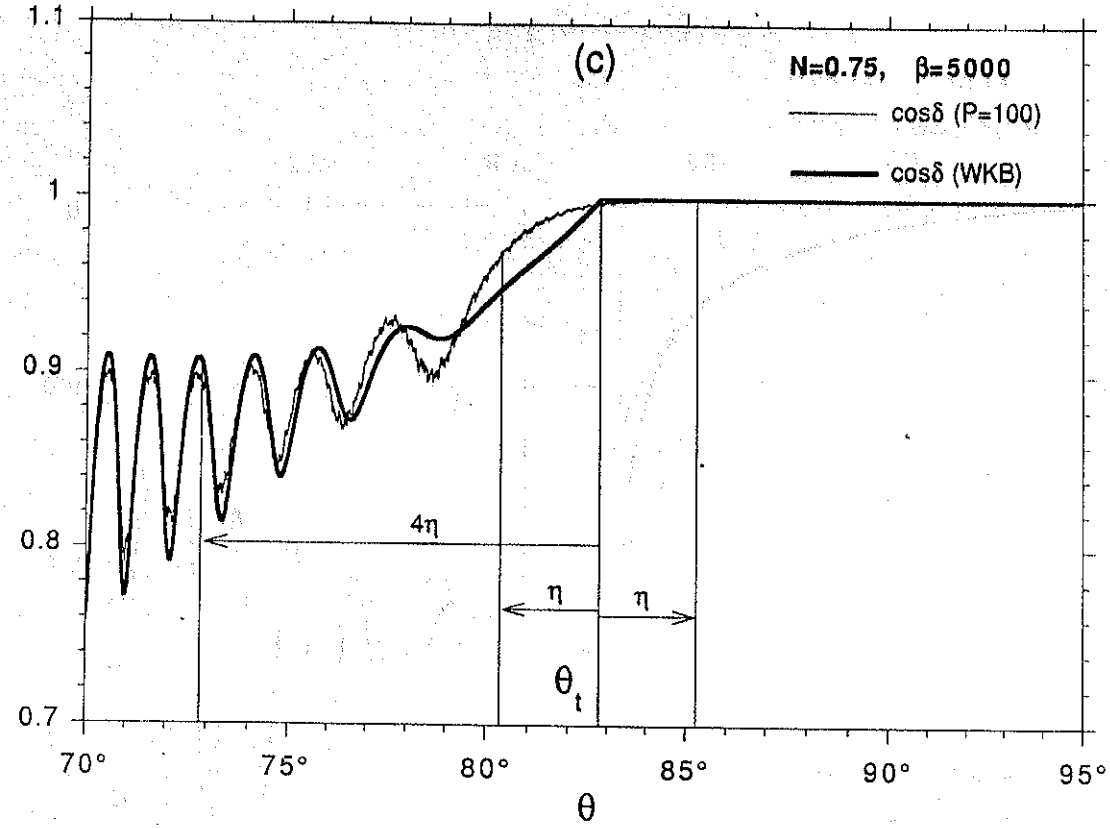

Figure 9(c)

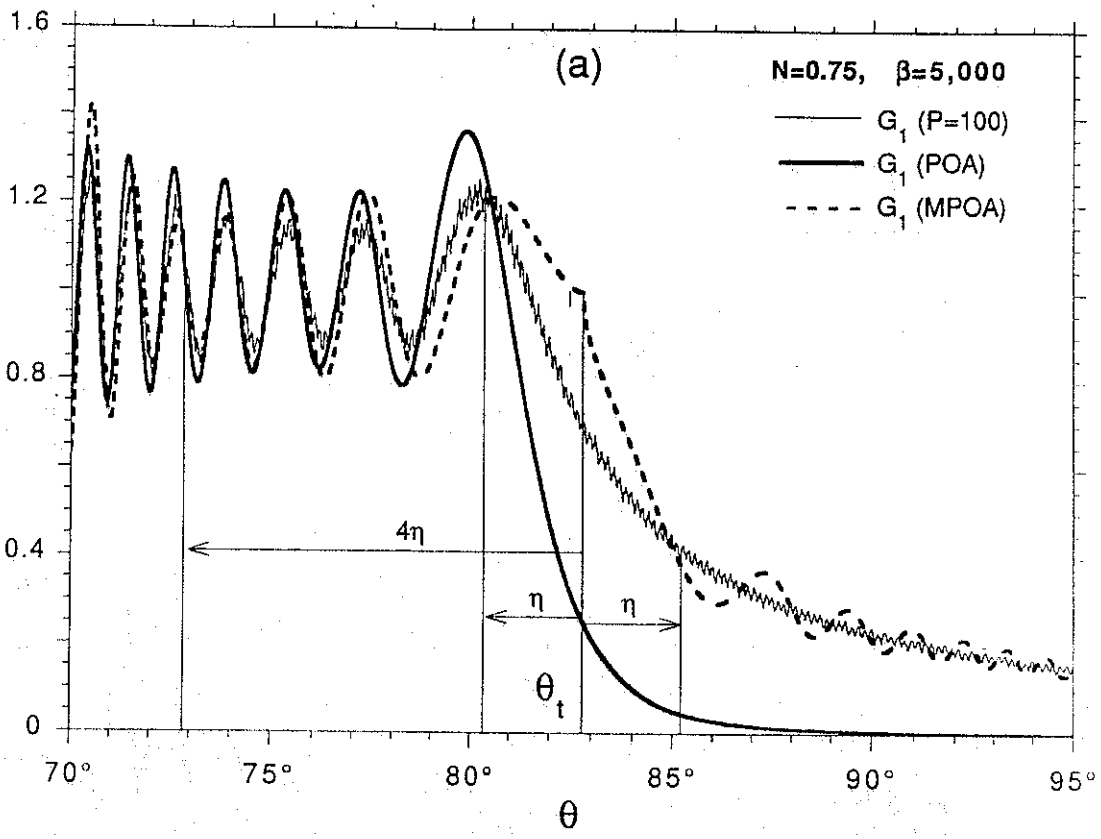

Figure 10(a)

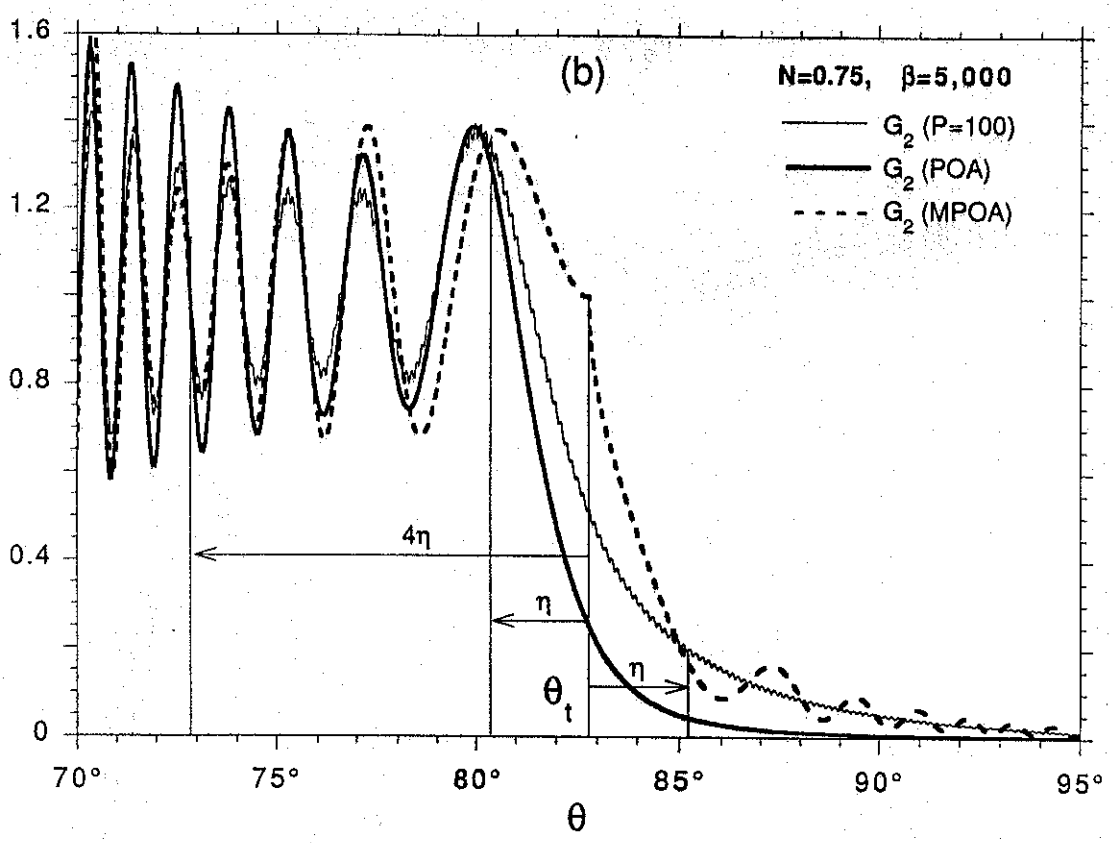

Figure 10(b)

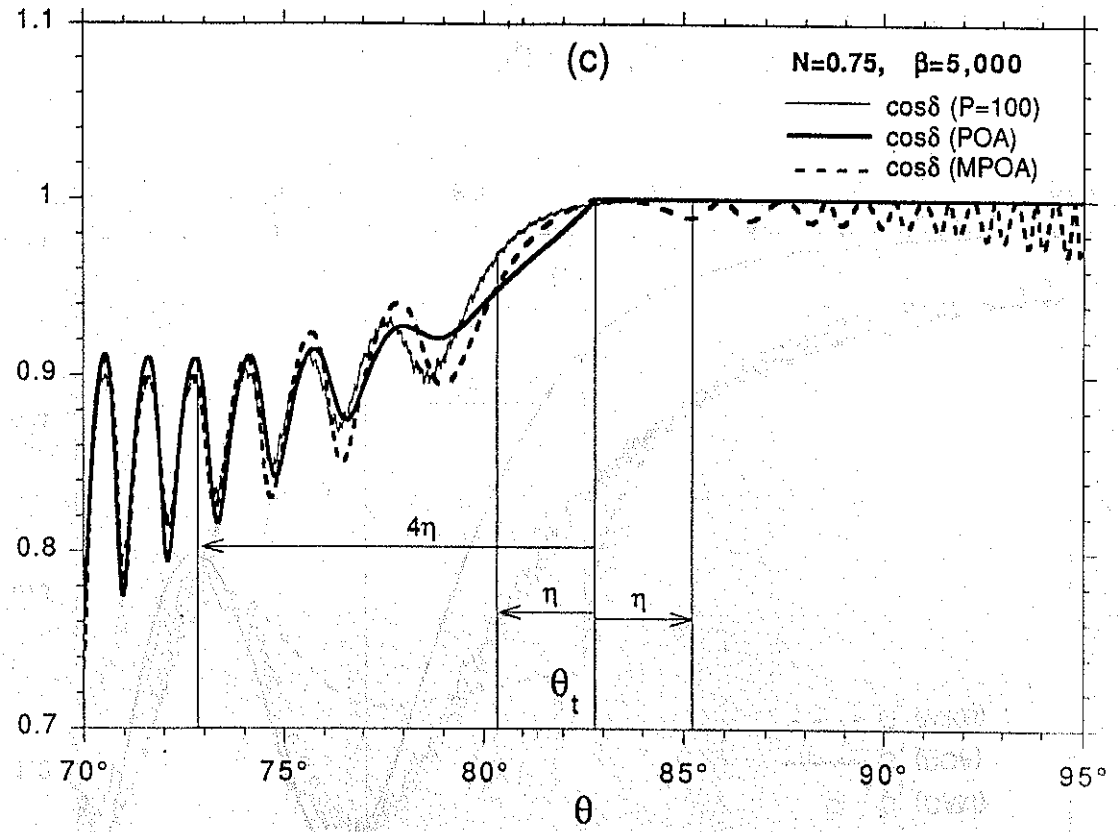

Figure 10(c)

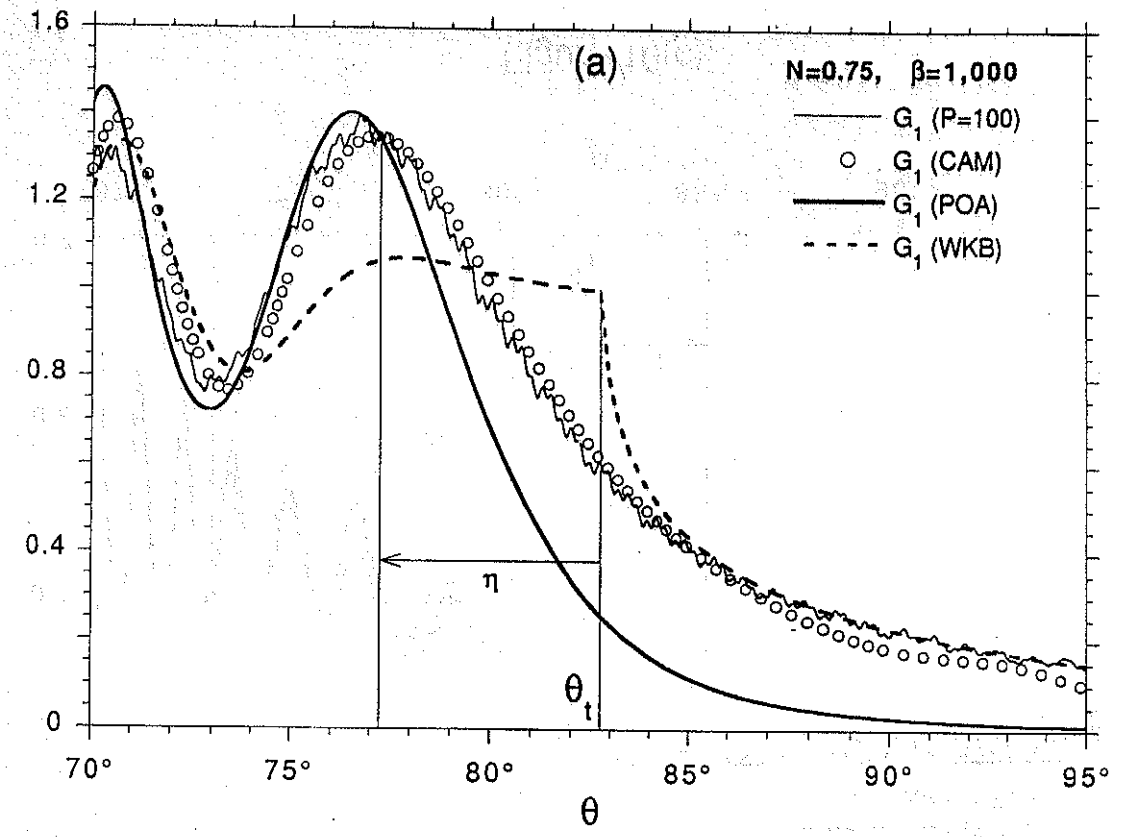

Figure 11(a)

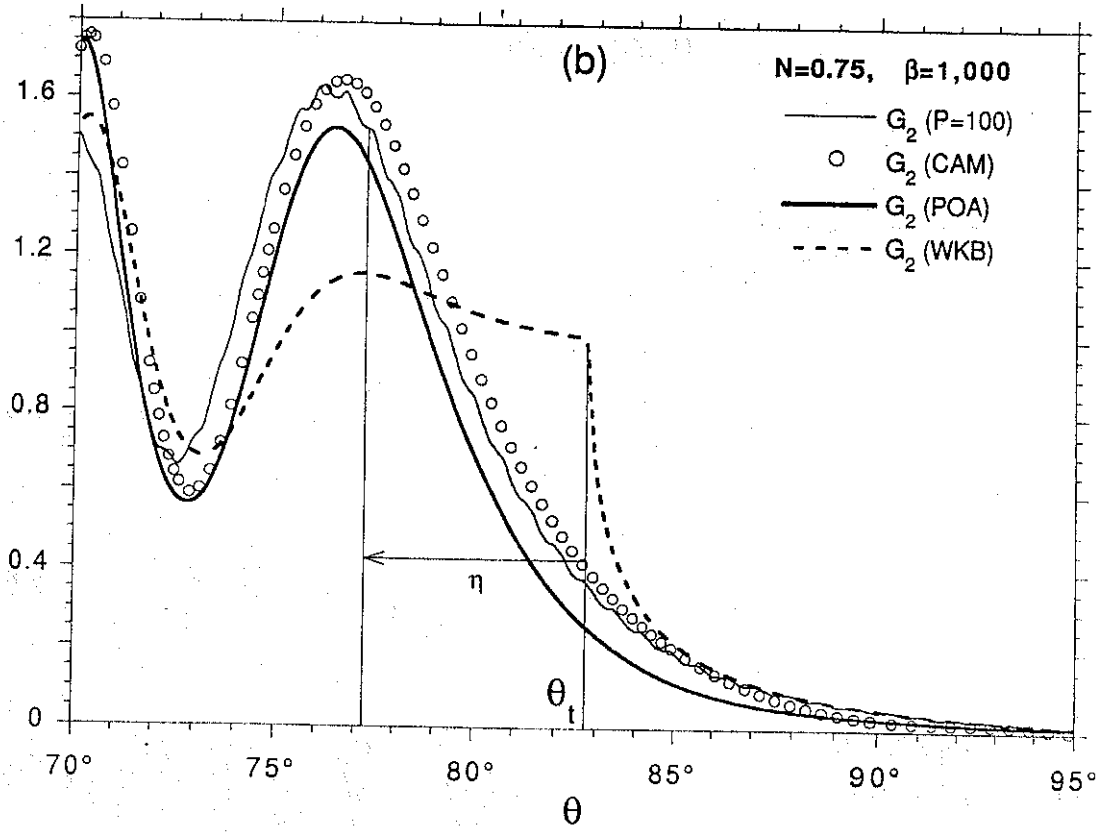

Figure 11(b)

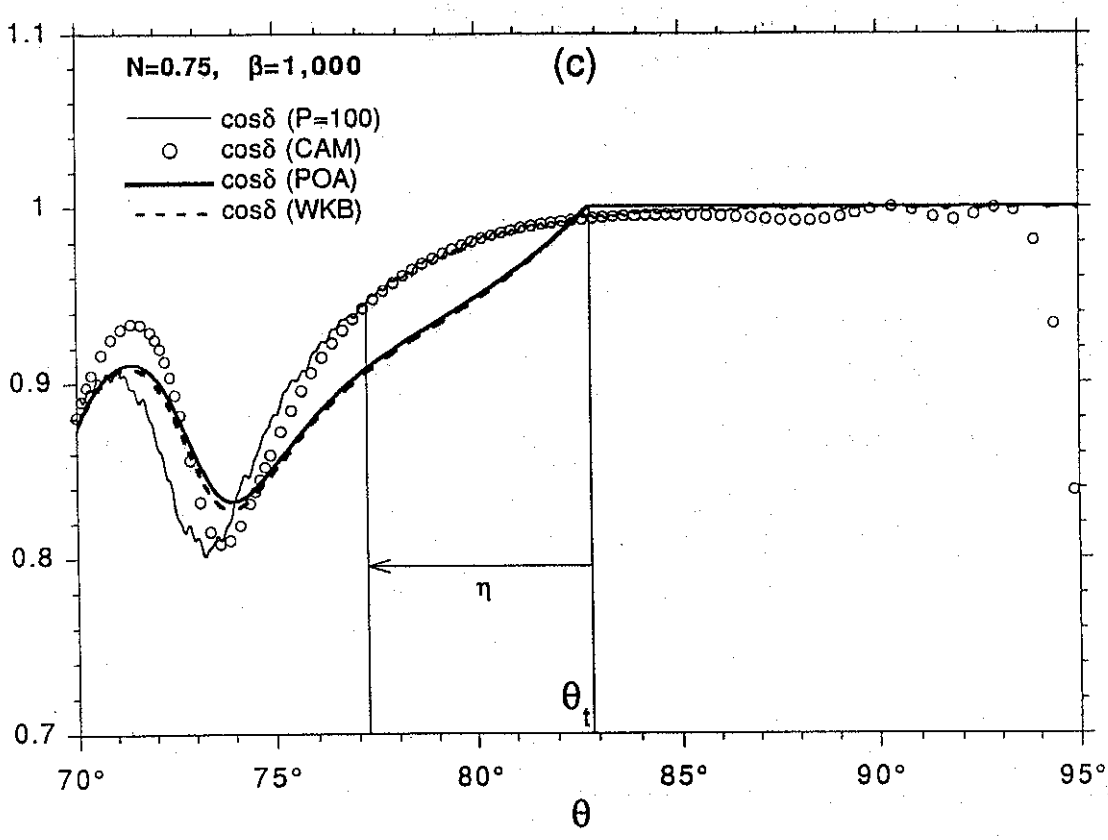

Figure 11(c)

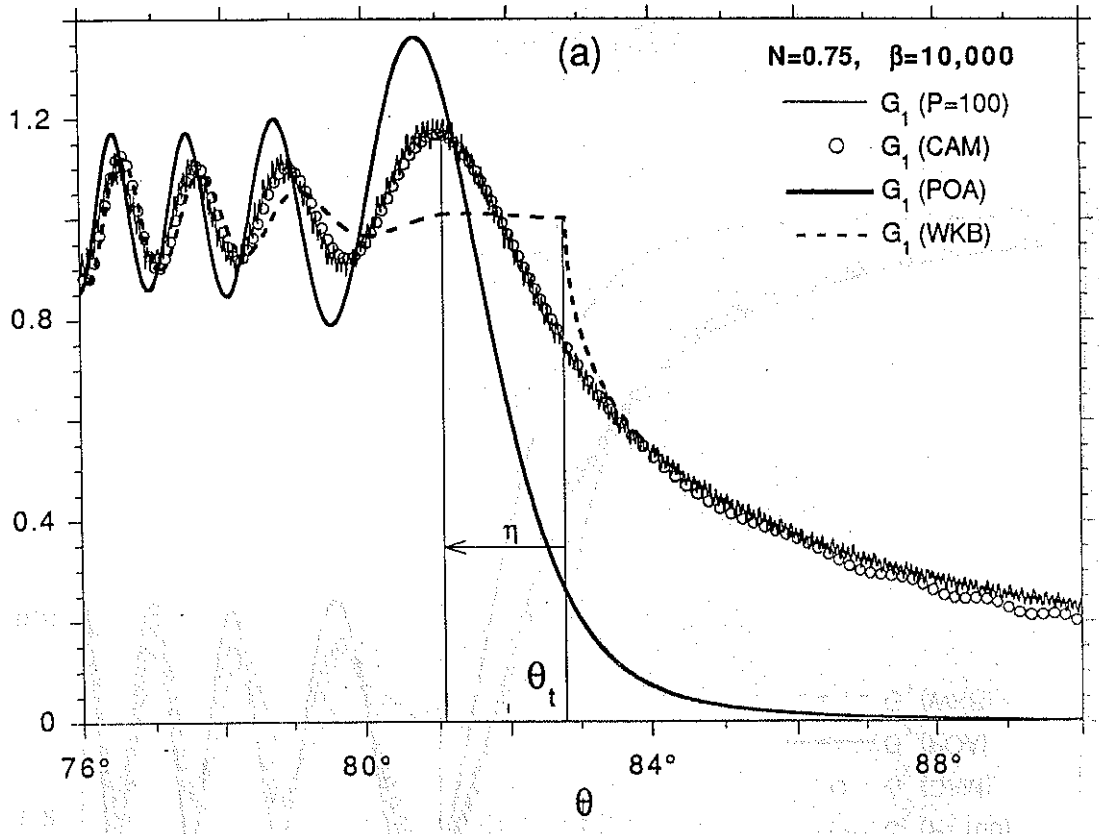

Figure 12(a)

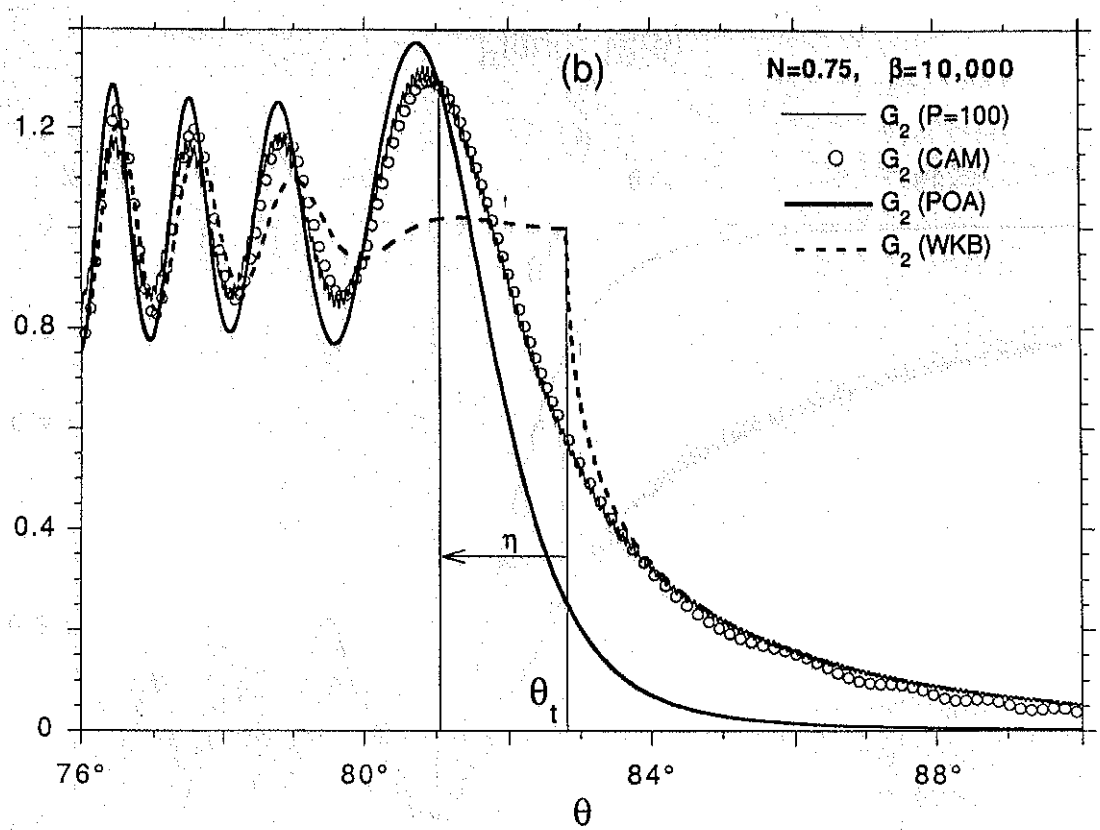

Figure 12(b)

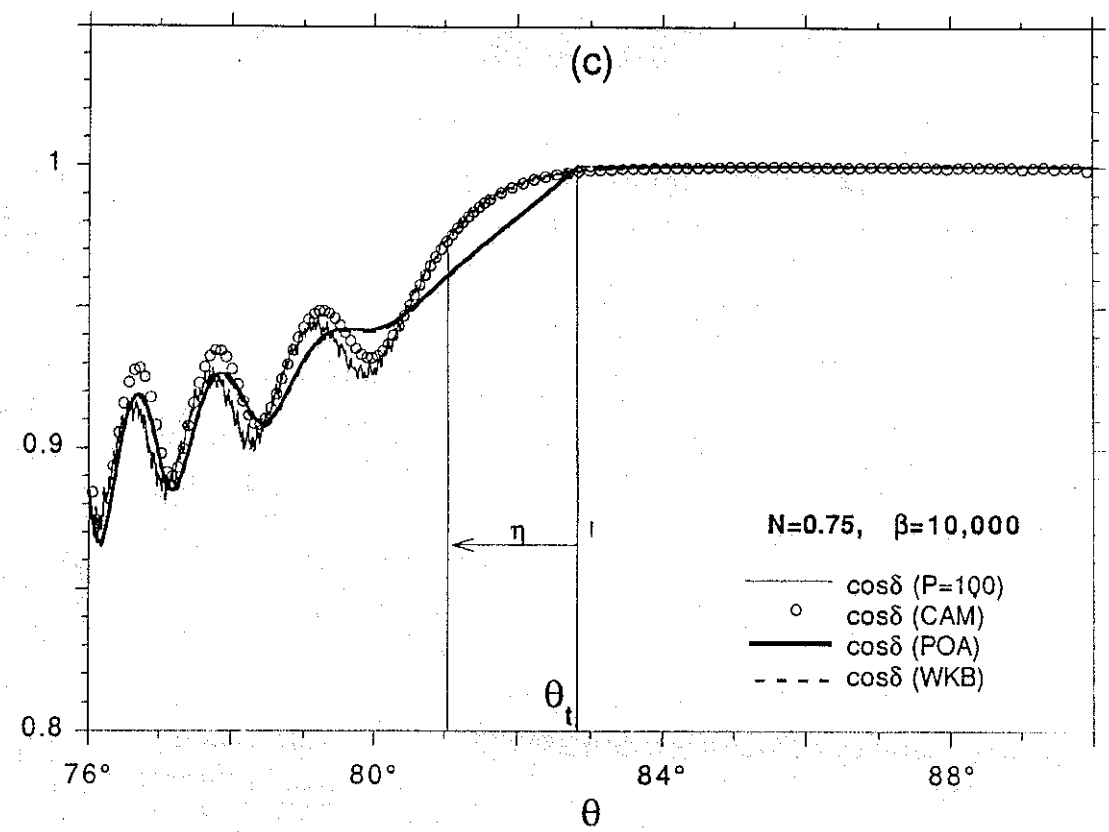

Figure 12(c)

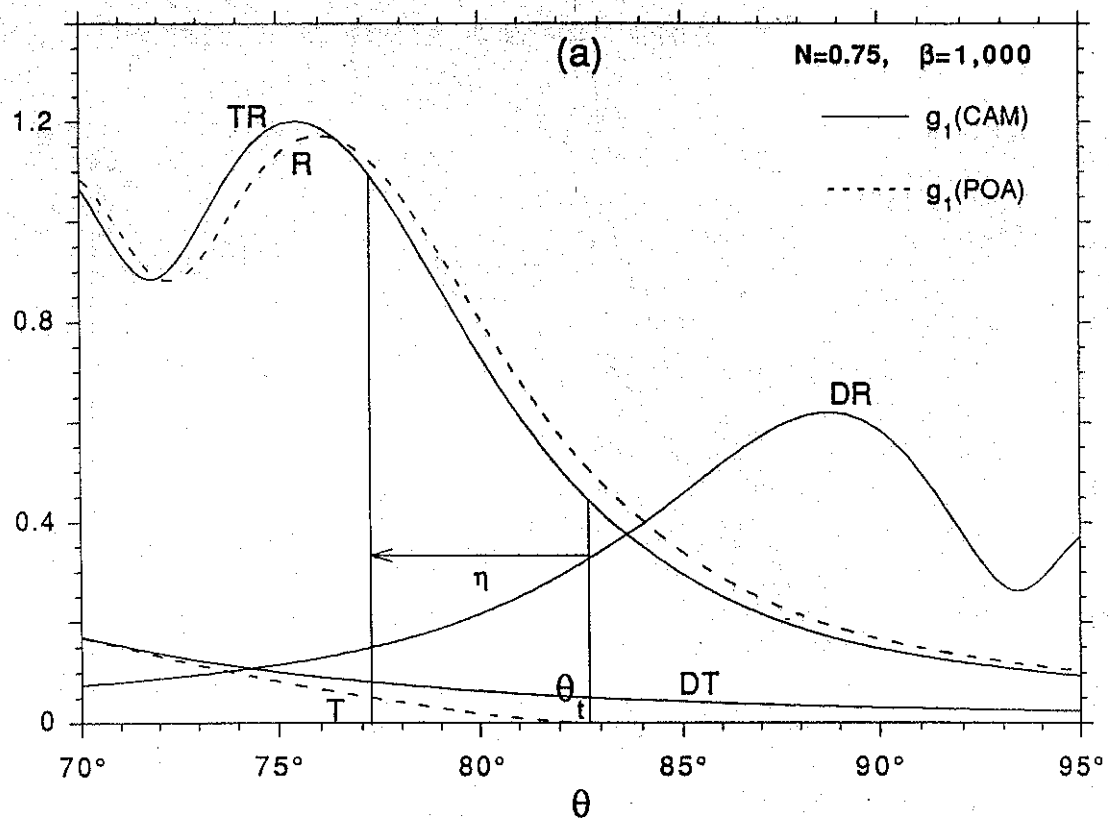

Figure 13(a)

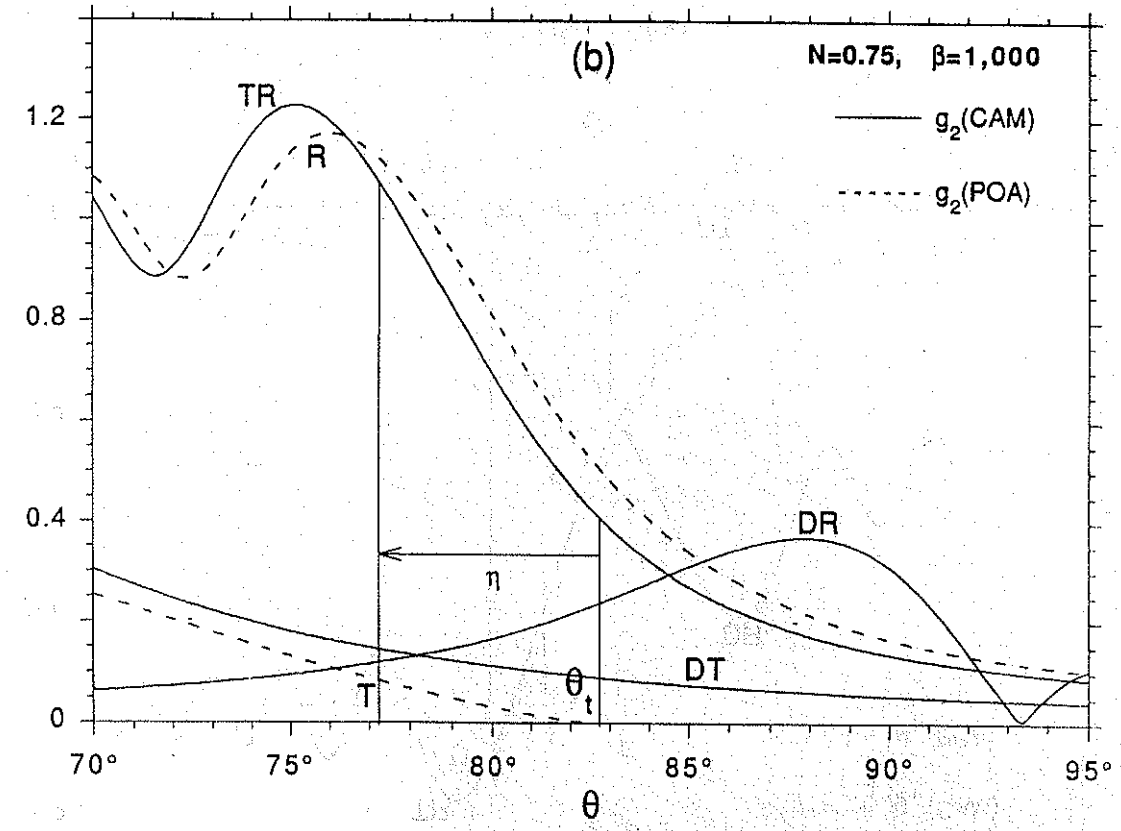

Figure 13(b)

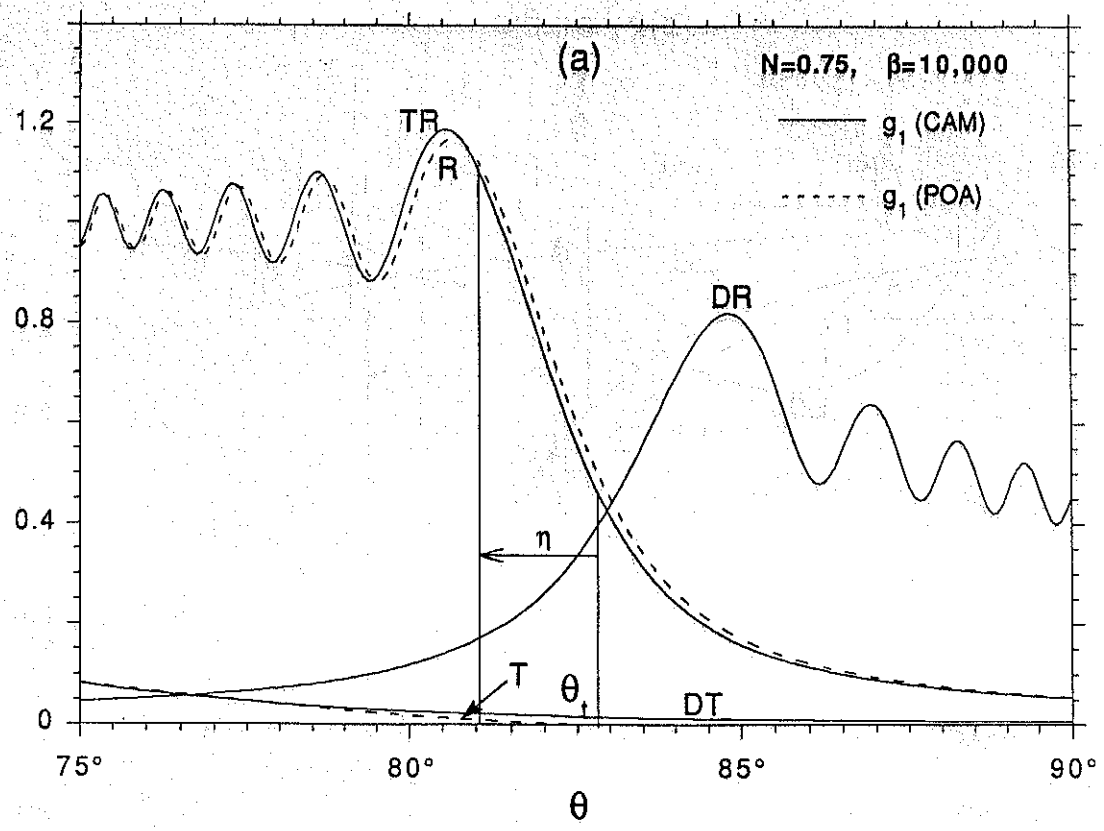

Figure 14(a)

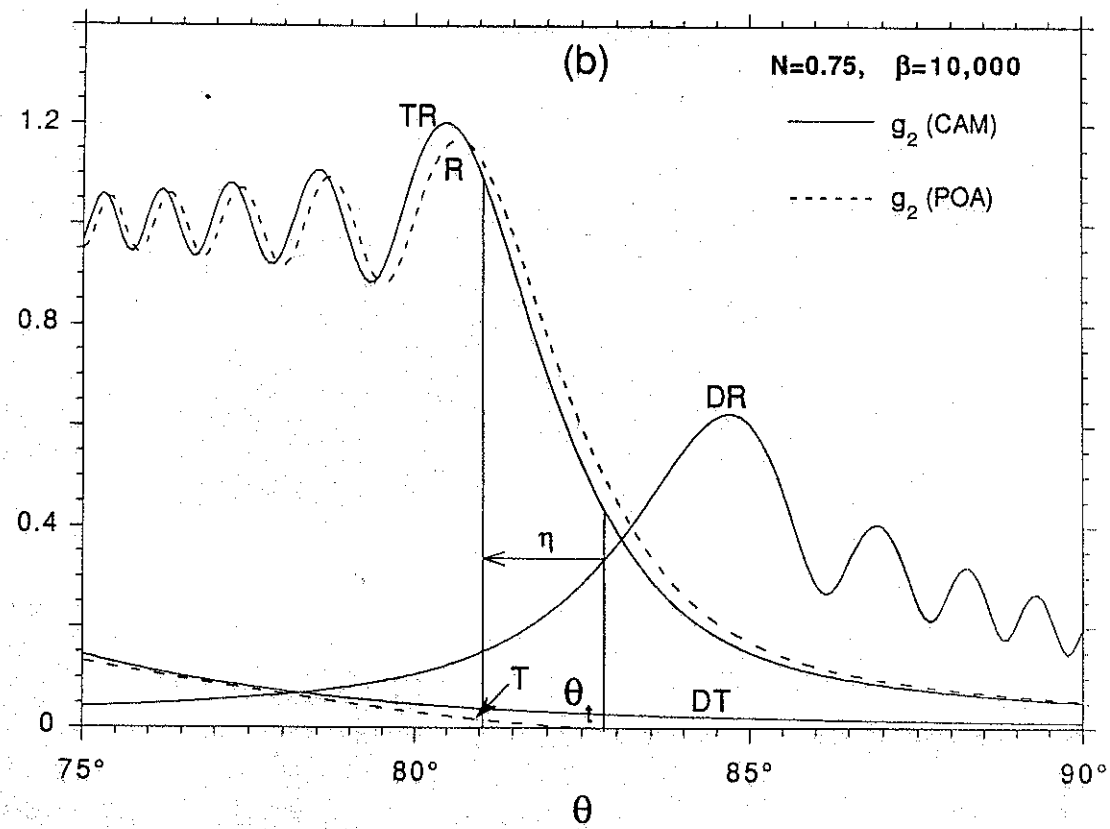

Figure 14(b)

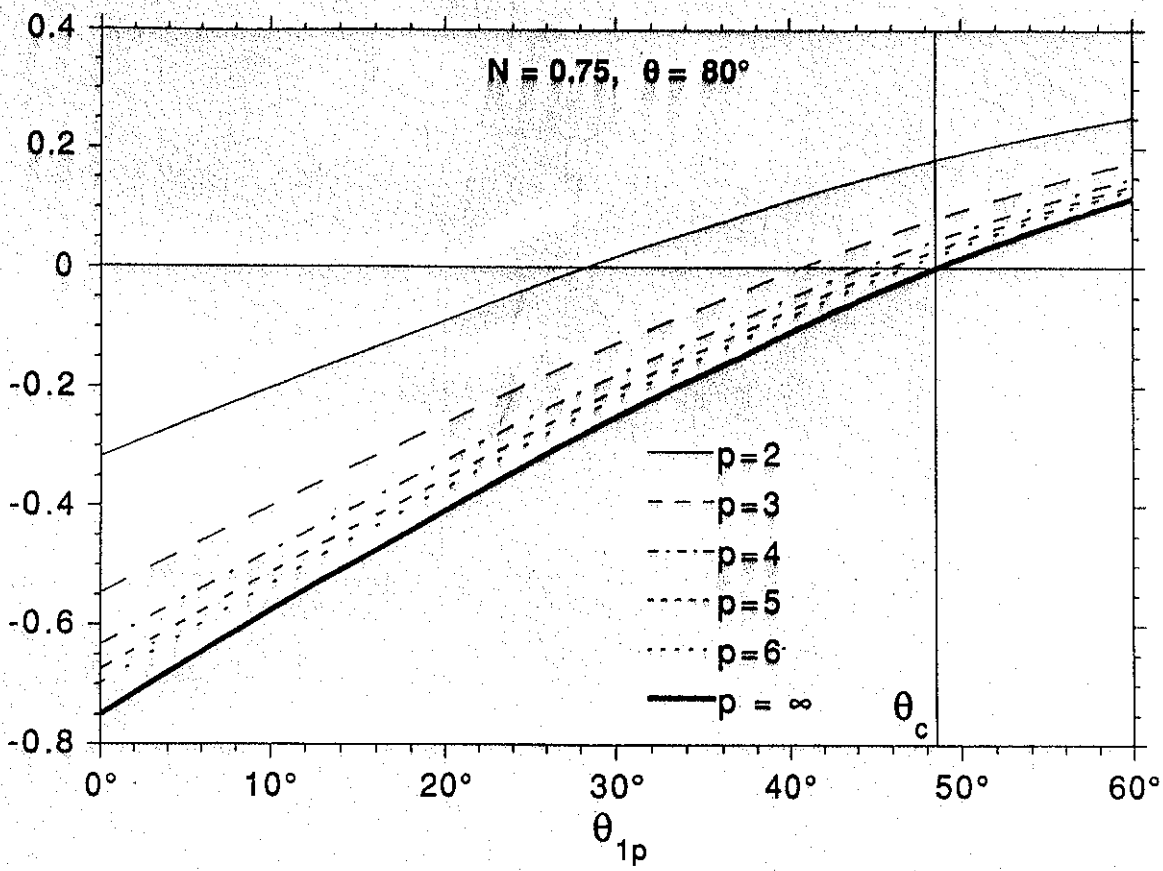

Figure 15